

**NASA CONTRACTOR
REPORT**



NASA CR-2370

NASA CR-2370

**PARAMETRIC STUDY OF RELAMINARIZATION
OF TURBULENT BOUNDARY LAYERS
ON NOZZLE WALLS**

by J. P. Kreskovsky, S. J. Shamroth, and H. McDonald

Prepared by

UNITED AIRCRAFT RESEARCH LABORATORIES

East Hartford, Conn. 06108

for Langley Research Center



NATIONAL AERONAUTICS AND SPACE ADMINISTRATION • WASHINGTON, D. C. • JUNE 1974

1. Report No. NASA CR-2370		2. Government Accession No.		3. Recipient's Catalog No.	
4. Title and Subtitle PARAMETRIC STUDY OF RELAMINARIZATION OF TURBULENT BOUNDARY LAYERS ON NOZZLE WALLS				5. Report Date June 1974	
				6. Performing Organization Code	
7. Author(s) J. P. Kreskovsky, S. J. Shamroth, and H. McDonald				8. Performing Organization Report No.	
9. Performing Organization Name and Address United Aircraft Research Laboratories East Hartford, CT 06108				10. Work Unit No. 501-06-07-03	
				11. Contract or Grant No. NAS1-11917	
12. Sponsoring Agency Name and Address National Aeronautics and Space Administration Washington, D.C. 20546				13. Type of Report and Period Covered Contractor Report	
				14. Sponsoring Agency Code	
15. Supplementary Notes Final report.					
16. Abstract By means of comparisons between theoretical predictions and experimental data the accuracy of a boundary layer procedure to predict the effect of large streamwise accelerations upon initially turbulent boundary layers is assessed. The boundary layer procedure is based upon simultaneous solution of the boundary layer partial differential equations and the integral turbulence kinetic energy equation. The results of the present investigation show the ability of the procedure to accurately predict properties of boundary layers subjected to large streamwise accelerations. The procedure is used to conduct a parametric study of the effect of free stream turbulence, heat transfer, Reynolds number, acceleration, and Mach number on boundary layers in supersonic nozzles to assist in the design of a quiet tunnel. Results of the investigation show that, even in the presence of moderate free-stream turbulence levels, the boundary layer in the approach section of the quiet tunnel nozzle relaminarizes and becomes thin enough to be removed by a small slot in the nozzle wall. Furthermore, the calculations indicate that it should be possible to maintain a laminar boundary layer for the entire length of the supersonic portion of the quiet tunnel nozzle.					
17. Key Words (Suggested by Author(s)) Laminar, transitional, turbulent boundary layers Boundary layers with large favorable pressure gradient. Mixing length, turbulence			18. Distribution Statement Unclassified - Unlimited STAR Category 12		
19. Security Classif. (of this report) Unclassified		20. Security Classif. (of this page) Unclassified		21. No. of Pages 91	22. Price* \$4.00

PARAMETRIC STUDY OF RELAMINARIZATION OF
TURBULENT BOUNDARY LAYERS ON NOZZLE WALLS

J. P. Kreskovsky, S. J. Shamroth, and H. McDonald
United Aircraft Research Laboratories

SUMMARY

By means of an extensive comparison between theoretical predictions and experimental data this investigation assesses the accuracy of a boundary layer procedure to predict the effect of large streamwise accelerations upon initially turbulent boundary layers. The boundary layer procedure under consideration is based upon simultaneous solution of the boundary layer partial differential equations and the integral turbulence kinetic energy equation and has previously been shown to yield satisfactory predictions for a large number of boundary layers in the subsonic to low hypersonic Mach number range. The results of the present investigation show the ability of the procedure to accurately predict properties of boundary layers subjected to large streamwise accelerations. The procedure is used to conduct a parametric study of the effect of free-stream turbulence, heat transfer, Reynolds number, acceleration, and Mach number on boundary layers in supersonic nozzles to assist in the design of a quiet tunnel. Results of the investigation show that, even in the presence of moderate free-stream turbulence levels, the boundary layer in the approach section of the quiet tunnel nozzle relaminarizes and becomes thin enough to be removed by a small slot in the nozzle wall. Furthermore, the calculations indicate that it should be possible to maintain a laminar boundary layer for the entire length of the supersonic portion of the quiet tunnel nozzle.

INTRODUCTION

The location of boundary layer transition is an important consideration in the successful design and operation of supersonic and hypersonic vehicles. In general, it is expected that the maximum wall heating at any point in the flight path will occur in the region where the boundary layer undergoes transition from a laminar to a turbulent state and the insurance of vehicle structural integrity requires an accurate prediction of both the transition location and the peak wall heating rate either by theoretical or experimental means. In addition to heat transfer considerations, boundary layer transition may play a significant role in determining the skin friction drag and vehicle wake flow field. At present the only method of determining the transition region for the complex three-dimensional flow fields developing on hypersonic vehicles other than flight testing is through accurate wind tunnel testing. If a model is tested in the proper environment, it should be possible to obtain a flow pattern in the wind tunnel corresponding to the flow pattern which would occur under free flight conditions. Two obvious free flight quantities which must be matched in the wind tunnel test are Mach number and Reynolds number. A third quantity which must be matched particularly in regard to determining the transition region is the free-stream disturbance level. It has long been recognized that the free-stream turbulence level has a dominant role in determining transition (e.g., refs. 1 and 2) and, therefore, it is important that the wind tunnel tests be characterized by the free-stream disturbance level expected to be present under flight conditions.

The problem of obtaining a specified free-stream disturbance level in a high Mach number wind tunnel is one which requires careful analysis during the tunnel design period as indicated by the fact that transition measurements carried out in different wind tunnel facilities have been inconclusive and even contradictory. For example, Pate and Schueler (ref. 3) and Pate (ref. 4) have shown that correlations based upon transition data from one supersonic wind tunnel do not necessarily correspond to correlations based upon data from a different tunnel. Upon examination of the data, Pate and Schueler (ref. 3) showed that for a large amount of data a direct relationship exists between the location of transition and the free-stream aerodynamic noise emanating from turbulent tunnel wall boundary layers, thus indicating that at high Mach numbers the acoustic mode is the dominant free-stream disturbance mode and that the source of the acoustic disturbance is the transitional and turbulent portions of the tunnel wall boundary layer. Bertram and Beckwith (ref. 5) have also demonstrated that a considerable portion of the noise found in a supersonic tunnel emanates from the turbulent tunnel wall boundary layer. Thus, the development of a quiet tunnel more representative of free flight conditions would require a laminar tunnel wall boundary layer in all regions which could

effect the test section of the tunnel. One method of suppressing the turbulent boundary layer is to cause the normally turbulent boundary layer which develops in the nozzle inlet section to revert to a laminar-like state by means of high streamwise acceleration (ref. 6). Furthermore, wall cooling may delay transition in the nozzle approach section and may suppress transition of the laminarized boundary layer in the supersonic section of the nozzle once the streamwise acceleration is removed. Reynolds number and Mach number effects are also expected to influence the relaminarizing boundary layer. Thus, an analytical procedure which could predict the effects of high streamwise acceleration, wall cooling, Reynolds number, and Mach number, as well as the effect of free-stream turbulence on transition and relaminarization, would be a tool of considerable assistance in the design of the quiet wind tunnel.

Presently, there exist three possible approaches for developing a boundary layer theory to predict transition and relaminarization: the semi-empirical approach, the stability theory approach, and the turbulence kinetic energy approach. Typical examples of the semiempirical approach for predicting transition location are discussed by Hairston (ref. 7) and such approaches could also be used for predictions of relaminarization; however, semiempirical procedures cannot be used with confidence to predict transition for flow conditions significantly different from the flow conditions of the correlating data. In addition to the limitations imposed by data correlations, most semiempirical theories are limited further by the crude assumption of instantaneous transition. Although the instantaneous transition assumption may be acceptable if flow conditions in the vicinity of transition are not of interest, the assumption clearly is unacceptable if predictions in the vicinity of transition are required. The instantaneous transition assumption has been relieved in the work of Harris (ref. 8) who assumes a finite length transition region in which the total shear stress is a linear combination of the laminar shear stress and the fully-turbulent shear stress. This model has successfully predicted the development of transitional boundary layers in the low hypersonic Mach number regime and represents a significant improvement over instantaneous transition models. This model could be extended to relaminarization, however, since it heavily depends upon empiricism and was not intended to predict the effect of phenomena such as free-stream turbulence, Mach number, wall temperature, etc. upon transitional behavior, it does not serve as a general boundary layer transition or relaminarization prediction procedure. The second possible approach which might lead to an analytical prediction of transitional boundary layers is based upon stability theory in which the flow is divided into a mean flow whose stability is the subject of the investigation and a superimposed disturbance of specified form. Attempts to predict the initiation of transition from classical stability theory (for example, ref. 9) have had only qualitative success and this approach has yet to be applied successfully to the problem of transitional boundary layer development. Furthermore, the application of stability theory to relaminarizing boundary layers is not obvious.

The third approach for predicting the behavior of transitional boundary layers is based upon the solution of the turbulence kinetic energy equation. The turbulence kinetic energy equation has proven to be a useful tool in predicting the behavior of a wide variety of turbulent boundary layers (e.g., refs. 10 and 11) and has been extended into the transitional regime by Glushko (ref. 12), Donaldson, Sullivan, and Yates (ref. 13), and McDonald and Fish (ref. 14). At the present time, neither the work of Glushko (ref. 12) or Donaldson, et al. (ref. 13) has been developed into a practical prediction procedure. However, the approach used by McDonald and Fish (ref. 14) has proven capable of accurately predicting the behavior of a wide variety of transitional boundary layers in the subsonic and low supersonic Mach number regimes and this approach has been extended by Shamroth and McDonald (ref. 15) to the low hypersonic Mach number regime.

In the present report the ability of the McDonald-Fish procedure (ref. 14) to predict the effect of strong favorable pressure gradients upon an initially turbulent boundary layer is assessed and the procedure is then used in conjunction with various inviscid flow calculation procedures to assist in developing a design for the NASA pilot model quiet tunnel (ref. 16). In the quiet tunnel the nozzle is preceded by a constant area entrance duct. The entrance duct is long enough so that a turbulent wall boundary layer is present at the junction between the entrance duct and the nozzle itself. In the subsonic portion of the nozzle the flow is subjected to a strong favorable pressure gradient which is expected to cause the initially turbulent boundary layer to relaminarize and become very thin. Slightly upstream of the throat the thin boundary layer is removed by a suction slot. A new boundary layer is formed at the suction slot which grows along the tunnel wall downstream of the throat region. This new boundary layer is initially laminar and the favorable pressure gradient inhibits transition. Eventually at some station downstream of the favorable pressure gradient the boundary layer may undergo transition and become turbulent.

In the present report a series of comparisons between theoretical predictions and experimental data for initially turbulent boundary layers under the influence of strong favorable pressure gradients are presented. These comparisons demonstrate the ability of the McDonald-Fish procedure to predict the effect of strong favorable pressure gradients on an initially turbulent boundary layer. The theoretical procedure is then used to calculate wall boundary layers for the pilot model quiet tunnel. In addition to these boundary layer calculations, results from inviscid flow predictions for the pilot tunnel geometry are presented and compared to predictions made independently by NASA.

LIST OF SYMBOLS

a_n	structural coefficients of turbulence
C_p	specific heat
C_f	skin friction coefficient
\mathcal{D}	sublayer damping factor
F	dimensionless stream function
G^i	dimensionless temperature ratio
H	shape factor
H^*	incompressible shape factor
K	acceleration parameter
k	thermal conductivity
L	dissipation length
L_{ref}	reference length
l	mixing length
l_∞	wake value of mixing length
M	Mach number
Pr	Prandtl number
Pr_T	turbulent Prandtl number
P	pressure
Q	heat flux
$\overline{q^2}$	turbulence kinetic energy

r	radius
R_T	turbulence Reynolds number
$\overline{R_T}$	layer averaged turbulence Reynolds number
Re	Reynolds number based upon momentum thickness
St	Stanton number
T	static temperature
T^0	total temperature
u	streamwise velocity
u_T	friction velocity
v	transverse velocity
w	cross flow velocity
x	streamwise coordinate
y	transverse coordinate
y^+	dimensionless transverse coordinate
α	indicator equal to one for axisymmetric flow, zero for two-dimensional flow
β	density ratio
Γ	intermittency factor
γ	ratio of specific heats
δ	boundary layer thickness
δ_s	sublayer thickness
δ^*	displacement thickness
δ^+	reference length

ϵ	turbulence dissipation
η	dimensionless transverse coordinate
θ	momentum thickness
μ	viscosity
ν	kinematic viscosity
ν_T	kinematic eddy viscosity
ρ	density
τ	shear stress
χ	dimensionless longitudinal distance
ϕ_1, ϕ_2, ϕ_3	integral functions (see Eqs. (A-19) through (A-21))

Subscripts

e	boundary layer edge condition
∞	free-stream condition
w	wall condition
t	throat

Superscripts

—	average quantity
'	fluctuating quantity

THEORY

The UARL prediction procedure is based upon a simultaneous solution of the boundary layer partial differential equations of conservation of mass, momentum, and energy. The partial differential equations are used in conjunction with an integral turbulence kinetic energy equation and a turbulence structure model to predict boundary layer development. The procedure has been used to predict a wide variety of boundary layers with Mach numbers varying from the incompressible to the low hypersonic regime. The procedure can include the effects of heat transfer and wall transpiration and, in addition, has a multiple species and chemical reaction capability. In brief, for a single component flow the procedure solves the governing momentum and energy equations by a Hartree-Womersley approach in which streamwise derivatives are replaced by finite-differences, the coordinate normal to the wall is nondimensionalized and a stream function is introduced. The resulting momentum and energy equations are third order and second order nonlinear ordinary differential equations, respectively, in the transverse coordinate. At each streamwise station the nonlinear coefficients are estimated from solutions at the previous stations and the resulting linearized equations are solved as two point boundary value problems. The resulting solutions are used to obtain better estimates of the nonlinear coefficients and the entire process is repeated until two solutions agree within a specified tolerance. When two successive solutions agree, the equations are considered solved at that streamwise station and the solution proceeds to the next streamwise station.

The integral turbulence kinetic energy equation is coupled iteratively to the momentum and energy conservation equations. At specified points in the calculation which iterate upon the nonlinear coefficients of the momentum and energy equations, the integral turbulence kinetic energy equation is solved to determine the turbulent contribution to the transport coefficients. The integral turbulence kinetic energy equation is solved even during laminar flow and in these cases the predicted turbulent transport properties are negligible compared to the laminar transport properties. Gradually as the boundary layer thickness increases the predicted turbulent transport becomes comparable and then much larger than the laminar transport (except, of course, in the sublayer region) indicating transitional and fully-turbulent flow. Similarly in the case of a fully-turbulent flow subjected to a strong favorable pressure gradient, the predicted turbulent contribution to the total transport may decrease leading to relaminarization and development of an effectively laminar boundary layer. It is important to note that in the UARL procedure transition and relaminarization are natural occurrences of the turbulence model rather than being triggered by some semiempirical criteria such as momentum thickness Reynolds number. In its present form the procedure does not include any effect of Taylor-Goertler vortices which if present may induce transition. However,

if information were available which could relate two-dimensional mean flow conditions to the formation of the vortices and to the subsequent development of the Reynolds stress tensor, it seems reasonable to assume that this information could be incorporated within the framework of the turbulence kinetic energy equation and models such as the present, which are based on energy considerations, could be extended to include the effect of the vortices.

A detailed description of the governing equations and the turbulence model has been presented in refs. 14 and 15. The description of the method presented in ref. 15 is repeated in Appendix A of the present report.

The primary purpose of the present investigation was to assist NASA in theoretically evaluating the design of the model pilot quiet tunnel through implementation of the UARL boundary layer prediction procedure. The first step in fulfilling this purpose was to evaluate the UARL procedure's ability to predict the behavior of boundary layers subjected to large favorable pressure gradients. Although the ability of the UARL procedure to predict the boundary layer mean flow behavior in going from the laminar to the turbulent state had been previously extensively assessed (refs. 14 and 15), no detailed assessment had been previously made of the procedure's ability to predict the effects of large favorable pressure gradients on an initially turbulent boundary layer. The experimental highly accelerated boundary layer data available for comparison with theoretical predictions falls into three broad areas; adiabatic wall low-speed flows, adiabatic wall moderately supersonic flows, and low-speed flows in the presence of wall heat transfer. The amount of data available with heat transfer in highly accelerated turbulent flows, in sufficient detail to enable predictions to be made, is limited. However, enough data is available to make some meaningful comparisons.

The Effect of Pressure Gradient Upon Transition

In general, it is expected that relaminarization will occur in regions of strong favorable pressure gradient and as a first step in evaluating the ability of the model to predict relaminarization, a series of calculations were made to compare theoretical predictions of the forward transition Reynolds number with the experimental data of Feindt (ref. 17) over a range of pressure gradients. The results of several calculations made for various pressure gradients are shown in Fig. 1 where the predicted variation of the momentum thickness Reynolds number at transition, R_{θ_T} with the pressure gradient parameter $(\theta^2/\nu)dU/dx$, is compared with the theory of van Driest and Blumer (ref. 18) and with the experimental data of Feindt (ref. 17) as presented by Hall and Gibbings (ref. 19). The predicted transition location was taken to be at the point of minimum skin friction. The UARL predictions and the data of Feindt are for a free-stream turbulence level of 1.2 percent. The van Driest-Blumer theory is presented for 1 percent free-stream turbulence. Both theories, as well as the experimental data, show only a mild effect of pressure gradient on transition Reynolds number over this moderately low range of the pressure gradient parameter. The UARL predictions are in good agreement with Feindt's data, showing an increase in transition Reynolds number with increasing pressure gradient parameter.

The Effect of Large Streamwise Accelerations
Upon the Boundary Layer in Supersonic Nozzles

As part of the present investigation predictions of the effect of large streamwise accelerations upon initially fully-turbulent boundary layers were made corresponding to boundary layer measurements obtained experimentally by Nash-Webber (ref. 6). The measured boundary layers were developed in nozzles constructed with a flat plate as one wall and a contoured surface as the opposite wall; the experimental data were taken for the boundary layer development on the flat plate wall. The nozzles, referred to as nozzle "A" and nozzle "C" in ref. 6, had exit Mach numbers of approximately 2.0 and had adiabatic walls. Both nozzles subjected the boundary layers to favorable pressure gradients. Since Nash-Webber (ref. 6) did not report a free-stream turbulence intensity, a level of 2 percent was assumed at the nozzle inlet. The free-stream turbulence kinetic energy, \bar{q}_e^2 , is assumed to remain constant under either acceleration or deceleration, therefore, the intensity, $(\bar{q}_e^2/3)^{1/2}/U_e$, varies inversely with free-stream velocity. Comparisons between predictions made using the UARL transition model, fully-turbulent theory (frozen mixing length), and the data of Nash-Webber (ref. 6) for three different stagnation pressures in nozzle "A" are shown in Figs. 2 through 4. Variation of the stagnation pressure provides a means of varying the free-stream unit Reynolds number, Reynolds number increasing with increasing pressure, while maintaining the same pressure gradient. The acceleration parameter, K,

$$K = \nu_w / U_\infty^2 \, dU_\infty / dx = \nu_w / \rho U_\infty^3 \, dP / dx \quad (1)$$

however, is reduced as the stagnation pressure is increased due to the increase in density. The results shown in Figs. 2 through 4 indicate that the predicted variation of momentum thickness Reynolds number and shape factor made using the UARL prediction procedure are in good agreement with the experimental data for the three values of stagnation pressure considered. In Figs. 2 through 4 (as well as Figs. 5 and 6) the distance along the nozzle has been nondimensionalized by a reference length, $L_{ref} = 30.5$ cm (12 in.). The variation of the dimensionless mixing length (l_∞/δ), indicates that the boundary layers effectively relaminarize at a dimensionless distance of about 2.0. The relaminarization is also indicated by the sharp increase in the boundary layer shape factor. The predictions made using fully-turbulent theory are significantly inferior as they do not correlate well either with the experimental data or the predictions made using the transition model past the region of relaminarization. The predictions of the boundary layer development in nozzle "C" at two values of stagnation pressure are shown in Figs. 5 and 6. The predictions made using the UARL procedure are again in good agreement with the experimental data for both values of stagnation pressure, however, the streamwise variation of the

momentum thickness Reynolds number at a stagnation pressure of 1.66×10^{-1} atm, shown in Fig. 5, is somewhat overpredicted. The sharp drop in the dimensionless mixing length occurs at approximately $\chi = 2.75$ for both values of stagnation pressure indicating the region of relaminarization, and it is downstream of this region that the fully-turbulent predictions deviate significantly from both the data and the transitional predictions.

The Effect of Large Streamwise Accelerations Upon Low-Speed Boundary Layers

Predictions for strongly accelerated flows. - A detailed investigation of a low-speed highly-accelerated boundary layer which is suitable for comparison with theory was carried out by Blackwelder and Kovaszny (ref. 20). In this investigation a flow in which the free-stream velocity was initially 295 cm per sec was accelerated smoothly to a velocity of 1260 cm per sec over a distance of 350 cm. During the acceleration the acceleration parameter, K , reached a maximum of 4.8×10^{-6} which is well above the usual value at which relaminarization is observed. This maximum acceleration parameter is reached at 984 cm and the acceleration then decreases to zero at 1200 cm. The free-stream turbulence level was of the order of 0.5 percent as determined from measurements of u' , v' , and w' . Theoretical predictions of the flow were made both with the UARL transition procedure using 0.5 percent free-stream turbulence and with the fully-turbulent (constant dimensionless mixing length) theory. Comparison of the two predictions with the experimental data are presented in Figs. 7 and 8. Figure 7 shows the variation of the momentum thickness Reynolds number and the shape factor. The predictions made using the UARL procedure are in good agreement with the experimental data. In contrast with the transition prediction, the fully-turbulent prediction does not give good quantitative predictions of the momentum thickness Reynolds number and shape factor downstream of the point of maximum acceleration. The variation of the skin friction coefficient and the dimensionless mixing length is shown in Fig. 8. The prediction of skin friction coefficient made using the UARL procedure shows qualitative agreement with the data but quantitative disagreement. Both theory and experiment show a drop in skin friction followed by a rise, however, the theoretically predicted rise anticipates the experimentally observed rise. It should be noted that the fully-turbulent theory is not even in qualitative agreement with experiment as far as skin friction or shape factor predictions are concerned. The dimensionless mixing length shows that relaminarization is effectively complete by $x = 960$ cm. This is close to the point of maximum acceleration and coincides with the point where the fully-turbulent prediction begins to show large discrepancies with the data. The dimensionless mixing length then shows a sharp increase indicating that transition back to turbulent flow occurs in the downstream section where the flow is subjected to zero pressure gradient. This result is consistent with the experimental results of Blackwelder and

Kovaszny (ref. 20). With regard to the predicted and experimental values of the skin friction coefficient it is of interest to note that the boundary layer is initially a fully-turbulent, zero pressure gradient boundary layer. At the initial value of the momentum thickness Reynolds number of 2500, the data correlation of Smith and Walker (ref. 21) would indicate that the skin friction coefficient should be close to 0.00315, a value in close agreement with the predicted value, but higher than that measured by Blackwelder and Kovaszny. Thus, some error in the experimental values of skin friction, which were determined by measurement of the velocity gradient in the viscous sublayer near the wall, may be present.

Predictions for sink-flows. - Jones and Launder (ref. 22) have made experimental measurements of sink-flow turbulent boundary layers which are of particular interest because they are the only turbulent boundary layers with varying free-stream velocity in which the characteristic turbulent and viscous length scales may develop at the same rate (ref. 23). In sink-flows the acceleration parameter, K , is constant and the momentum thickness Reynolds number and shape factor obtain approximately constant asymptotic values over a considerable streamwise distance. The velocity profiles also become similar once these asymptotic conditions are reached. Two predictions were made under conditions investigated by Jones and Launder (ref. 22) for $K = 1.5 \times 10^{-6}$ and $K = 2.5 \times 10^{-6}$. The theoretical predictions for a given value of K were carried out until a sensibly constant value of the momentum thickness Reynolds number was reached. Curves and experimental data taken from ref. 22 for the asymptotic values of momentum thickness Reynolds number and shape factor as a function of the acceleration parameter are shown in Fig. 9. The symbols represent data taken from five sources (refs. 24 through 28), all of which show relaminarization except for the data of Julien, et al. (ref. 26) taken in the Stanford tunnel. This discrepancy has been noted by Jones and Launder (ref. 22) who attribute it to the inability of the Stanford tunnel to produce high- K sink-flows because of no independent means of adjusting Reynolds number. However, an alternative possibility may be the presence of some turbulence generating mechanism. Because of the discrepancy, no comparisons between theoretical predictions and the Stanford data for high accelerating flows were made except for the Moretti heat transfer runs discussed subsequently. The triangular data points indicate the new data of Jones and Launder (ref. 22) and the flagged circles represent the asymptotic values obtained from the UARL prediction procedure. The theoretically predicted and the experimentally measured values of R_θ and H are in excellent agreement. A more stringent test of the theory is the comparison of the predicted and measured velocity profiles when the momentum thickness Reynolds number becomes constant. The predicted velocity profile for $K = 1.5 \times 10^{-6}$ is compared with the experimental data at three values of R_θ for the given value of K in Fig. 10. The agreement between the prediction and the data is quite good, particularly for the experimental profile at $R_\theta = 711$. Some discrepancy is evident for the other two experimental profiles in the vicinity of a normal distance Reynolds number of one.

Similar results are presented in Fig. 11 for $K = 2.5 \times 10^{-6}$. The comparisons are generally good at this higher value of K with discrepancies occurring again at a normal distance Reynolds number of one. The comparisons shown in Figs. 10 and 11 indicate that the UARL prediction procedure may not adequately allow for the thickening of the viscous sublayer, which is known to occur during strong acceleration.

Effect of acceleration on heat transfer. - Three comparisons between theoretical predictions and experimental data were made to determine how well the UARL procedure could predict the variation of Stanton number in a strongly accelerated flow. The three experimental cases which were used for comparison were measured by Moretti and Kays (ref. 29) and termed Runs 12, 41, and F-2. All three of these experimental cases were basically similar in that a constant velocity low-speed flow was first subject to a nearly step reduction in wall temperature. The flow was then allowed to undergo some thermal development before accelerations of varying strength were applied. In Run 12, the acceleration parameter increases sharply to a maximum K of 3.39×10^{-6} and then rapidly returns to zero. The comparison between the predicted and measured variation of Stanton number along with the wall temperature variation for Run 12 is shown in Fig. 12. The location of the initiation and end of the acceleration are indicated in the figure. Both the prediction using the UARL transition model and the experimental data indicate that there is no effect on the Stanton number until the dimensionless distance $\chi = 5.0$ is reached with good agreement to that point even though the acceleration was initiated at $\chi = 4.5$. At $\chi = 5.0$ the UARL prediction and the data indicate a sharp decline in Stanton number although the prediction gives a larger decrease than that experimentally observed. The fully-turbulent prediction shows no decrease. At $\chi = 5.5$ the data show an increase in Stanton number. This behavior also is predicted by the transitional theory, however, the predicted increase is somewhat delayed compared to the data. The variation of the dimensionless mixing length, also shown in Fig. 12, shows that effectively relaminarization occurs just past $\chi = 5.0$ and also indicates that the failure of the UARL prediction to follow the data once the pressure gradient is removed may be due to incomplete transition back to turbulent flow. However, on a qualitative basis, the prediction made using the UARL procedure shows significantly better results than the prediction made using fully-turbulent theory. Figure 13 shows similar results for Run 41. In Run 41 the maximum value of K is 1.84×10^{-6} and K is nearly constant at this value over the distance from $\chi = 4.0$ to $\chi = 5.0$. Again, qualitative agreement is shown between the data and the UARL predictions. However, although the data only indicate a slight degree of relaminarization, the theory indicates a strong relaminarization. Based upon the sink-flow

boundary layer results of Fig. 9, a flow subject to an acceleration parameter of 1.8×10^{-6} should show a significant relaminarization effect. Figure 14 then shows the results for Run F-2 where K reached a maximum value of 3.04×10^{-6} and was nearly constant from $\chi = 4.0$ to $\chi = 5.3$. Here, too, the prediction using the transition model shows qualitative agreement. From the results shown in Figs. 12 through 14 it is noted that although only qualitative predictions of Stanton number through the strongly accelerated regions are obtainable, the onset of the effect of acceleration is well predicted by the UARL procedure, whereas the fully-turbulent theory gives no indication of feeling the effect of acceleration.

CALCULATIONS FOR A QUIET TUNNEL

The quiet tunnel program currently being undertaken by NASA (ref. 16) uses a converging-diverging nozzle with an annular slot just upstream of the nozzle throat. The slot is used to remove the boundary layer which develops on the inlet duct and convergent nozzle section walls thus reducing the boundary layer thickness at the throat station. Predictions of the boundary layer behavior in the inlet duct and approach section of the NASA nozzle (convergent portion) were made to give an indication of the nozzle slot height required to remove the approaching boundary layer. A new boundary layer then develops from the edge of the slot and continues to grow as the flow moves downstream into the supersonic section of the nozzle. If the tunnel wall boundary layer in the supersonic portion of the nozzle undergoes transition and becomes turbulent, the acoustic radiation emanating from the boundary layer will dominate the transition process occurring on a model placed in the tunnel and result in the model transition measurements being tunnel dependent. Therefore, it is necessary to maintain a laminar boundary layer in the supersonic section of the nozzle as far downstream as possible. With these considerations in mind, a parametric study of the effects of free-stream turbulence, heat transfer, Reynolds number, acceleration and Mach number on the boundary layer development in the supersonic section was conducted to determine both if the boundary layer developing in supersonic regions of the contemplated NASA tunnel would remain laminar and how varying various parameters would effect the transition location. As a portion of these parametric studies, inviscid flow pressure distributions were computed for various nozzle geometries to facilitate the calculations of Mach number and acceleration effects. In addition, transonic and supersonic inviscid flow computations were made for the nozzle geometry specified by NASA to compare with the pressure distribution supplied by NASA in these regions of the nozzle.

Inviscid Flow Calculations

Pressure distribution in the transonic section of the NASA nozzle. -

Although pressure distributions were supplied by NASA for the transonic and supersonic sections of the NASA nozzle, several inviscid flow field predictions were made for NASA specified nozzle geometry using United Aircraft Corporation inviscid computer codes. The calculations were made at NASA's request to compare the inviscid flow predictions made using UAC codes with the predictions made using NASA codes. The nozzle coordinates and pressure distribution supplied by NASA are given in TABLE I. Transonic flow field computations were performed using the UAC SUB code (ref. 30). The present version of the SUB code cannot account directly for the presence of the slot in the nozzle wall, thus, two predictions of the transonic flow region were made each modifying

the approach section nozzle wall to represent the slot. Since the computation of the inviscid flow field in the supersonic section of the nozzle is dependent on the Mach number and pressure distributions predicted from the SUB code in the region of the sonic line, the location of the resulting sonic lines from the two predictions were then compared to determine how sensitive the sonic line was to changes in the upstream geometry.

The first prediction was made for a nozzle in which the slot lip was smoothly faired into the approach section nozzle wall. The predicted streamlines and sonic line for this contour, referred to as contour "A", are shown in Fig. 15. The broken line indicates the original NASA contour and the heavy solid line indicates the contour used in the computation. The NASA contour and contour "A" are identical downstream of the slot. The second computation was made for an approach section outer contour which corresponds to the estimated stagnation streamline which divides the flow passing through the nozzle throat from that passing through the slot. The coordinates of this streamline were obtained by mass conservation of the flow through the sonic slot. The predicted streamlines and sonic line for this contour, referred to as contour "B", are shown in Fig. 16. Downstream of the slot contour "B" is also identical to the NASA contour. An enlarged comparison of the sonic lines predicted using contours "A" and "B" presented in Fig. 17 shows that the effect of the modifications to the nozzle wall does not affect significantly either the shape or location of the sonic line. A comparison between the wall pressure distribution, normalized by stagnation pressure, predicted using contours "A" and "B" and the NASA distribution is shown in Fig. 18. The pressure distributions for contours "A" and "B", and the NASA pressure distribution show only small differences in the upstream region between $\chi = -3.0$ and $\chi = -0.5$ and the distributions are nearly identical in the throat region between $\chi = -0.5$ and $\chi = 0.0$. The pressure distributions downstream of the throat predicted for both contours "A" and "B" are slightly different from the NASA distribution. Furthermore, the NASA distribution shows a small discontinuity in slope at $\chi = 0.350$ which does not appear in either UAC calculation. It should be pointed out that the NASA pressure distribution was calculated using the theory of Hopkins and Hill (ref. 31) from $\chi = -0.90$ to $\chi = 0.294$ and using the method of characteristics downstream of $\chi = 0.294$. Thus, the apparent discontinuity of slope in the NASA pressure distribution may be the result of slightly incompatible initial conditions for the method of characteristics computation.

Pressure distributions in the supersonic section of the nozzle. - A computation of the flow field in the supersonic section of the NASA nozzle was made using the UAC SUPER code (ref. 32) with initial Mach number and pressure distributions obtained from the SUB code along a plane perpendicular to the nozzle axis at $\chi = 0.25$. The predicted wall pressure distribution, shown in Fig. 19, is in excellent agreement with the NASA pressure distribution. The predicted flow field contains no expansion fans or shocks and the predicted

exit plane Mach number is close to uniform with a maximum of 4.98 at the centerline and a minimum of 4.93 at the nozzle wall. Figure 20 shows an enlarged comparison between pressure distributions in the vicinity of the throat as predicted by the SUB and SUPER codes, and that specified by NASA. All three pressure distributions show good agreement. The SUPER prediction fares smoothly into the prediction made using the SUB code at $\chi = 0.25$. The SUPER prediction initially gives slightly higher values of wall pressure ratio than the NASA prediction, however, by $\chi = 0.5$ both distributions are in good agreement. Neither the SUB prediction, nor the combined SUB-SUPER prediction exhibit the discontinuities of slope observed in the NASA pressure distribution.

Inviscid calculations for acceleration and Mach number effects. - Several additional inviscid flow field calculations were made using the UAC Perfect Nozzle code to obtain pressure distributions to be used in boundary layer calculations showing the effect of acceleration and the effect of Mach number. The Perfect Nozzle code generates the coordinates and pressure distribution of a sharp corner throat bell nozzle with a uniform exit Mach number for a specified throat-to-exit area ratio. Nozzle contours and pressure distributions were computed for area ratios corresponding to exit Mach numbers of 4.1, 5.0, and 6.0. The resulting wall pressure distributions for these nozzles are shown in Fig. 21.

Viscous Flow Calculations

Boundary layers in subsonic portion of NASA nozzle. - Calculations of the boundary layer flow field on the inlet duct and nozzle approach section walls of the NASA nozzle were carried out using the pressure distribution specified by NASA given in TABLE II, with a wall temperature of 65.5 deg C (150 deg F), a free-stream temperature of 104.4 deg C (220 deg F), and a total pressure of 10.2 atm (150 psia). The inlet duct extends from $\chi = -6.91$ to $\chi = -0.911$ and the approach section extends from $\chi = -0.911$ to $\chi = -0.023$ where $\chi = x/L_{ref}$ and L_{ref} is taken as 30.5 cm (12 in.). Calculations performed for free-stream turbulence levels of 0.18 and 1.0 percent based on a reference velocity of approximately 1176 cm per sec (40 ft per sec) were initiated from an assumed stagnation point at the upstream end of the inlet duct. These turbulence levels correspond to 1 and 6 percent based on the actual initial velocity in the inlet duct of 213 cm per sec (7 ft per sec). Transition from laminar to turbulent flow was predicted to occur in the inlet duct well upstream of the approach section of the nozzle for both turbulence levels. The predicted boundary layer behavior in the approach section of the nozzle downstream of the inlet duct is shown in Figs. 22 through 24 where the boundary layer thicknesses are nondimensionalized with respect to the nozzle throat radius of 1.27 cm (0.5 in.). In the nozzle approach section the boundary layer thickness decreases continuously under the influence of the strong favorable pressure

gradient for both turbulence levels, as shown in Fig. 22. The distribution of the dimensionless mixing length, also shown in Fig. 22, indicates that for 1.0 percent free-stream turbulence relaminarization of the boundary layer is initiated at $\chi = -0.65$ and is nearly complete at $\chi = -0.4$. The mixing length distribution predicted for 6.0 percent free-stream turbulence indicates that relaminarization is completed over a longer distance being initiated at $\chi = -0.67$ and showing effectively complete relaminarization by $\chi = -0.3$. However, for both turbulence levels the boundary layer is laminar at the throat. The momentum thickness also decreases continuously for both levels of turbulence as the throat is approached, as shown in Fig. 23. The behavior of the boundary layer thickness near the throat of the nozzle is shown on an enlarged scale in Fig. 24 with an indication of the location and height of the slot. As can be seen in this figure, the predicted boundary layer thickness is almost identical to the slot height, thus indicating that the slot is large enough to remove the entire velocity boundary layer.

Boundary layer downstream of the slot in the NASA nozzle. - Predictions of the boundary layer development in the transonic and supersonic section of the NASA nozzle were made for free-stream turbulence levels of 1, 3, and 6 percent based on a reference velocity of 1176 cm per sec (40 ft per sec). The results of these calculations, which were initiated at the slot with a negligible displacement thickness ($\delta^* = 0.000254$ cm = 0.0001 in.), are presented in Figs. 25 through 27. The flow conditions are indicated on the figures. In Figs. 25 through 27, as well as all the figures which follow, the boundary layer thicknesses are normalized by the nozzle throat radius $r_t = 1.27$ cm (0.5 in.) and axial distances are nondimensionalized by the reference length $L_{ref} = 30.5$ cm (12 in.). The acceleration parameter, shown in Fig. 25, has a maximum value of 1.53×10^{-6} at the slot and decreases continuously through the throat. At an axial distance of $\chi = 0.1$, the acceleration parameter has dropped to less than 10 percent of its maximum value and between $\chi = 0.1$ and the exit of the nozzle, at $\chi = 1.289$, K decreases almost linearly to a value of 0.03×10^{-6} .

The incompressible shape factor, H^* , i.e., the locally evaluated shape factor obtained from the incompressible definitions of momentum and displacement thicknesses, is also presented in Fig. 25. The incompressible shape factor is presented rather than the true shape factor since it more satisfactorily indicates the laminar or turbulent state of the boundary layer when density gradients across the boundary layer are significant. For the 1 percent turbulence level H^* decreases sharply under the influence of the strong acceleration in the throat region. As the acceleration is relaxed, the incompressible shape factor increases to a relatively constant value of about 2.5 indicating a laminar boundary layer for the entire nozzle length. For the 6 percent turbulence level H^* shows the same initial trend, but near $\chi = 0.1$ H^* drops to a constant value of 1.4 which indicates that the boundary layer has

undergone transition to turbulent flow. This behavior is also observed at $\chi = 0.2$ for 3 percent free-stream turbulence. The streamwise variations of the momentum thickness and the compressible shape factor are shown for the three levels of free-stream turbulence in Fig. 26. For the higher free-stream turbulence levels the turbulent nature of the boundary layer is indicated by the more rapid growth of the momentum thickness. Finally, the variations of the dimensionless mixing and boundary layer thicknesses are shown in Fig. 27. The variation of the dimensionless mixing length shows that the boundary layer remains laminar for the 1 percent turbulence level. The sharp rise to nearly constant values of 0.11 for the higher turbulence levels indicates the rapid transition to a turbulent boundary layer in the presence of the higher free-stream turbulence.

Parametric Variation in the Supersonic Portion of the Nozzle

Effect of heat transfer. - Since wall cooling is known to have a stabilizing effect for a constant pressure boundary layer, it may also be expected to maintain a laminar boundary layer in a nozzle where large favorable pressure gradients are present. Thus, predictions of the effect of wall cooling on the boundary layer in the NASA nozzle were made for wall temperatures of -17.8 deg C (0 deg F) and -73.3 deg C (-100 deg F) for turbulence levels of 1 and 3 percent. The results of the calculations made for 1 percent free-stream turbulence are compared with predictions made for an adiabatic wall in Figs. 28 through 30. These comparisons indicate that for this low value of free-stream turbulence wall cooling promotes earlier boundary layer transition as can be seen in the plots of incompressible shape factor, presented in Fig. 28, momentum thickness, shown in Fig. 29, and dimensionless mixing length, shown in Fig. 30. Predictions made for the same wall temperatures and flow conditions with a free-stream turbulence level of 3 percent are presented in Figs. 31 through 33. The predicted variations of incompressible shape factor, momentum thickness, and mixing length indicate that for this higher turbulence level wall cooling has little effect on the location of transition.

The apparent discrepancy of the prediction of wall cooling promoting transition can be explained by citing the dual role of wall cooling in the presence of a pressure gradient. In the absence of wall roughness and pressure gradients, wall cooling stabilizes the boundary layer retarding transition. However, in the presence of a favorable pressure gradient this direct stabilizing effect is offset by the destabilizing effect resulting from the reduction of the acceleration parameter, K , as is shown in Figs. 28 and 31. This reduction of the acceleration parameter is due solely to the reduction of the kinematic viscosity near the wall. It appears that this dual effect of wall cooling may either enhance or inhibit transition depending upon whether the

direct stabilizing effect of wall cooling is greater or less than the indirect destabilizing effect of the reduced acceleration parameter. Since the transition point varied with wall temperature for the case of 1 percent free-stream turbulence while showing relative insensitivity to wall temperature at a 3 percent free-stream turbulence, the integrated effects of wall cooling could be, and apparently were, different for the two different turbulence levels. The important observation is that in the presence of a favorable pressure gradient wall cooling may not necessarily inhibit transition.

Effect of Reynolds number. - The effect of variation of the free-stream unit Reynolds number on the boundary layer development in the transonic and supersonic sections of the NASA nozzle was achieved by varying the nozzle stagnation pressure; the variation of stagnation pressure then being reflected in the value of the kinematic viscosity. The results of the calculations, which were performed for stagnation pressures of 5.1, 10.2, and 25.5 atm (75, 150, and 375 psia), are shown in Figs. 34 through 36. All calculations were made for a free-stream turbulence level of 1 percent. The calculation made using a stagnation pressure of 5.1 atm (75 psia) corresponds to a low Reynolds number case, whereas the 25.5 atm (375 psia) stagnation pressure calculation represents a higher Reynolds number. Within this range of stagnation pressure the free-stream unit Reynolds number at a given axial location varies by a factor of 5 between the three calculations. The variation of the incompressible shape factor, shown in Fig. 34, indicates that for both the low (5.1 atm (75 psia)) and intermediate (10.2 atm (150 psia)) values of Reynolds number a laminar boundary layer is maintained for the entire length of the nozzle; however, the higher Reynolds number prediction shows that the boundary layer undergoes transition from laminar to turbulent slightly downstream of the throat. The acceleration parameter, also shown in Fig. 34, shows substantial variation with Reynolds number. This is a direct result of the variation of the kinematic viscosity. The variation of the momentum thickness and compressible shape factor along the nozzle are shown in Fig. 35. These results again indicate the laminar state of the boundary layer for both low and intermediate Reynolds numbers. It is also noted that the predicted variation of the momentum thickness with axial distance for low and intermediate Reynolds numbers, and for the higher Reynolds number prediction prior to transition, is consistent with the usual laminar boundary layer theory; the momentum thickness grows more rapidly for lower Reynolds numbers. Finally, the variation of the dimensionless mixing length and the boundary layer thickness is shown in Fig. 36. The variation of the dimensionless mixing length indicates that transition occurs only for the higher Reynolds number prediction.

Effect of acceleration. - Calculations were made to determine the effect of varying the acceleration parameter upon the boundary layer development. The calculations were made using the pressure distribution obtained from the Perfect Nozzle deck for a Mach 5 exit sharp corner throat, shown in Fig. 21. The sharp corner throat represents a zero radius of curvature and gives the

greatest possible wall pressure gradient in the throat region. The resulting nozzle geometry generated by the UAC Perfect Nozzle deck differed from the NASA nozzle primarily in the region of the throat leading to different static pressure distributions. The effects of this variation of the nozzle geometry on the acceleration parameter, incompressible shape factor, and momentum thickness are shown in Fig. 37 where they are compared with the values predicted for the specified NASA nozzle geometry. The calculations for the sharp corner throat nozzle were initiated at the throat with a displacement thickness equal to that at the throat of the NASA nozzle. The acceleration parameter for the sharp cornered throat nozzle only differed slightly from that of the NASA nozzle, as shown in Fig. 37. The slight difference in acceleration parameter did not lead to any significant difference in boundary layer development, as shown in Figs. 37 and 38. The major differences between the two calculations were in the throat region where differences were predicted in the incompressible shape factor.

Effect of exit Mach number. - The effect of variation of the nozzle exit Mach number was studied by making boundary layer predictions for the pressure distributions shown in Fig. 21 for exit Mach numbers of 4.1, 5, and 6. The pressure distributions are for nozzles having sharp corner throats and uniform exit flow. The predictions were initiated at the nozzle throat with a displacement thickness equal to that predicted for the NASA nozzle with a free-stream turbulence of 1 percent. The predicted variations of acceleration parameter, incompressible shape factor, and momentum thickness are compared in Fig. 39. The variation of the acceleration parameter shows that there is very little effect due to exit Mach number in the throat region; however, the characteristic linear decrease in acceleration parameter downstream of the throat shows that as the exit Mach number is increased, the acceleration parameter decreases more slowly. The variation of the incompressible shape factor shows a drop near the throat and then an increase to a relatively constant value of 2.5 in the Mach 5.0 and Mach 6.0 nozzles while continually increasing to a value of 2.7 in the Mach 4.1 nozzle. These variations of the incompressible shape factor, as well as the smooth continuous rise in momentum thickness, indicate that a laminar boundary layer is maintained for the entire length of all three nozzles. The variations of the compressible shape factor, dimensionless mixing length, and boundary layer thickness are shown in Fig. 40. The variation of the dimensionless mixing length indicates the laminar state of the predicted boundary layers. It is interesting to note that, although still small, the value of the dimensionless mixing length at the nozzle exit shows a trend of increasing with exit Mach number. This trend is probably due, at least in part, to the longer distance over which the boundary layer develops in higher Mach number nozzles.

DISCUSSION

The inconsistencies found when attempting to correlate transition data from several supersonic wind tunnels (refs. 3 and 4) and the evidence that the cause of these inconsistencies is the aerodynamic noise radiating from the tunnel wall turbulent boundary layer clearly indicates the need for a quiet supersonic wind tunnel. In addition, a recent investigation by McDonald and Kreskovsky (ref. 33) shows that the level of free-stream turbulence can significantly alter the structure of even fully-turbulent boundary layers and since the fluctuating pressure associated with an acoustic disturbance can be easily related to a fluctuating velocity (ref. 15), it is reasonable to assume that the varying magnitude of aerodynamic noise found in different tunnels could effect the fully-turbulent boundary layer development as well as transition location. Therefore, to aid in the design of a quiet tunnel, a parametric study of boundary layers in supersonic nozzles has been conducted in this investigation.

Prior to performing the parametric study it was necessary to ascertain that the boundary layer prediction procedure used would give accurate predictions of relaminarizing flows. Comparisons of theoretical predictions of momentum thickness and shape factor with the supersonic data of Nash-Webber (ref. 6) and the low-speed experimental data of Blackwelder and Kovasznay (ref. 20) were very good. However, comparison between theoretical predictions of skin friction and the data of ref. 20, although showing qualitative agreement, showed quantitative discrepancies. Similarly, comparisons between theory and experiment for sink-flow boundary layer shape factors and momentum thicknesses were very good, however, comparisons of velocity profiles, although very good in the outer region, showed discrepancies in the wall region. Finally, predictions of Stanton number through relaminarization (when compared with the data of Moretti and Kays (ref. 29)) indicate that the onset of the effect of acceleration is accurately predicted although the actual variation of Stanton number through relaminarization is somewhat overpredicted. Thus, in general, the theory predicts the initiation of relaminarization and the variation of integral thicknesses through relaminarization very well. Comparisons between theory and experiment for skin friction and Stanton number, although showing qualitative agreement, show quantitative discrepancies. However, as discussed in the Comparison section, neither skin friction nor Stanton number data are completely reliable and in any event present a much more difficult measurement task than the mean flow or integral thicknesses.

The subsequent calculations made for the quiet tunnel study indicate that, perhaps not surprisingly, transition from laminar to turbulent flow is sensitive to the level of free-stream disturbance (see Figs. 25 through 27); a laminar boundary layer being maintained only for the lowest turbulence level prediction. With regard to the effect of wall cooling, it was found (see Figs. 28 through 33) that a destabilizing effect may result from wall cooling in the

presence of favorable pressure gradients. A possible explanation for this result is the dual role played by wall cooling in the presence of a favorable pressure gradient, the direct stabilizing effect and the destabilizing effect of reduction of the acceleration parameter. Predictions of the effect of Reynolds number indicate that, as one would expect, increasing Reynolds number promotes transition (Figs. 34 through 36). Predictions of the effect of variation of the pressure gradient (via variation of nozzle geometry) show only slight differences for the geometries examined (see Figs. 37 and 38). A significant variation of the pressure distribution in the supersonic section of the nozzle cannot be achieved since the major portion of the potential energy associated with the flow is converted to kinetic energy in the transonic region near the throat. Finally, calculations made for the effect of Mach number show that laminar boundary layers may be maintained for the entire nozzle length for nozzles with exit Mach number of at least 6.0 for low free-stream turbulence levels (see Figs. 39 and 40).

CONCLUSIONS

Conclusions Regarding the Assessment of the UARL Boundary Layer Prediction Procedure

1. The UARL boundary layer prediction procedure, previously shown by McDonald and Fish to account for the influence of such items as free-stream turbulence and wall roughness upon the transition from laminar to turbulent flow in a zero pressure gradient boundary layer, has been shown in the present study also to account for the movement of the transition region due to moderate pressure gradients.
2. The UARL procedure was also found to accurately predict the variation of boundary layer integral parameters in an initially turbulent boundary layer subject to large accelerations in both low-speed and supersonic flows.
3. The UARL procedure apparently predicts the onset of the effect of strong acceleration on wall-dominated properties such as Stanton number. However, the variation of wall-dominated properties in boundary layers undergoing relaminarization is in only qualitative agreement with presently available data.

Conclusions Regarding the Quiet Tunnel

1. The predicted boundary layer in the approach section of the NASA nozzle effectively relaminarizes for free-stream turbulence levels as high as 6 percent based upon an inlet velocity of 213 cm per sec (7 ft per sec).
2. The predicted boundary layer thickness at the slot is approximately equal to the slot height.
3. It should be possible to maintain a laminar boundary layer for the full length of the NASA nozzle with adiabatic walls, provided that the free-stream turbulence level is of the order of 6 percent or less in the approach section based upon a mean velocity of 213 cm per sec (7 ft per sec).
4. The predicted effect of wall cooling promotes early transition at 1 percent free-stream turbulence but shows little effect on transition location at 3 percent free-stream turbulence.

5. Transition is predicted to occur earlier with higher free-stream unit Reynolds number.

6. Variation of the acceleration parameter downstream of the nozzle throat could not be increased significantly by changes in geometry and only insignificant effects of the resulting changes in acceleration were observed on the boundary layer.

7. The indications are that a laminar boundary layer may be maintained in nozzles with exit Mach numbers as high as 6.0.

APPENDIX A

The Basic Equations

Within the framework of boundary layer theory, various authors (for example, Schubauer and Tchen (ref. 34)) have reduced the time-averaged Navier-Stokes equations to the compressible boundary layer equations of motion. For two-dimensional or axisymmetric flows, steady in the mean, the boundary layer approximations to the momentum, energy, and continuity equation become

$$\bar{\rho} \bar{u} \frac{\partial \bar{u}}{\partial x} + \bar{\rho} \bar{v} \frac{\partial \bar{u}}{\partial y} = - \frac{d\bar{P}}{dx} + \frac{\partial \tau}{\partial y} \quad (\text{A-1})$$

$$\bar{\rho} \bar{u} C_p \frac{\partial \bar{T}^o}{\partial x} + \bar{\rho} \bar{v} C_p \frac{\partial \bar{T}^o}{\partial y} = \frac{\partial}{\partial y} (Q + \bar{u} \tau) \quad (\text{A-2})$$

$$\frac{\partial \bar{\rho} \bar{u} r^\alpha}{\partial x} + \frac{\partial \bar{\rho} \bar{v} r^\alpha}{\partial y} = 0 \quad (\text{A-3})$$

where x and y are coordinates in the streamwise and transverse directions, u and v are velocity components in the x and y directions, ρ is density, P is pressure, C_p is specific heat, T^o is total temperature, r is the radius of curvature for an axisymmetric body, and the exponent α is zero for two-dimensional flows and unity for axisymmetric flows. The effective shear stress, τ , and the effective heat transfer, Q , are defined as

$$\tau = \bar{\mu} \frac{\partial \bar{u}}{\partial y} - \bar{\rho} \overline{u'v'} \quad (\text{A-4})$$

$$Q = \bar{k} \frac{\partial \bar{T}}{\partial y} - \bar{\rho} C_p \overline{v'T'} \quad (\text{A-5})$$

where μ is viscosity, k is thermal conductivity, T is static temperature. In Eqs. (A-1) through (A-5) overbars indicate averaged quantities and primes indicate fluctuating quantities. The equations are valid for laminar, transitional, or turbulent flows; obviously, for laminar flows the primed quantities are zero. For turbulent and transitional boundary layers it is convenient to represent the contribution of the apparent turbulent stress, τ_T , to the total shear stress, τ , by an effective turbulent viscosity, ν_T , and similarly the turbulent contribution to the total heat flux, Q , is represented conveniently by an effective turbulent conductivity, k_T , such that

$$\bar{\rho} \nu_T \frac{\partial \bar{u}}{\partial y} = - \bar{\rho} \overline{u'v'} \quad (\text{A-6})$$

$$k_T \frac{\partial \bar{T}}{\partial y} = - \bar{\rho} c_p \overline{v'T'} \quad (\text{A-7})$$

The turbulent conductivity, k_T , is related to the turbulent viscosity, ν_T , by a turbulent Prandtl number, Pr_T , defined as

$$Pr_T = \bar{\rho} c_p \nu_T / k_T \quad (\text{A-8})$$

and the boundary layer momentum and energy equations, Eqs. (A-1) and (A-2), become

$$\bar{\rho} \bar{u} \frac{\partial \bar{u}}{\partial x} + \bar{\rho} \bar{v} \frac{\partial \bar{u}}{\partial y} = - \frac{\partial \bar{P}}{\partial x} + \frac{\partial}{\partial y} \left\{ (\bar{\mu} + \bar{\rho} \nu_T) \frac{\partial \bar{u}}{\partial y} \right\} \quad (\text{A-9})$$

$$\begin{aligned} \bar{\rho} \bar{u} c_p \frac{\partial \bar{T}^o}{\partial x} + \bar{\rho} \bar{v} c_p \frac{\partial \bar{T}^o}{\partial y} = \frac{\partial}{\partial y} \left\{ \left(\frac{\bar{\mu}}{Pr} + \frac{\bar{\rho} \nu_T}{Pr_T} \right) c_p \frac{\partial \bar{T}^o}{\partial y} \right\} \\ + \frac{\partial}{\partial y} \left\{ \left[\left(1 - \frac{1}{Pr} \right) \bar{\mu} + \left(1 - \frac{1}{Pr_T} \right) \bar{\rho} \nu_T \right] \bar{u} \frac{\partial \bar{u}}{\partial y} \right\} \end{aligned} \quad (\text{A-10})$$

In deriving Eq. (A-10) use has been made of the definition of total temperature

$$\tau^o = \tau + \frac{u^2}{2Cp} \quad (A-11)$$

With the flow laminar, Eqs. (A-3), (A-9), and (A-10) are solved with $v_T = 0$ to determine the boundary layer development. If the flow is transitional or turbulent, it is necessary to model v_T and Pr_T . The specification of the turbulent viscosity, v_T , and the turbulent Prandtl number, Pr_T , is carried out through the turbulence model described in detail in the subsequent section.

After specification of the turbulent viscosity and Prandtl number, Eqs. (A-3), (A-9), and (A-10) are solved by first eliminating $\bar{\rho v}$ from the momentum and energy equations by application of the continuity equation. When the streamwise static pressure distribution, $P(x)$, is specified, the momentum and energy equations, in conjunction with an equation of state and equations governing v_T and Pr_T , form a closed set of nonlinear, parabolic, partial differential equations, which can be solved upon specification of boundary conditions. The wall and free-stream boundary conditions employed in the solution are given by:

at the wall $y = 0$

$$\bar{\rho v} = (\bar{\rho v})_w, u = 0, \bar{T}^o = T_w \text{ or } \frac{\partial T}{\partial y} = 0 \quad (A-12)$$

at the free-stream, $y \rightarrow \infty$

$$\bar{\rho u} = \bar{\rho}_\infty \bar{u}_\infty, \bar{T}^o = \bar{T}_\infty^o \quad (A-13)$$

Details of the solution procedure are presented in ref. 15.

The Turbulence Model

Fully-developed turbulence model. - The fully-developed turbulence model originally presented by McDonald and Camarata (ref. 11) for two-dimensional incompressible flow, forms the basis for the transitional turbulence model used in the McDonald-Fish transitional boundary layer theory and, therefore, at this juncture it is useful to describe the model in some detail. The fully-developed turbulence model, which is described in greater detail in ref. 14, is based

upon a solution of the turbulence kinetic energy equation. The turbulence kinetic energy equation is a conservation equation derived from the Navier-Stokes equations by writing the instantaneous quantities as a sum of mean and fluctuating parts. The i^{th} Navier-Stokes momentum conservation equation ($i = 1, 2, 3$, referring to the three coordinate directions) is multiplied by the i^{th} component of fluctuating velocity and the average of the resulting three equations is taken. The three averaged equations are summed to obtain the turbulence kinetic energy equation. The derivation of the turbulence kinetic energy equation has been given by Favre (ref. 35) for compressible flow and approximated by Bradshaw and Ferris (ref. 10) to boundary layer flows; a derivation and discussion of the turbulence kinetic energy equation used in the present theory is given in ref. 15.

As shown in ref. 15, the boundary layer approximation to the turbulence kinetic energy equation is given by

$$\begin{aligned}
 & \frac{\partial}{\partial x} \left(\frac{1}{2} \bar{\rho} \bar{u} \bar{q}^2 \right) + \frac{\partial}{\partial y} \left(\frac{1}{2} \bar{\rho} \bar{v} \bar{q}^2 \right) = -\bar{\rho} \overline{u'v'} \frac{\partial \bar{u}}{\partial y} \\
 & \text{advection} \qquad \qquad \qquad \qquad \qquad \qquad \qquad \qquad \qquad \text{production} \\
 & - \frac{\partial}{\partial y} \left(\overline{P'v'} + \frac{1}{2} \overline{(\rho v)'} \bar{q}^2 \right) - \bar{\rho} \epsilon \\
 & \text{diffusion} \qquad \qquad \qquad \qquad \qquad \qquad \qquad \qquad \qquad \text{dissipation} \\
 & - \bar{\rho} \overline{(u'^2 - v'^2)} \frac{\partial \bar{u}}{\partial x} + \overline{\rho' \frac{\partial u'_i}{\partial x_i}} \\
 & \text{normal stress production} \qquad \qquad \qquad \text{pressure-dilatation}
 \end{aligned} \tag{A-14}$$

All calculations reported in the investigation were made with the usual assumption of zero pressure-dilatation contribution to the energy balance (ref. 10). The turbulence model is developed by integrating Eq. (A-14) with respect to y between the limits $y = 0$ and $y = \delta$ which leads to

$$\begin{aligned}
 \frac{1}{2} \frac{d}{dx} \int_0^\delta \bar{\rho} \bar{u} \bar{q}^2 dy &= \int_0^\delta -\bar{\rho} \overline{u'v'} \frac{\partial \bar{u}}{\partial y} dy - \int_0^\delta \bar{\rho} \epsilon dy \\
 - \int_0^\delta \bar{\rho} \overline{(u'^2 - v'^2)} \frac{\partial \bar{u}}{\partial x} dy &+ \int_0^\delta \overline{\rho' \frac{\partial u'_i}{\partial x_i}} dy + E
 \end{aligned} \tag{A-15}$$

where

$$E = \left[\frac{1}{2} \bar{q}^2 \left(\bar{\rho} \bar{u} \frac{\partial \delta}{\partial x} - \bar{\rho} \bar{v} \right) - \overline{P'v'} + \frac{1}{2} \overline{(\rho v)'} \bar{q}^2 \right]_e \tag{A-16}$$

Following Townsend (ref. 36) and Bradshaw and Ferris (ref. 10) structural coefficients a_1 and L are introduced, together with a mixing length l ; these scales are defined as

$$\begin{aligned} \overline{u'v'} &= a_1 \overline{q^2}, \quad \overline{u'^2} = a_2 \overline{q^2}, \quad \overline{v'^2} = a_3 \overline{q^2}, \\ \overline{w'^2} &= (1 - a_2 - a_3) \overline{q^2} \end{aligned} \quad (\text{A-17})$$

$$\epsilon = (\overline{u'v'})^{3/2} / L, \quad (\overline{u'v'})^{1/2} = l \frac{\partial \bar{u}}{\partial y}$$

For fully-developed turbulence the structural coefficients a_1 , a_2 , and a_3 are assumed constant having values 0.15, 0.50, and 0.20, respectively (refs. 11 and 37). As is discussed subsequently, a_1 becomes a variable in the transitional regime. Using Eq. (A-17), Eq. (A-16) is put in the form

$$\frac{d}{dx} \left(\frac{\phi_1 \rho_e u_e^3 \delta^+}{2a_1} \right) = \rho_e u_e^3 \left(\phi_2 - \phi_3 + \frac{E}{\rho_e u_e^3} \right) + \int_0^\delta \overline{\rho' \frac{\partial u_i'}{\partial x_i}} dy \quad (\text{A-18})$$

where

$$\phi_1 = \int_0^{\delta/\delta^+} \frac{\bar{\rho} \bar{u}}{\rho_e u_e} \left(\frac{l}{\delta^+} \frac{\partial \bar{u}/u_e}{\partial \eta} \right)^2 d\eta \quad (\text{A-19})$$

$$\phi_2 = \int_0^{\delta/\delta^+} \frac{\bar{\rho}}{\rho_e} \left(\frac{l}{\delta^+} \right)^2 \left(\frac{\partial \bar{u}/u_e}{\partial \eta} \right)^3 \left(1 - \frac{l}{L} \right) d\eta \quad (\text{A-20})$$

$$\phi_3 = \int_0^{\delta/\delta^+} \frac{\bar{\rho}}{\rho_e} \left(\frac{a_2 - a_3}{a_1} \right) \left(\frac{l}{\delta^+} \frac{\partial \bar{u}/u_e}{\partial \eta} \right)^2 \frac{\delta}{u_e} \frac{\partial \bar{u}}{\partial x} d\eta \quad (\text{A-21})$$

where η is a nondimensional transverse distance y/δ^+ , δ^+ is an arbitrary reference length, and δ the boundary layer thickness.

The left-hand side of Eq. (A-18) represents the streamwise rate of change of turbulence kinetic energy and is derived directly from the turbulence kinetic energy advection term. The term $\rho_e U_e^3 \phi_2$ represents the integral of turbulence production minus dissipation and $\rho_e U_e^3 \phi_3$ is the normal stress production. The terms designated by E are turbulent source terms resulting from disturbances imposed upon the boundary layer by the free stream. As shown in Eq. (A-16), E is the sum of two major contributions the first, $(q^2/2)(\bar{\rho} u \partial \delta / \partial x - \bar{\rho} v)$ representing the free-stream velocity disturbance (i.e., free-stream turbulence entrained by the boundary layer) and the second, $-P'v' + (\rho v)' q^2/2$, representing the direct absorption of acoustic energy. In subsonic and moderately supersonic flows the acoustic source term is negligible compared to the free-stream turbulent velocity disturbance. At higher Mach numbers the acoustic term may become the dominant source and, as indicated by Pate and Schueler (ref. 3), the acoustic disturbance is the dominating disturbance in high Mach number wind tunnels having turbulent tunnel wall boundary layers. In the present investigation of the NASA pilot model quiet wind tunnel it is the tunnel wall boundary layer itself which is under investigation and when this is laminar there is not expected to be an acoustic disturbance source. Thus, in the present calculation for the tunnel wall boundary layers the acoustic disturbance has been assumed negligible.

For fully-developed turbulent flow, as in ref. 11, L and l are given by

$$\frac{L}{\delta} = 0.1 \tanh \left[\kappa y / (0.1 \delta) \right] \quad (\text{A-22})$$

$$\frac{l}{\delta} = \frac{l_\infty}{\delta} \tanh \left[\kappa y / l_\infty \right] \quad (\text{A-23})$$

where l_∞ is the "wake" value of the mixing length at any particular streamwise station. Although Eqs. (A-22) and (A-23) give accurate representations of L and l through most of the turbulent boundary layer, it is well-known that they overestimate the length scales within the viscous sublayer and are somewhat inaccurate at low Reynolds numbers. Following McDonald and Fish (ref. 14) the experimentally observed damping effect in the viscous sublayer is modeled by assuming intermittent turbulence within the sublayer leading to the relation

$$\overline{-u'v'} = \Gamma \overline{(-u'v')}_{\tau} = \Gamma (\ell \partial \bar{u} / \partial y)_{\tau}^2 = \left(\mathcal{D} \ell_{\tau} \frac{\partial \bar{u}}{\partial y} \right)^2 \quad (\text{A-24})$$

In Eq. (A-24) Γ is the intermittency factor, \mathcal{D} the damping factor, and the subscript T indicates the value with turbulent flow. Obviously, \mathcal{D} is equal to the square root of Γ . As in ref. 14, the present investigation assumes that the damping distributes normally about mean height y^+ ($y^+ = y\sqrt{\tau/\rho\nu}$) with a standard deviation σ leading to the equation

$$\mathcal{D} = P^{1/2} \{ (y^+ - \bar{y}^+) / \sigma \} \quad (\text{A-25})$$

where P is the normal probability function; y^+ is taken as 23, and σ as 8. A detailed discussion of the sublayer damping treatment is presented in ref. 14. In the present calculations the von Karman constant K was taken to be 0.43.

In regard to the low Reynolds number effects, Coles (ref. 38) has observed and correlated the departure of the mean velocity profile of a flat plate turbulent boundary layer from the usual similarity laws known to hold at higher Reynolds numbers. Using Coles' correlation of the mean velocity profile in the low Reynolds number regime, McDonald (ref. 39) integrated the boundary layer equations of mean motion to obtain local distributions of turbulent shear stress and evaluated the local mixing length distributions from the assumed mean velocity distribution and the computed shear stress distributions. Based upon these calculations, a low Reynolds number correction for the dissipation length of the form

$$L = L_{\infty} \left[1 + \exp(-1.63 \ln R_{\theta} + 9.7) \right] \quad (\text{A-26})$$

was derived where L_{∞}/δ is given by Eq. (A-22). In the calculations presented in the present report the dissipation length used was obtained by multiplying Eq. (A-26) by the sublayer damping factor \mathcal{D} .

When numerical values of the structural coefficients a_n are specified, Eqs. (A-22), (A-23), (A-25), and (A-26) are used to represent L and ℓ , and the pressure dilatation is either neglected or modeled, the turbulence kinetic energy equation, Eq. (A-18), becomes an ordinary differential equation with

the dependent parameter $l_\infty(x)$ which is solved in conjunction with the boundary layer momentum and energy equations to predict the development of both the mean flow field and the turbulent shear stress.

In addition to including the turbulence kinetic energy equation in the set of equations governing the boundary layer development it is necessary to specify the turbulent heat flux contribution, $-\bar{\rho}C_p v'T'$. As previously stated, in the present procedure, $v'T'$ is specified by assuming a turbulent Prandtl number, Pr_T , which relates the velocity-temperature correlation, $v'T'$, to the Reynolds stress, $u'v'$, through Eq. (A-8). The turbulent Prandtl number distribution used in the present procedure varies with distance from the wall in the manner suggested by Meier and Rotta (ref. 40). At this juncture it should be pointed out that an alternative procedure can be used to determine $v'T'$, based upon an easily derived conservation equation for either the quantity T'^2 or the correlation, $v'T'$, which is similar in form to the turbulence kinetic energy equation, Eq. (A-14). However, to solve this new conservation equation it is necessary to assume a universal structure relating quantities analogous to dissipation, production, etc. While sufficient experimental data exists to allow valid modeling of the required terms for the turbulence kinetic energy equation, the existing data does not indicate how proper modeling could be carried out for the $v'T'$ conservation equation. Thus, at least for the present, the approach based upon a turbulent Prandtl number appears preferable to an approach based upon the $v'T'$ conservation equation.

Transitional turbulence model. - The McDonald-Fish transitional turbulence model is based upon a solution of the turbulence kinetic energy equation with the structural coefficients modified from their fully-developed turbulence values. The following discussion of the model condenses the presentation in ref. 14. For fully-developed turbulent flows the structural coefficients a_1 , a_2 , and a_3 are assumed constant and are set equal to 0.15, 0.50, and 0.20, respectively. Although it is probable that all coefficients vary in the transitional regime only the coefficient a_1 contributes significantly to the energy balance when the boundary layer is far removed from separation, as shown by Bradshaw (ref. 37). Therefore, the transition model assumes a_2 and a_3 are equal to their fully-developed values and that only a_1 need be modified. The McDonald-Fish model modifies a_1 through the introduction of a turbulence Reynolds number, R_τ , defined by

$$R_\tau = \frac{(-u'v')^{1/2} \delta}{\nu} \quad (A-27)$$

Noting that

$$(-\overline{u'v'}) = \delta^2 \left(\frac{\partial \bar{u}}{\partial y} \right)^2 = \nu_T \frac{\partial \bar{u}}{\partial y} \quad (\text{A-28})$$

the turbulence Reynolds number becomes

$$R_T = \frac{\nu_T}{\nu} \quad (\text{A-29})$$

To be consistent with the integral turbulence kinetic energy equation, Eq. (A-18), a layer-averaged turbulence Reynolds number, \bar{R}_T , is introduced as

$$\bar{R}_T = \frac{1}{\delta} \int_0^{\delta} \nu_T dy / \frac{1}{\delta_s} \int_0^{\delta_s} \nu dy \quad (\text{A-30})$$

where δ_s , the sublayer thickness, is defined as the location at which the laminar stress has fallen to four percent of the total stress (the four percent definition gave a sublayer mean temperature in very good agreement with the so-called Eckert reference temperature).

The McDonald-Fish model assumes that the turbulence Reynolds number, \bar{R}_T , is the sole variable influencing the development of a_1 and a relationship between a_1 and \bar{R}_T is obtained by considering the development of an incompressible constant pressure flat plate equilibrium turbulent boundary layer. It should be noted that under the assumption that a_1 is solely dependent upon \bar{R}_T it is only necessary to derive a relation for one set of flow conditions to obtain a universally valid relationship. Based upon experimental observation, it is readily ascertained that for the incompressible, constant pressure equilibrium turbulent boundary layer, ϕ_3 , E , and $\partial \phi_1 / \partial x$ are negligible which leads to the reduced turbulence kinetic energy equation

$$\frac{d \ln a_1}{d R_{\theta}} = \frac{d \ln \delta}{d R_{\theta}} - \frac{4 a_1 \phi_2 \theta}{R_{\theta} C_f \phi_1 \delta} \quad (\text{A-31})$$

In Eq. (A-31), C_f is the skin friction coefficient and the independent variable has been changed from streamwise distance, x , to momentum thickness Reynolds

number, R_θ , using the momentum integral equation. Equation (A-31) has the general form of a Bernoulli equation

$$\frac{d \ln a}{d R_\theta} = f(R_\theta) + a_1 g(R_\theta) \quad (A-32)$$

which has the general solution

$$a_1 = (\exp \int f dR_\theta) / (C - \int g \exp \int f dR_\theta dR_\theta) \quad (A-33)$$

When the mutual dependence between \bar{R}_T , f , g , and R_θ is determined for the flat plate equilibrium boundary layer, Eq. (A-33) provides the required general relationship between a_1 and \bar{R}_T . The quantities f and g are evaluated by first noting that for the flat plate equilibrium boundary layer θ/δ varies very slowly with R_θ . Neglecting this variation leads to the result

$$f = \frac{1}{R_\theta} \quad (A-34)$$

The quantity g which is equal to the factor $-4\phi_2\theta/(C_F\phi_1\delta)$ is evaluated numerically by integrating the profiles of Maise and McDonald (ref. 41). Over a wide range of Reynolds numbers the grouping is found to be sensibly constant with a value approximately 6.66. Thus, Eq. (A-33) becomes

$$a_1 = a_0 (R_\theta/R_{\theta_0}) / [1 + 6.666 a_0 (R_\theta/R_{\theta_0} - 1)] \quad (A-35)$$

where the arbitrary constant a_0 is the value of a_1 when R_θ is equal to R_{θ_0} . It should be pointed out that at large values of R_θ/R_{θ_0} , a_1 asymptotes to the fully-developed value of 0.15. The independent variable of Eqs. (A-35) and (A-26) is changed from R_θ to \bar{R}_T by using the profiles of Maise and McDonald (ref. 41) which integrate to give

$$R_\theta = 68.1 \bar{R}_T + 614.3 \quad R_T > 40 \quad (A-36)$$

At low Reynolds numbers good results are obtained using the equation

$$R_\theta = 100 \bar{R}_\tau^{0.22} \quad \bar{R}_\tau \leq 1 \quad (\text{A-37})$$

In the intermediate range $1 < \bar{R}_\tau < 40$, the two distributions, Eqs. (A-36) and (A-37), are joined by a cubic constructed to match the value and slope at the join points. Finally, the constant of integration, a_0 , is determined on the basis of comparison between experiment and theory. Best agreement between theory and experiment for low Mach number, adiabatic wall boundary layers is obtained by setting a_0 equal to 0.0115 when \bar{R}_τ is equal to unity. During the assessment of theory as applied to low hypersonic Mach number boundary layers Shamroth and McDonald (ref. 15) showed that good results for transitional boundary layers could be obtained over a range of Mach numbers and wall to free stream temperature ratios by allowing a_0 to be a function of the wall-to-free-stream static temperature ratio, T_w/T_e . The functional relationship was chosen so that for incompressible flow the theory would agree with the incompressible data of Zysina-Molozhen and Kuznetsova (ref. 42) in the range $0.5 < T_w/T_e < 2.8$. For $T_w/T_e > 2.8$ the transition Reynolds number is assumed to be independent of wall temperature ratio. The variation of a_0 with T_w/T_e is shown in Fig. 41. The functional relationship based upon incompressible data shown in Fig. 41 leads to good comparisons between theoretical predictions and experimental data for a variety of boundary layers in the supersonic and low hypersonic Mach number regimes (ref. 15).

REFERENCES

1. Reynolds, W. C., Kays, W. M., and Kline, S. J.: Heat Transfer in the Turbulent Incompressible Boundary Layer, IV - Effect of Location and Transition and Prediction of Heat Transfer in a Known Transition Region. NASA Memorandum 12-4-58W, 1958.
2. Dryden, H. L.: Transition from Laminar to Turbulent Flow. Turbulent Flow and Heat Transfer. Princeton University Press, Princeton, New Jersey, 1959, pp. 3-74.
3. Pate, S. R. and Schueler, C. J.: Radiated Aerodynamic Noise Effects on Boundary Layer Transition in Supersonic and Hypersonic Wind Tunnels. AIAA Journal, Vol. 7, No. 3, March 1969, pp. 450-457.
4. Pate, S. R.: Measurements and Correlations of Transition Reynolds Numbers on Sharp Slender Cones at High Speeds. AIAA Journal, Vol. 9, No. 6, June 1971, pp. 1082-1090.
5. Bertram, M. H. and Beckwith, I. E.: NASA Langley Studies on Stability and Transition in High Speed Shear Layers. Proceedings of the Boundary Layer Transition Workshop, Vol. I, Report No. TOR-0172(S2816-16)-5 (Contract No. F04701-71-C-0172), Aerospace Corp., 1971.
6. Nash-Webber, J. L.: Wall Shear Stress and Laminarization in Accelerated Turbulent Compressible Boundary Layers. M.I.T. Report 94, April 1968.
7. Hairston, D. E.: Survey and Analysis of Current Boundary Layer Transition Prediction Techniques. Preprint No. 71-985, AIAA, October 1971.
8. Harris, J. E.: Numerical Solution of the Equations for Compressible Laminar, Transitional and Turbulent Boundary Layers and Comparison with Experimental Data. NASA TR R-369, August 1971.
9. Jaffe, N. A., Okamura, T. T., and Smith, A. M. O.: The Determination of Spatial Amplification Factors and Their Application to Predicting Transition. Preprint No. 69-10, AIAA, January 1969.
10. Bradshaw, P. and Ferris, D. H.: Calibration of Boundary Layer Development Using the Turbulent Kinetic Energy Equation: Compressible Flow on Adiabatic Walls. Journal of Fluid Mechanics, Vol. 46, 1971, pp. 83-110.

11. McDonald, H. and Camarata, F. J.: Computation of Turbulent Boundary Layers - 1968 AFOSR-IFP-Stanford Conference, Vol. I, S. J. Kline, M. V. Morkovin, G. Sovran, and D. J. Cockrell, eds., Stanford University, c.1969, pp. 83-98.
12. Glushko, G. S.: Turbulent Boundary Layer on a Flat Plate in an Incompressible Fluid. NASA TT F-10080, 1965. Translation from Izvestiya Akademii Navk SSRR, Seriya Mekhanika, No. 4, pp. 13-23.
13. Donaldson, C duP., Sullivan, R. D., and Yates, J. E.: An Attempt to Construct an Analytical Model of the Start of Compressible Transition. Air Force Flight Dynamics Laboratory Technical Report TR-70-153, 1970.
14. McDonald, H. and Fish, R. W.: Practical Calculations of Transitional Boundary Layers. International Journal of Heat and Mass Transfer, Vol. 16, No. 9, 1973, pp. 1729-1744.
15. Shamroth, S. J. and McDonald, H.: Assessment of a Transitional Boundary Layer Theory at Low Hypersonic Mach Numbers. NASA CR-2131, November 1972.
16. Beckwith, I. E. and Bertram, M. H.: A Survey of NASA Langley Studies on High Speed Transition and the Quiet Tunnel. NASA TMX-2566, June 1972.
17. Feindt, E. G.: untersuchungen uber die Abhangigkeit des Umschlages Laminar-turbulent von der Oberflachenrauhigkeit und der Druckverteilung. Diss. Braunschweig 1956; Jb. 1956 der Schiffbautechn. Gesellschaft, 50, 180-203, 1951.
18. van Driest, E. R. and Blumer, C. B.: Boundary Layer Transition: Free Stream Turbulence and Pressure Gradient Effects. AIAA Journal, Vol. 1, June 1963, pp. 1303-1306.
19. Hall, D. J. and Gibbings, J. C.: Influence of Free Stream Turbulence and Pressure Gradient Upon Boundary Layer Transition. Journal of Mechanical Engineering Science, Vol. 14, No. 2, 1972, pp. 134-146.
20. Blackwelder, R. F. and Kovasznay, L. S. G.: Large-Scale Motion of a Turbulent Boundary Layer During Relaminarization. Journal of Fluid Mechanics, Vol. 53, 1972, pp. 61-83.
21. Smith, D. W. and Walker, J. H.: Skin-Friction Measurements in Incompressible Flow. NASA TR R-26, 1959.

22. Jones, W. P. and Launder, B. E.: Some Properties of Sink-Flow Turbulent Boundary Layers. *Journal of Fluid Mechanics*, Vol. 46, 1972, pp. 337-351.
23. Launder, B. E. and Jones, W. P.: Sink Flow Turbulent Boundary Layers. *Journal of Fluid Mechanics*, Vol. 38, 1969, pp. 817-831.
24. Herring, H. J. and Norbury, J. F.: Experiments on Equilibrium Turbulent Boundary Layers in Favorable Pressure Gradients. *Journal of Fluid Mechanics*, Vol. 27, 1967, p. 541.
25. Badri Narayanan, M. A. and Ramjee, V.: On the Criteria for Reverse Transition in a Two-Dimensional Boundary Layer Flow. *Journal of Fluid Mechanics*, Vol. 35, 1969, pp. 225-241.
26. Julien, H. L., Kays, W. M., and Moffat, R. J.: The Turbulent Boundary Layer on a Porous Plate: Experimental Study of the Effects of a Favorable Pressure Gradient. Stanford University, Thermo Science Division Report HMT-4, 1969.
27. Launder, B. E. and Stinchcombe, H. S.: Non-Normal Similar Boundary Layers. Imperial College, Mechanical Engineering Department Report TWF/TN/21, 1967.
28. Jones, W. P.: Laminarization in Strongly Accelerated Boundary Layers. Ph.D. Thesis, University of London, 1971.
29. Moretti, P. M. and Kays, W. M.: Heat Transfer to a Turbulent Boundary Layer With Varying Free-Stream Velocity and Varying Surface Temperature - An Experimental Study. *International Journal of Heat and Mass Transfer*, Vol. 8, 1965, pp. 1187-1202.
30. Bronfin, R. B., Cohen, L. S., Coulter, L. J., McDonald, H., Shamroth, S. J., and Tripodi, R.: Development of Chemical Laser Computer Models, Vol. III, User's Manual for the SUB Code. United Aircraft Research Laboratories Report M911252-14, January 1973.
31. Hopkins, D. F. and Hill, D. E.: Effect of Small Radius of Curvature on Transonic Flow in Axisymmetric Nozzles. *AIAA Journal*, Vol. 4, No. 8, August 1966, pp. 1337-1343.
32. Bronfin, R. B., Cohen, L. S., Coulter, L. J., McDonald, H., Shamroth, S. J., and Tripodi, R.: Development of Chemical Laser Computer Models, Vol. VI, User's Manual for the SUPER Code. United Aircraft Research Laboratories Report M911252-14, January 1973.

33. McDonald, H. and Kreskovsky, J. P.: Effect of Free-Stream Turbulence on the Turbulent Boundary Layer. United Aircraft Research Laboratories Report ML10887-1, June 1973.
34. Schubauer, C. G. and Tchen, C. M.: Turbulent Flow. Princeton University Press, Princeton, New Jersey, 1961.
35. Favre, A. J.: The Equations of Compressible Turbulent Gases. Annual Summary Report No. 1, Institute de Mechanique Statistique de la Turbulence, January 1965.
36. Townsend, A. A.: Equilibrium Layers and Wall Turbulence. Journal of Fluid Mechanics, Vol. 11, 1961, pp. 97-120.
37. Bradshaw, P.: The Turbulence Structure of Equilibrium Boundary Layers. Journal of Fluid Mechanics, Vol. 39, 1967, pp. 625-645.
38. Coles, D. E.: The Turbulent Boundary Layer in a Compressible Fluid. Rand Report R403 PR, September 1962.
39. McDonald, H.: Mixing Length and Kinematic Eddy Viscosity in a Low Reynolds Number Boundary Layer. United Aircraft Research Laboratories Report J214453-1, September 1970.
40. Meier, H. V. and Rotta, J. C.: Experimental and Theoretical Investigations of Temperature Distribution in Supersonic Boundary Layers. Preprint No. 70-744, AIAA, 1970.
41. Maise, G. and McDonald, H.: Mixing Length and Eddy Kinematic Viscosity in a Compressible Boundary Layer. AIAA Journal, Vol. 6, January 1968, pp. 73-80.
42. Zysina-Molozhen, L. M. and Kuznetsova, V. M.: Investigation of Turbulent Conditions in a Boundary Layer. Thermal Engineering (Teploenergetika), Vol. 16, No. 7, 1969, pp. 16-20.

TABLE I. - NASA SUPPLIED PRESSURE DISTRIBUTION IN
THE MACH 5 LAMINAR FLOW SLOTTED NOZZLE

Dimensionless distance from throat, $\chi = x/r_t$	Dimensionless Radius, r/r_t	Pressure Ratio P/P_0
Approach section and outer wall of slot		
-21.878 -21.400 -20.900 -20.400 -19.900 -19.400 -18.900 -18.400 -17.900 -17.400 -16.900 -16.400 -15.900 -15.400 -14.900 -13.900 -13.400 -12.900 -12.400 -11.900 -11.400 -10.900 -10.400 - 9.900 - 9.400 - 8.900 - 8.400 - 8.378 - 7.878 - 7.378 - 6.878 - 6.378	11.5000 11.4890 11.4686 11.4390 11.3990 11.3530 11.3040 11.2530 11.2020 11.1460 11.0890 11.0300 10.9690 10.9080 10.8480 10.7240 10.6550 10.5816 10.4960 10.3980 10.2760 10.1090 9.8810 9.6320 9.3380 8.9930 8.6190 8.6030 8.2160 7.8260 7.4210 7.4210	1.0000  0.9999 0.9999 0.9999 0.9998 0.9998

TABLE I. - NASA SUPPLIED PRESSURE DISTRIBUTION IN
THE MACH 5 LAMINAR FLOW SLOTTED NOZZLE - Continued

- 5.878	6.1360	0.9997
- 5.378	6.1360	0.9997
- 4.878	5.6870	0.9996
- 4.378	5.2320	0.9994
- 3.878	4.7680	0.9991
- 3.378	4.2960	0.9988
- 2.878	3.8190	0.9981
- 2.378	3.3420	0.9967
- 1.878	2.8480	0.9947
- 1.678	2.6450	0.9931
- 1.638	2.6020	0.9926
- 1.520	2.4730	0.9910
- 1.360	2.2820	0.9880
- 1.190	2.0600	0.9828
- 1.072	1.8980	0.9746
- 0.982	1.7760	0.9649
- 0.908	1.6780	0.9536
- 0.848	1.6060	0.9410
- 0.788	1.5380	0.9272
- 0.720	1.4680	0.8485
- 0.688	1.4400	0.7853
- 0.646	1.4140	0.6968
- 0.604	1.4020	0.6376
- 0.558	1.4000	0.5283
- 0.504	1.4100	0.3343
- 0.448	1.4410	0.1619
Inner wall of slot		
- 0.900	1.3740	0.92716
- 0.854	1.3560	0.88677
- 0.796	1.3320	0.84846
- 0.736	1.3100	0.78525
- 0.682	1.2940	0.69678
- 0.624	1.2840	0.63764
- 0.560	1.2800	0.52828
- 0.484	1.2800	0.33427
- 0.390	1.2800	0.16191

TABLE I. - NASA SUPPLIED PRESSURE DISTRIBUTION IN
THE MACH 5 LAMINAR FLOW SLOTTED NOZZLE - Continued

Transonic throat section		
- 0.9000	1.374	0.92716
- 0.8552	1.334	0.91208
- 0.7980	1.2902	0.89588
- 0.7450	1.253	0.87863
- 0.6952	1.220	0.86039
- 0.6482	1.1906	0.84123
- 0.6034	1.1650	0.82120
- 0.5604	1.1424	0.80037
- 0.5194	1.1224	0.77880
- 0.4796	1.1044	0.75654
- 0.4412	1.0884	0.73365
- 0.4040	1.0742	0.71014
- 0.3678	1.0616	0.68622
- 0.3324	1.0506	0.66179
- 0.2980	1.0408	0.63695
- 0.2642	1.0322	0.61178
- 0.2312	1.0246	0.58633
- 0.1988	1.0184	0.56066
- 0.1670	1.0130	0.53483
- 0.1356	1.0086	0.50892
- 0.1048	1.0052	0.48298
- 0.0742	1.0026	0.45709
- 0.0442	1.0010	0.43130
- 0.0146	1.0002	0.40570
0.0000	1.0000	0.39320
0.0148	1.0002	0.38036
0.0438	1.0010	0.35535
0.0724	1.0026	0.33074
0.1010	1.0050	0.30662
0.1280	1.0084	0.28909
0.1572	1.0124	0.26015
0.1850	1.0174	0.23839
0.2400	1.0300	0.19603
0.2944	1.0460	0.15789

TABLE I. - NASA SUPPLIED PRESSURE DISTRIBUTION IN
THE MACH 5 LAMINAR FLOW SLOTTED NOZZLE - Continued

Supersonic section		
0.3512	1.0654	0.15700
0.3992	1.0824	0.14861
0.4558	1.1036	0.14018
0.5218	1.1286	0.13162
0.5972	1.1438	0.12287
0.6826	1.1924	0.11437
0.7766	1.2306	0.10628
0.8788	1.2728	0.09851
0.9902	1.3190	0.09087
1.1118	1.3696	0.08355
1.2420	1.4238	0.07667
1.3804	1.4812	0.07027
1.5256	1.5410	0.06448
1.6778	1.6028	0.05916
1.8358	1.6662	0.05435
1.9992	1.7310	0.05000
2.3440	1.8640	0.04257
2.7080	1.9996	0.03622
3.0940	2.1368	0.03091
3.5020	2.2740	0.02660
3.9300	2.4106	0.02302
4.3760	2.5464	0.02006
4.8400	2.6804	0.01758
5.3240	2.8122	0.01549
5.8280	2.9418	0.01373
6.3520	3.0648	0.01222
6.8960	3.1914	0.01093
7.4600	3.3112	0.00982
8.0380	3.4280	0.00887
8.6360	3.5408	0.00805
9.2580	3.6488	0.00732
9.8900	3.7542	0.00670
10.5440	3.8548	0.00614
11.2220	3.9500	0.00566
11.9040	4.0436	0.00523
12.6200	4.1294	0.00484
13.3360	4.2140	0.00451
14.0900	4.2900	0.00420

TABLE I. - NASA SUPPLIED PRESSURE DISTRIBUTION IN
 THE MACH 5 LAMINAR FLOW SLOTTED NOZZLE - Concluded

14.8380	4.3664	0.00394
15.6240	4.4334	0.00369
16.4060	4.5005	0.00348
17.2240	4.5582	0.00328
18.0380	4.6158	0.00311
18.8920	4.6634	0.00295
19.7440	4.7106	0.00281
20.6040	4.7550	0.00269
21.4860	4.7928	0.00257
22.3840	4.8258	0.00247
23.2900	4.8564	0.00237
24.2160	4.8806	0.00229
25.1500	4.9026	0.00222
26.0920	4.9214	0.00215
27.0500	4.9354	0.00210
28.0140	4.9475	0.00205
28.9860	4.9568	0.00200
29.9640	4.9636	0.00197
30.9500	4.9680	0.00194

TABLE II. - NASA SUPPLIED PRESSURE DISTRIBUTION FOR
INLET DUCT AND APPROACH SECTION BOUNDARY
LAYER CALCULATION

Dimensionless Distance From Throat, $\chi = x/r_t$	Contour Distance From Last Screen, S		Dimensionless Radius, r/r_t	Pressure Ratio
	m.	ft.		
-165.878	0.0	0.0	11.5000	0.9999770
- 21.878	1.8288	6.000000	11.5000	0.9999770
- 17.400	1.8345	6.018718	11.1460	0.9999673
- 15.900	1.9050	6.250103	10.9690	0.9999714
- 14.900	1.9178	6.292076	10.8480	0.9999583
- 13.900	1.9306	6.334054	10.7240	0.9999432
- 12.900	1.9434	6.376114	10.5810	0.9999342
- 11.900	1.9563	6.418391	10.3980	0.9999304
- 11.400	1.9694	6.461433	10.2760	0.9999281
- 10.900	1.9763	6.483864	10.1090	0.9999240
- 10.400	1.9833	6.506949	9.8810	0.9999169
- 9.900	1.9905	6.530670	9.6320	0.9999052
- 9.400	1.9981	6.55541	9.3380	0.9998876
- 8.900	2.0059	6.581074	8.9930	0.9998619
- 8.400	2.0063	6.582213	8.6190	0.9998309
- 8.378	2.0142	6.608265	8.6030	0.9998293
- 7.878	2.0222	6.634649	8.2160	0.9997898
- 7.378	2.0326	6.6688233	7.8260	0.9997433
- 8.900	2.0977	6.688233	7.4210	0.9996898
- 6.378	2.0469	6.715564	7.0040	0.9996292
- 5.878	2.0553	6.743150	6.5720	0.9995614
- 4.878	2.0638	6.770971	6.1360	0.9994841
			5.6870	0.9993846
- 4.378	2.0723	6.799056	5.2320	0.9992465
- 3.878	2.0810	6.827351	4.7680	0.9990510
- 3.378	2.0897	6.855887	4.2960	0.9987087
- 2.878	2.0984	6.884608	3.8190	0.9980443
- 2.378	2.1072	6.913401	3.3420	0.9968761
- 1.878	2.1160	6.942441	2.8480	0.9946463
- 1.678	2.1196	6.954235	2.6450	0.9930038
- 1.638	2.1204	6.956646	2.6020	0.9925850
- 1.520	2.1226	6.963898	2.4730	0.9910844
- 1.360	2.1257	6.973979	2.2820	0.9881970
- 1.300	2.1269	6.977909	2.2036	0.9867291

TABLE II. - NASA SUPPLIED PRESSURE DISTRIBUTION FOR
 INLET DUCT AND APPROACH SECTION BOUNDARY
 LAYER CALCULATION - Concluded

- 1.190	2.1292	6.985453	2.0600	0.9827085
- 1.120	2.1307	6.990462	1.9638	0.9785564
- 1.072	2.1317	6.993906	1.8980	0.9747525
- 1.030	2.1326	6.996885	1.8410	0.9652792
- 0.982	2.1337	7.000220	1.7760	0.9652792
- 0.940	2.1346	7.003150	1.7204	0.9595346
- 0.908	2.1352	7.005320	1.6780	0.9542777
- 0.870	2.1360	7.007820	1.6324	0.9465237
- 0.848	2.1364	7.009240	1.606	0.9406963
- 0.820	2.1369	7.011020	1.5742	0.9306027
- 0.788	2.1376	7.013090	1.5298	0.9076510
- 0.760	2.1377	7.013590	1.5298	0.9076510
- 0.758	2.1381	7.014920	1.5070	0.8888883
- 0.740	2.1396	7.01980	1.4886	0.8683142
- 0.720	2.1388	7.017170	1.4680	0.8393871
- 0.710	2.1390	7.017740	1.4592	0.823443
- 0.688	2.1394	7.018890	1.4400	0.7873495
- 0.666	2.1397	7.020020	1.4264	0.7470208
- 0.646	2.1400	7.021010	1.4140	0.7079584
- 0.630	2.1402	7.021760	1.4094	0.6761727
- 0.604	2.1406	7.022910	1.4020	0.6239762
- 0.585	2.1408	7.023710	1.4012	0.5853385
- 0.568	2.1410	7.024420	1.4004	0.5495445
- 0.558	2.1411	7.024840	1.4000	0.5277362
- 0.552	2.1412	7.025090	1.4012	0.5145390

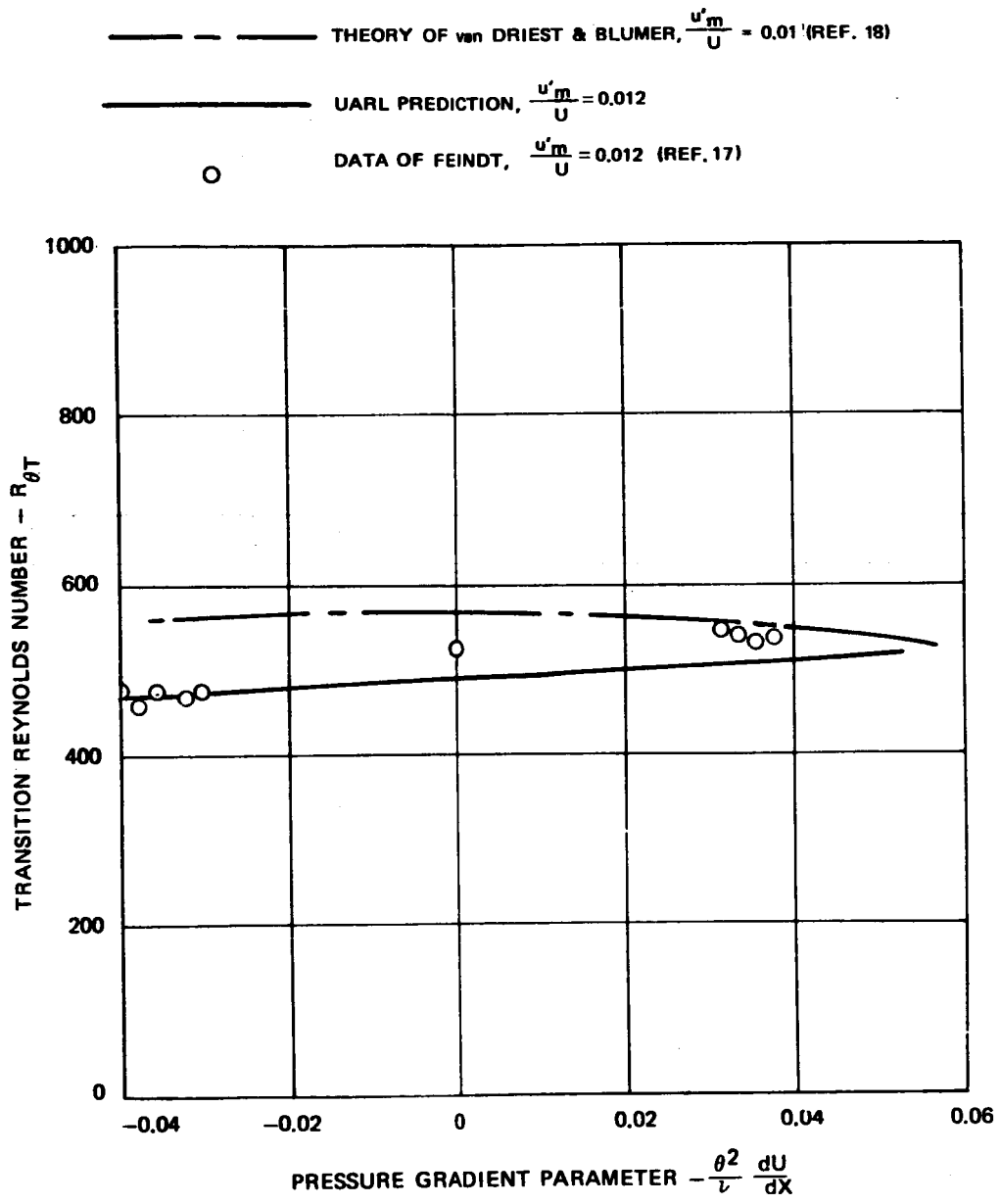


Figure 1. — Comparison between measured and predicted transition Reynolds number.

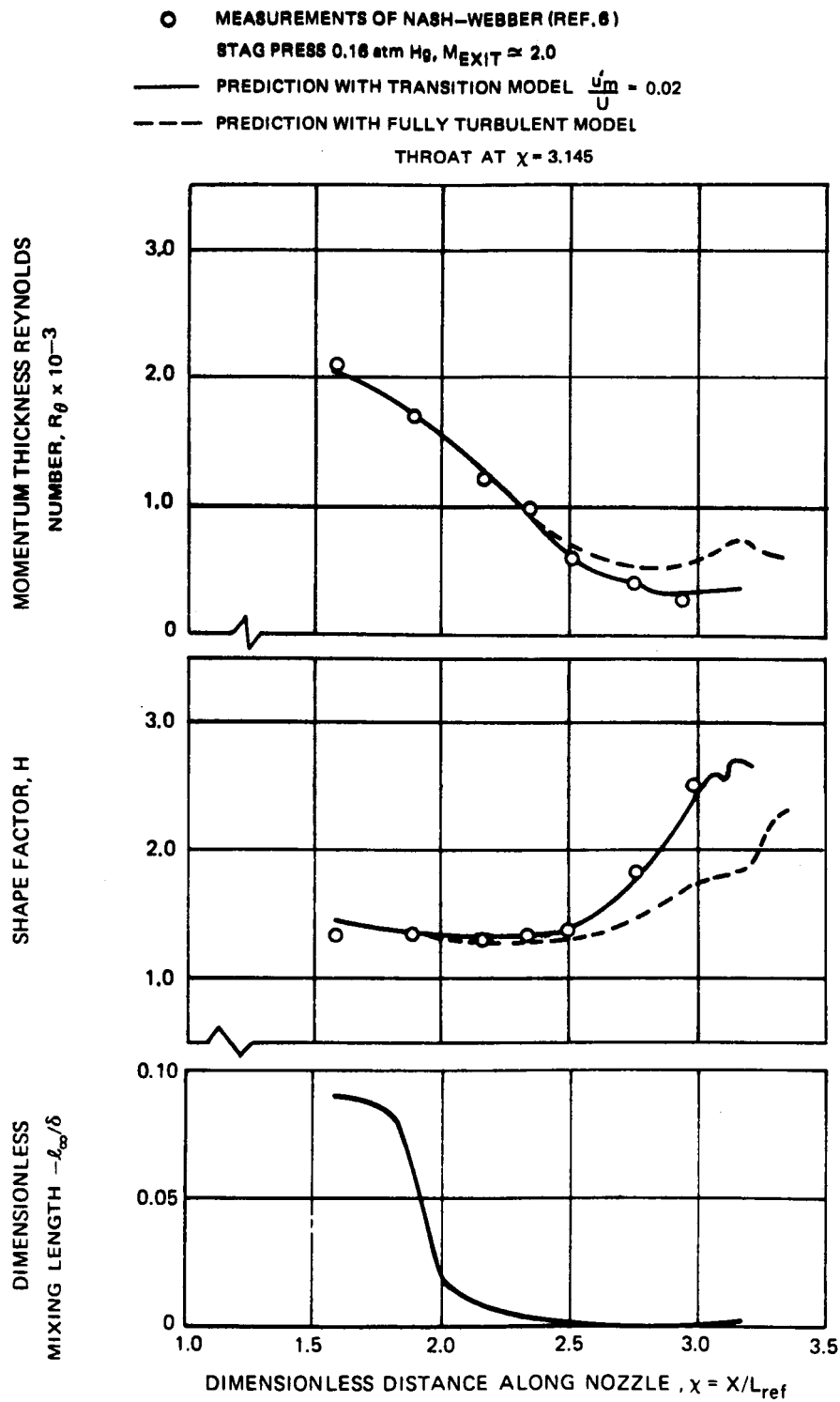


Figure 2. - Comparison between predictions and measurements for supersonic nozzle "A".

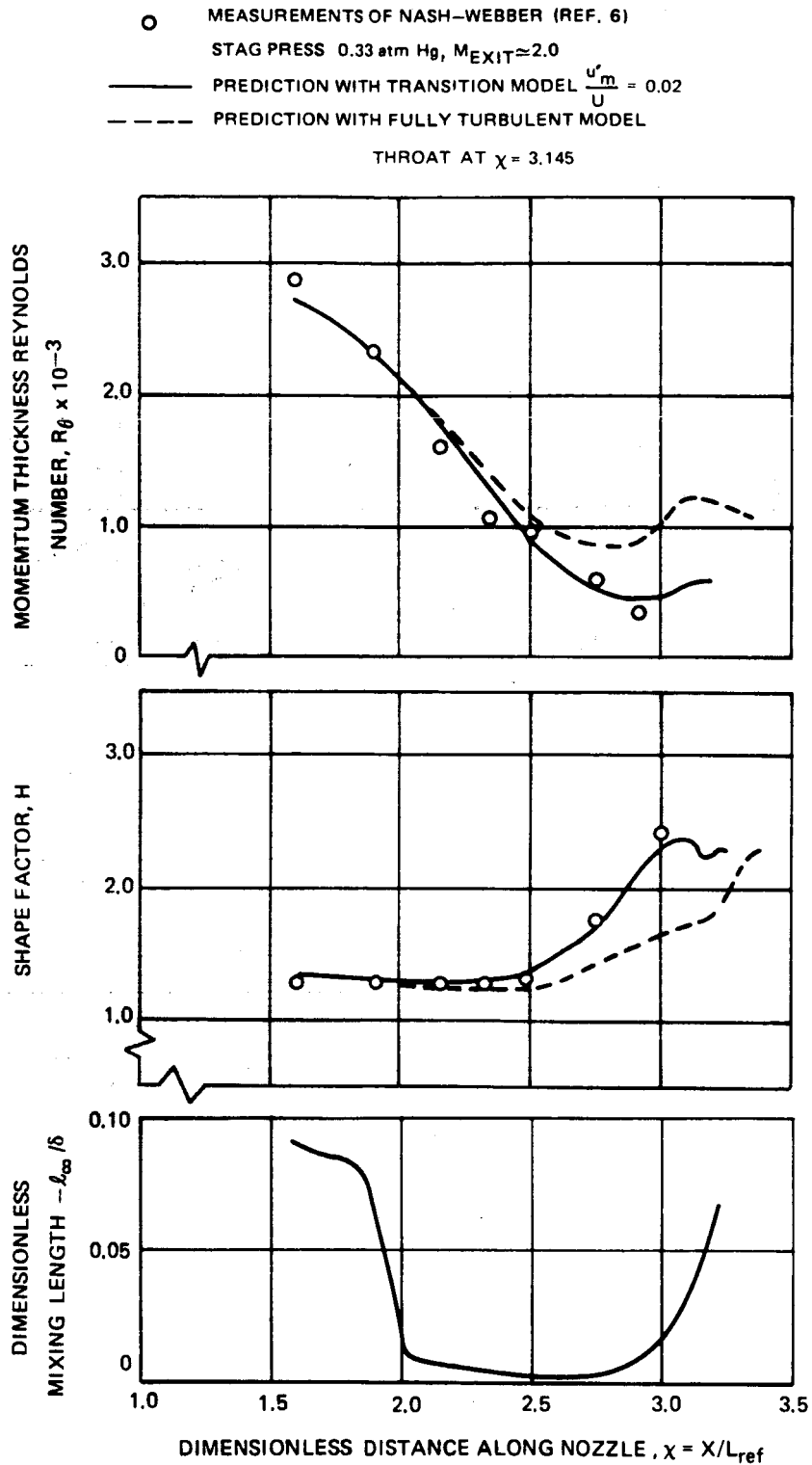


Figure 3. — Comparison between predictions and measurements for supersonic nozzle "A".

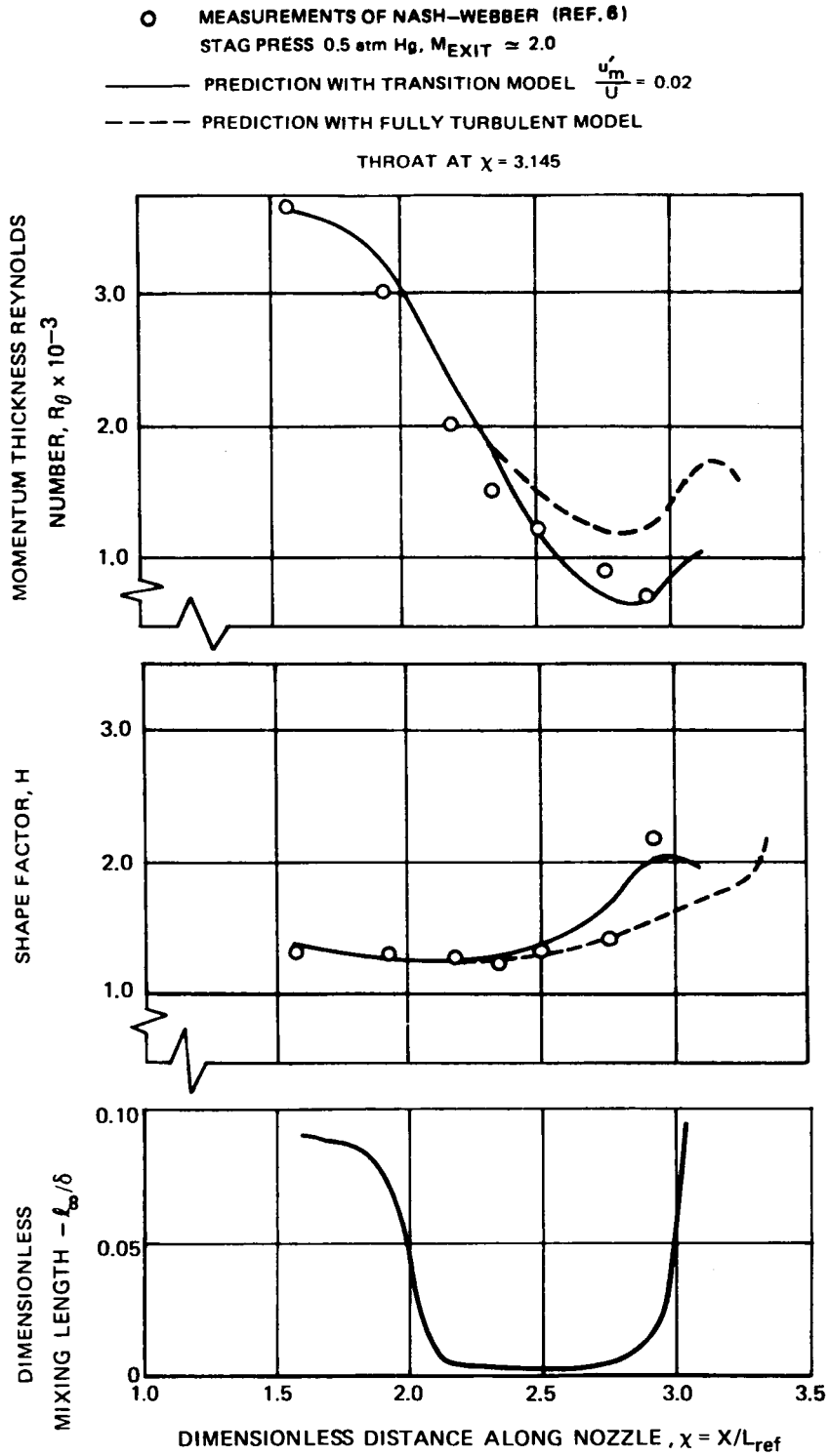


Figure 4. - Comparison between predictions and measurements for supersonic nozzle "A".

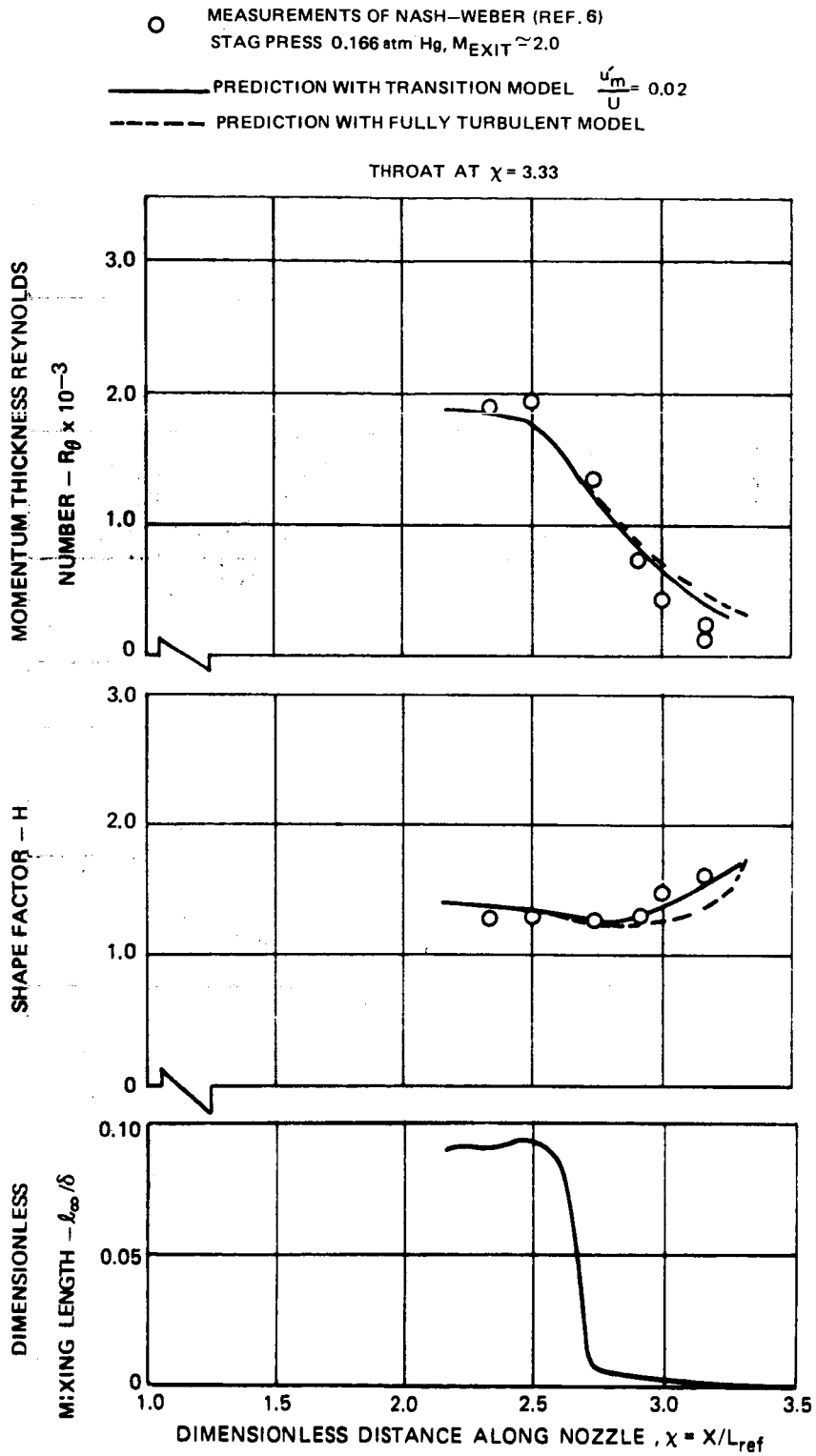


Figure 5. - Comparison between predictions and measurements for supersonic nozzle "C".

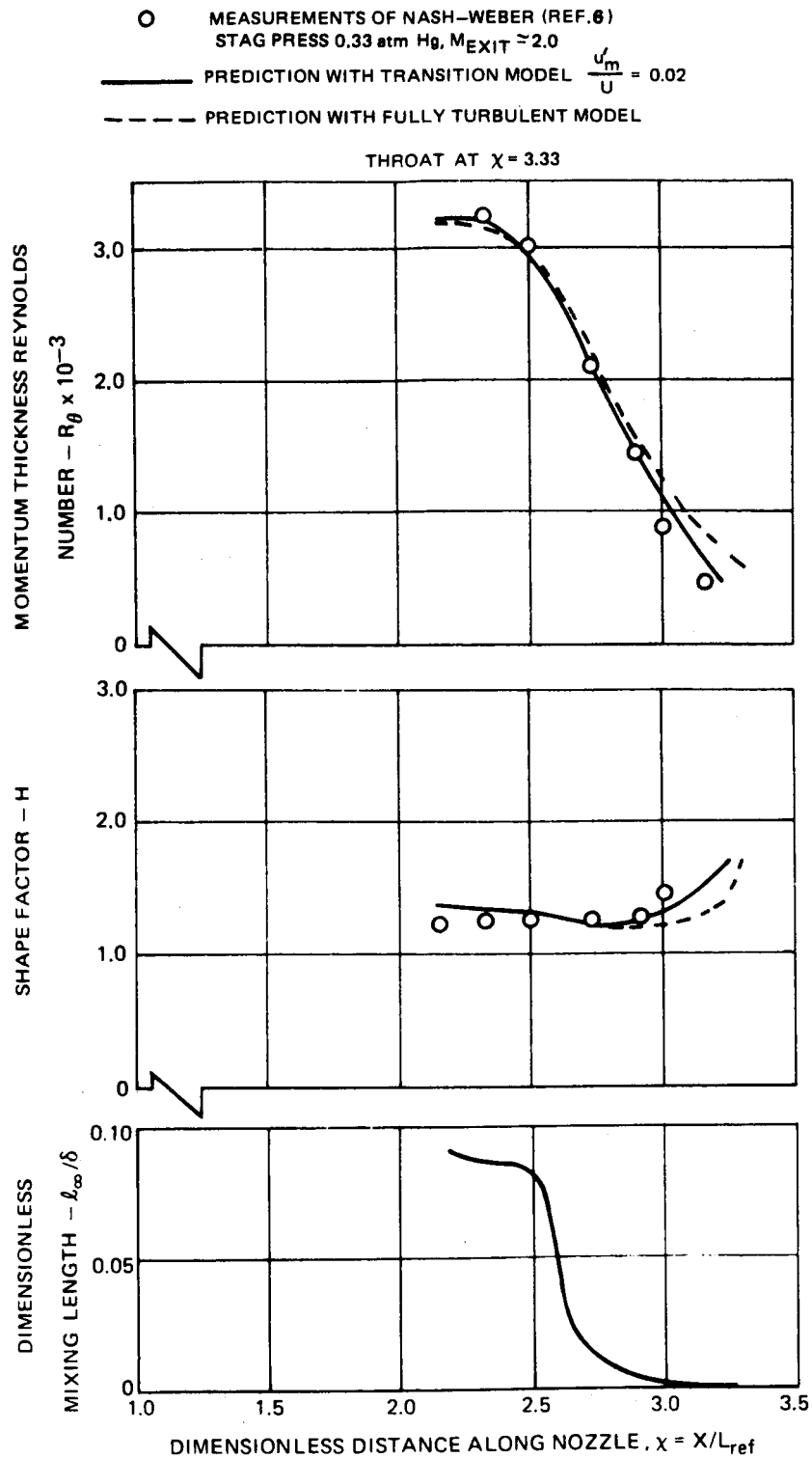


Figure 6. - Comparison between predictions and measurements for supersonic nozzle "C".

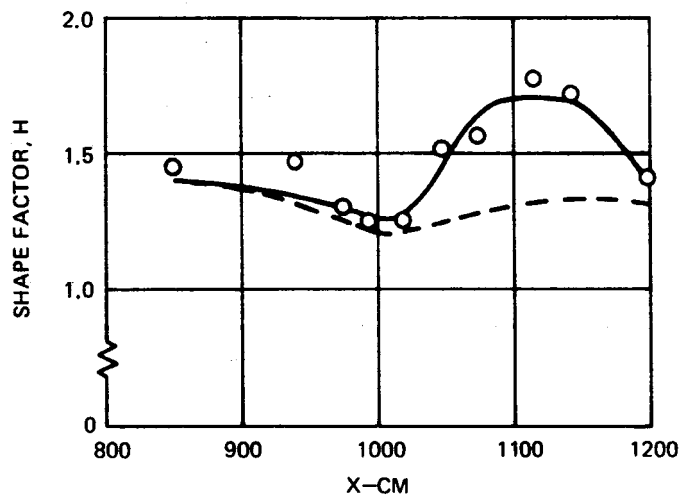
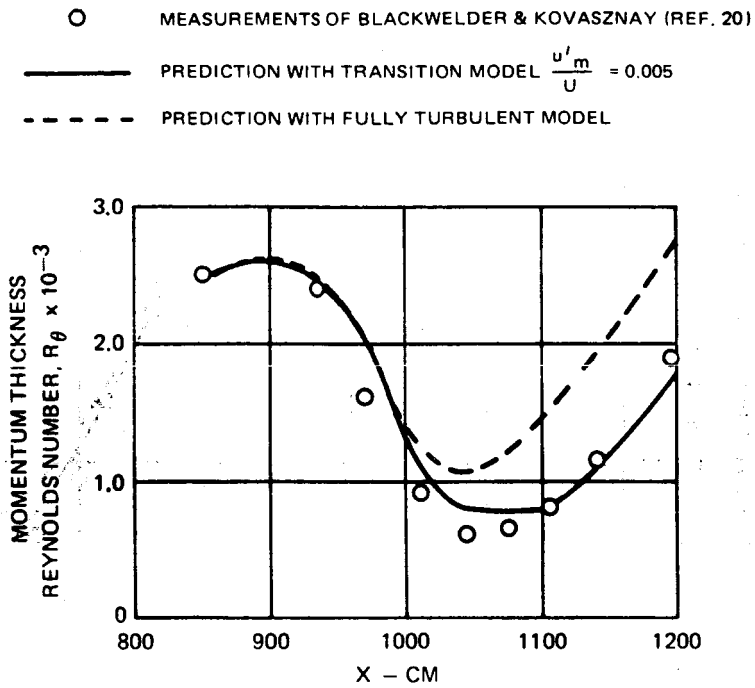


Figure 7. — Comparison between predictions and measurements of momentum thickness and shape factor for low speed flow.

○ MEASUREMENTS OF BLACKWELDER & KOVASZNAY (REF. 20)
 — PREDICTION WITH TRANSITION MODEL $\frac{u'_m}{U} = 0.005$
 - - - PREDICTION WITH FULLY TURBULENT MODEL

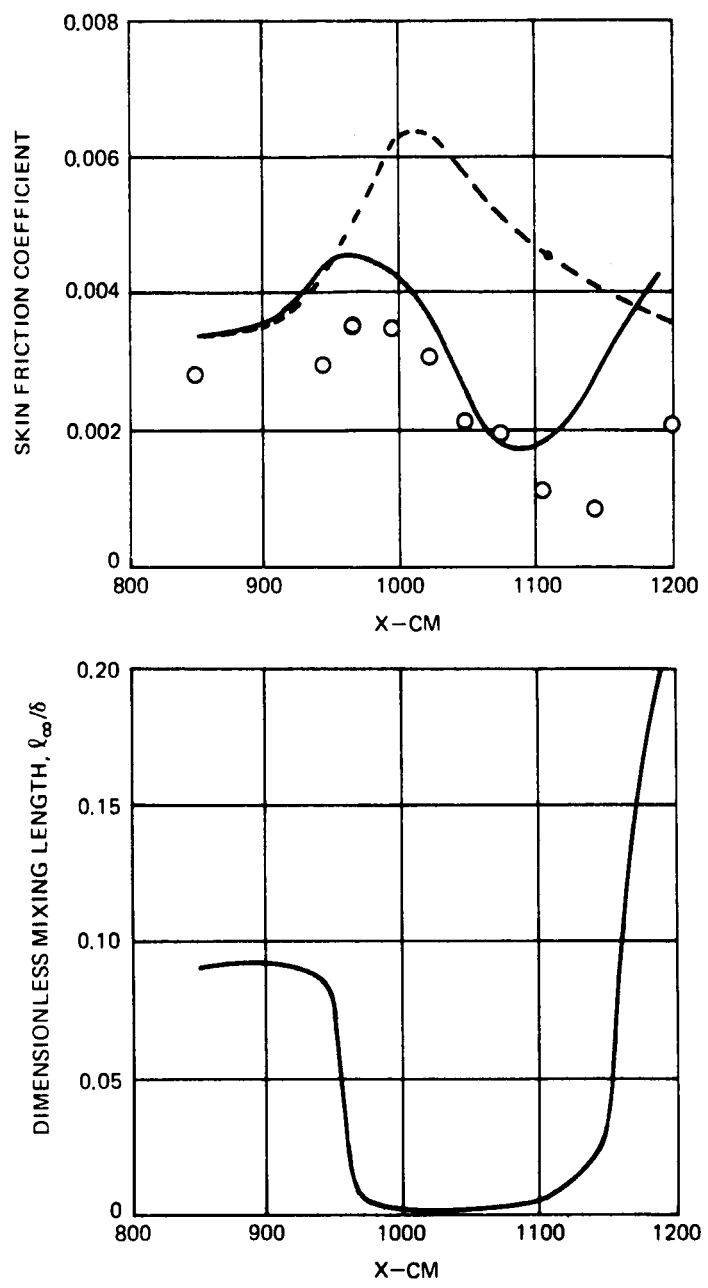


Figure 8. — Comparison between predictions and measurements of skin friction coefficient and predicted mixing length for low speed flow.

CURVES AND EXPERIMENTAL DATA FROM JONES AND LAUNDER (REF. 22)
 O—PREDICTIONS UNDER THE CONDITION OF JONES AND LAUNDER, $\frac{u'_m}{U} = 0.01$
 Δ—NEW DATA OF JONES AND LAUNDER (REF. 22)

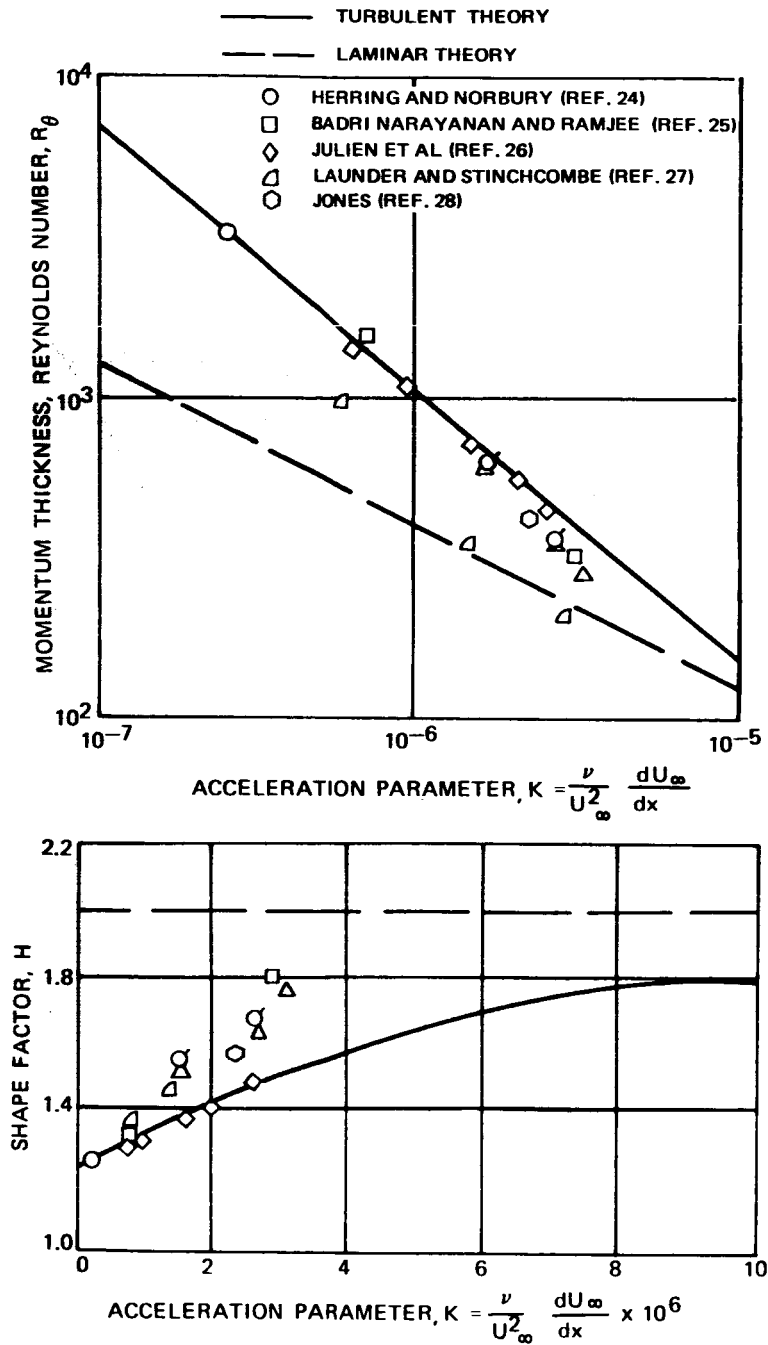


Figure 9. — Comparison between predictions and measurements of momentum thickness Reynolds number and shape factor for sink flow boundary layers.

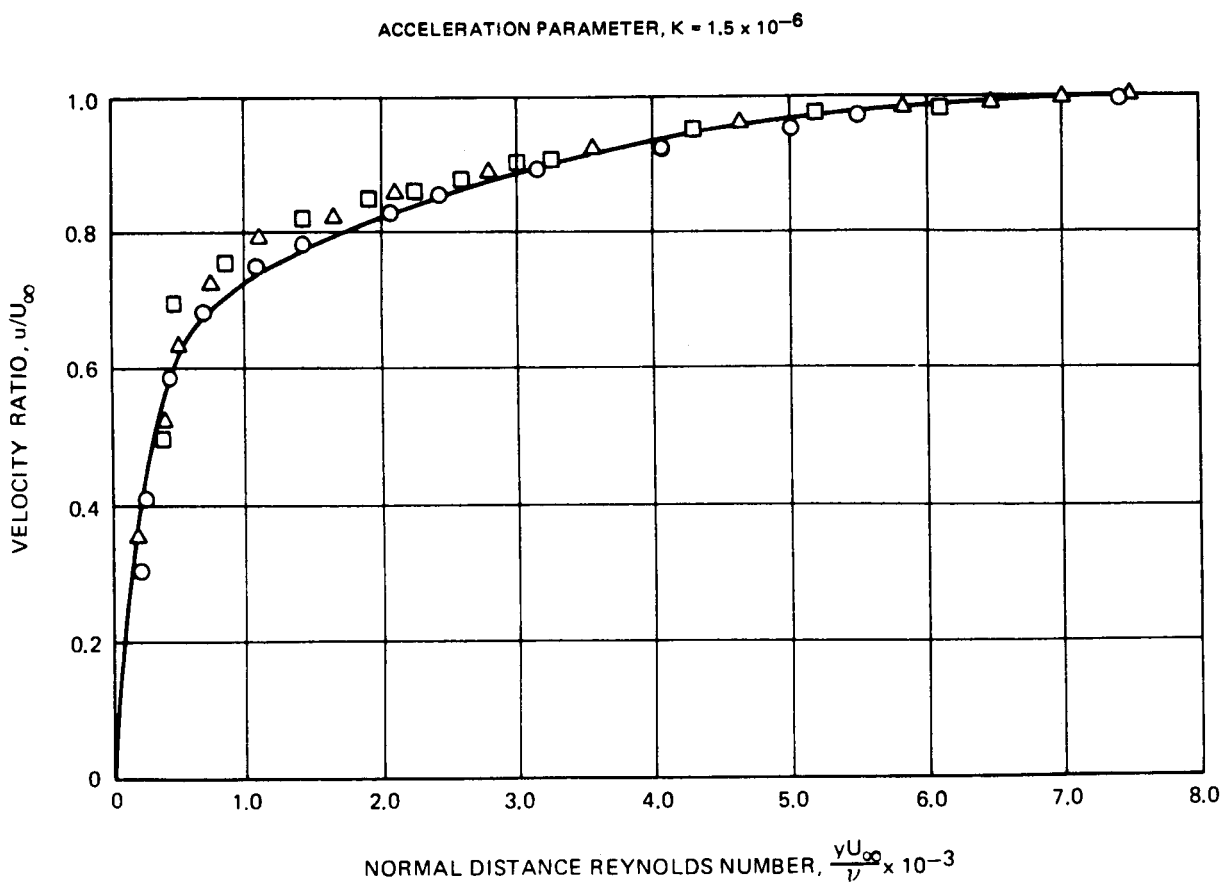
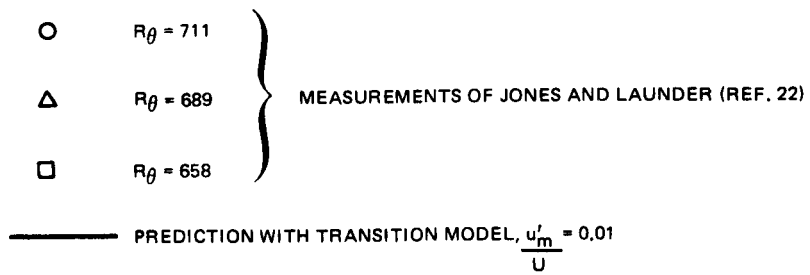


Figure 10. — Comparison between predictions and measurements for a sink flow boundary layer.

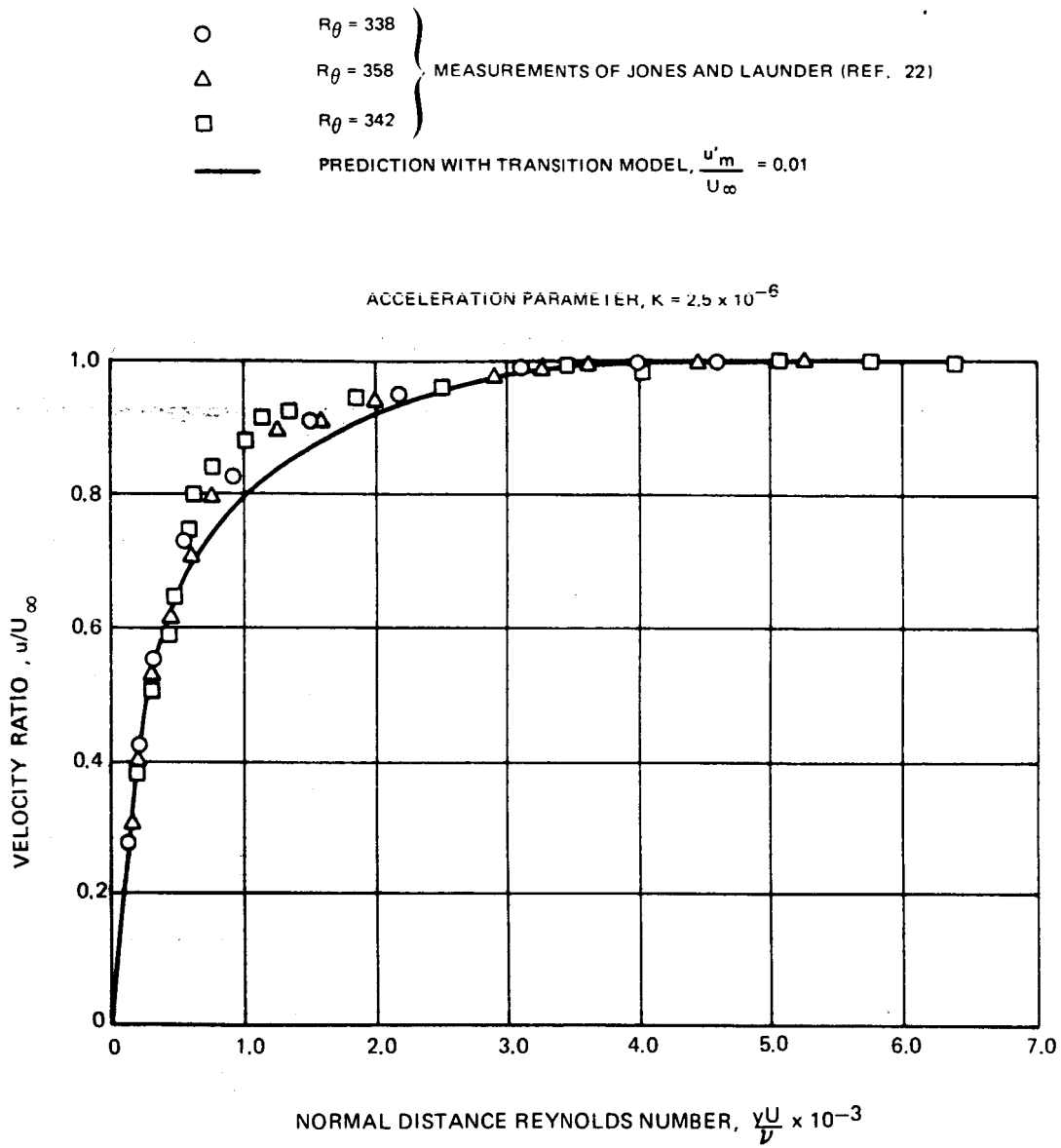


Figure 11.— Comparison between predictions and measurements for a sink flow boundary layer.

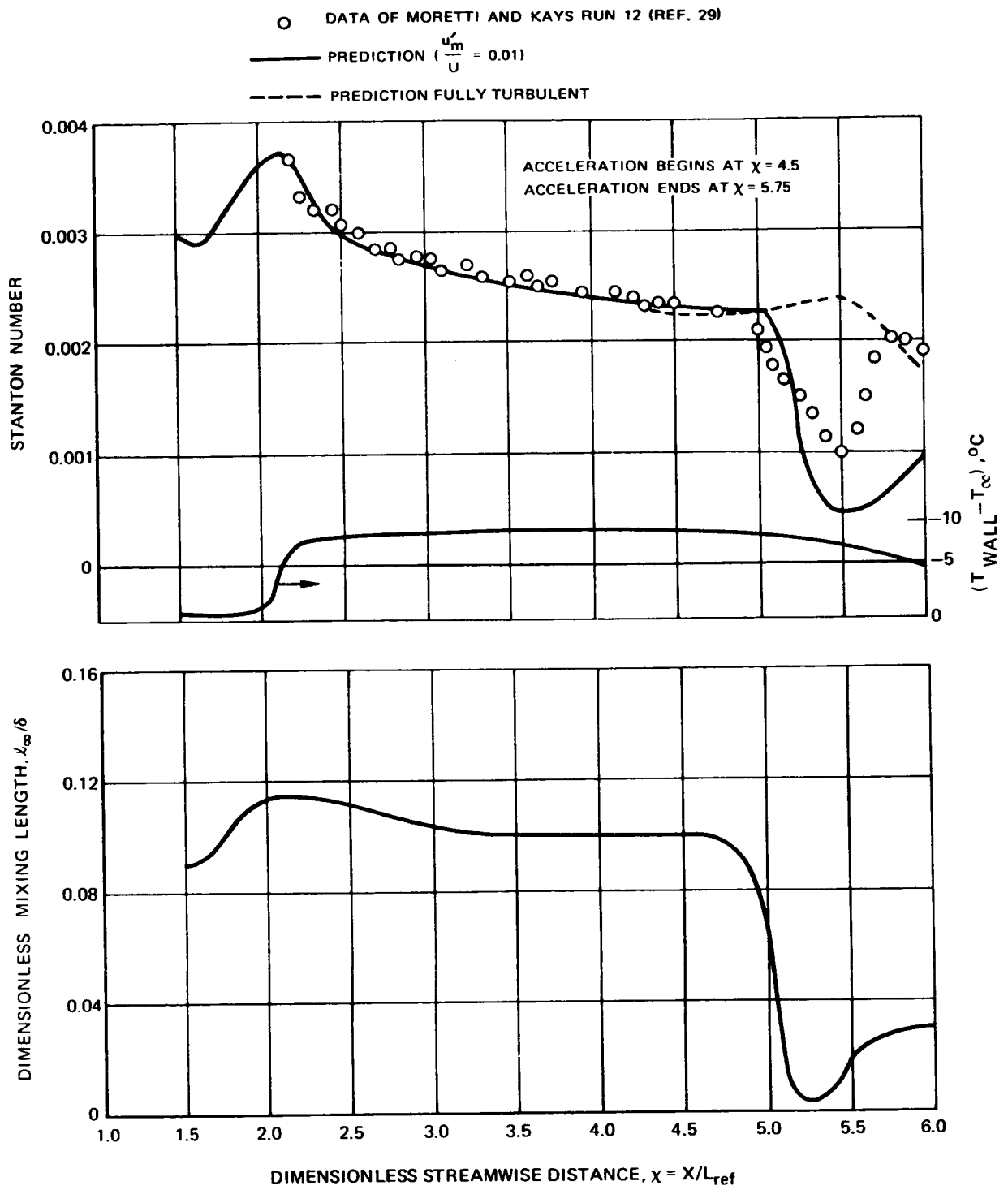


Figure 12. — Comparison between predicted and experimental results for heat transfer in an accelerated flow.

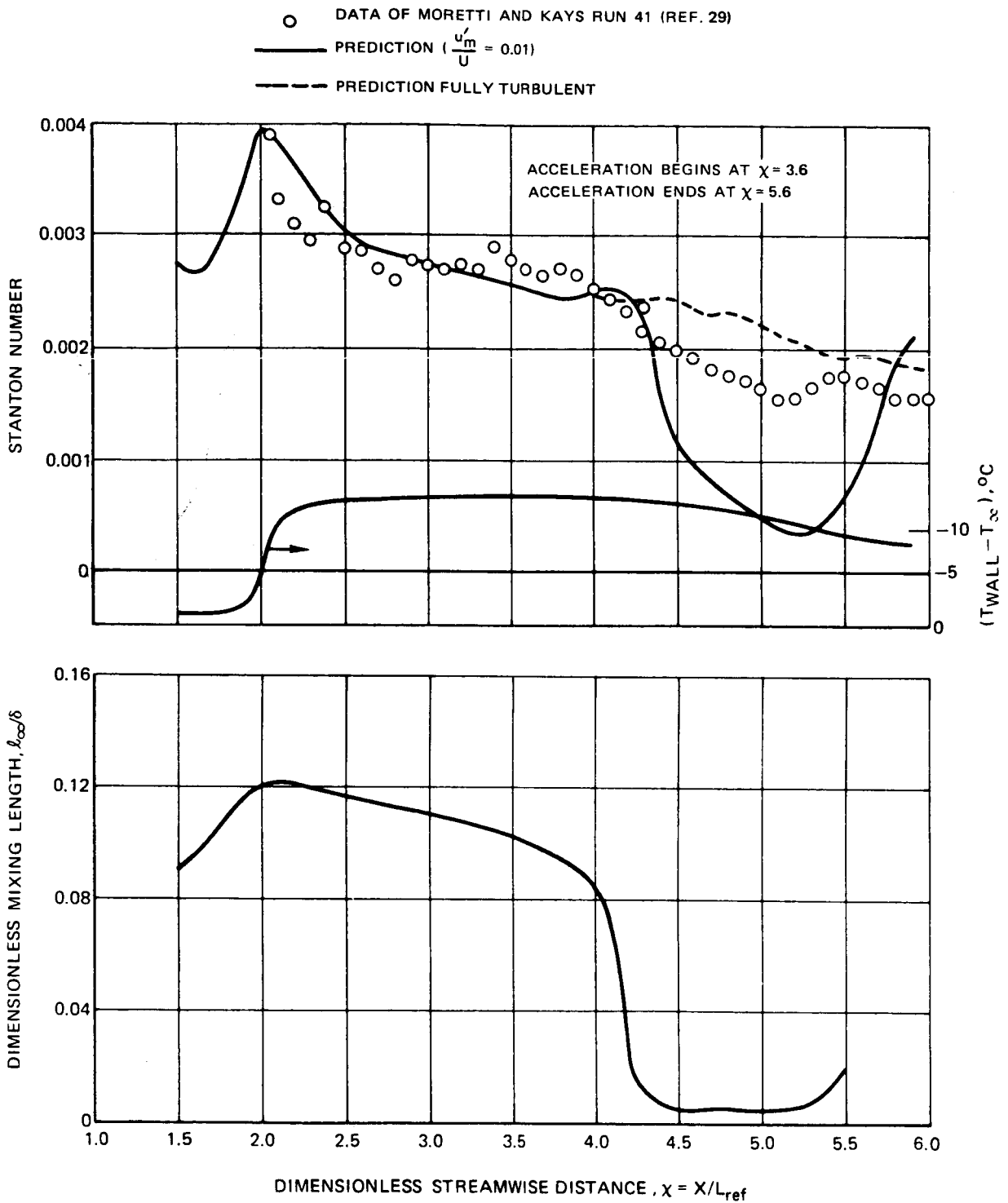


Figure 13. — Comparison between predicted and experimental results for heat transfer in an accelerated flow.

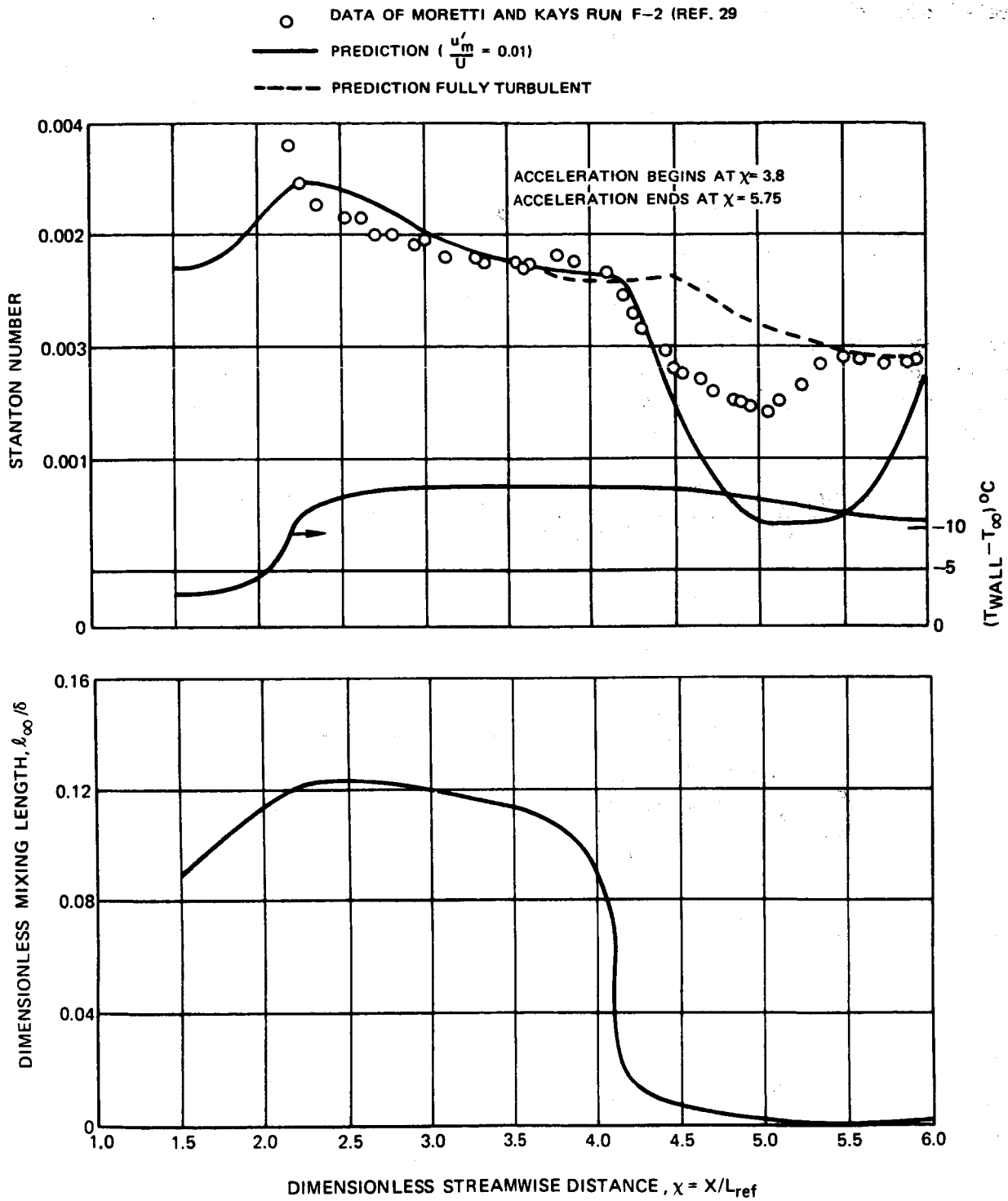


Figure 14. — Comparison between predicted and experimental results for heat transfer in an accelerated flow.

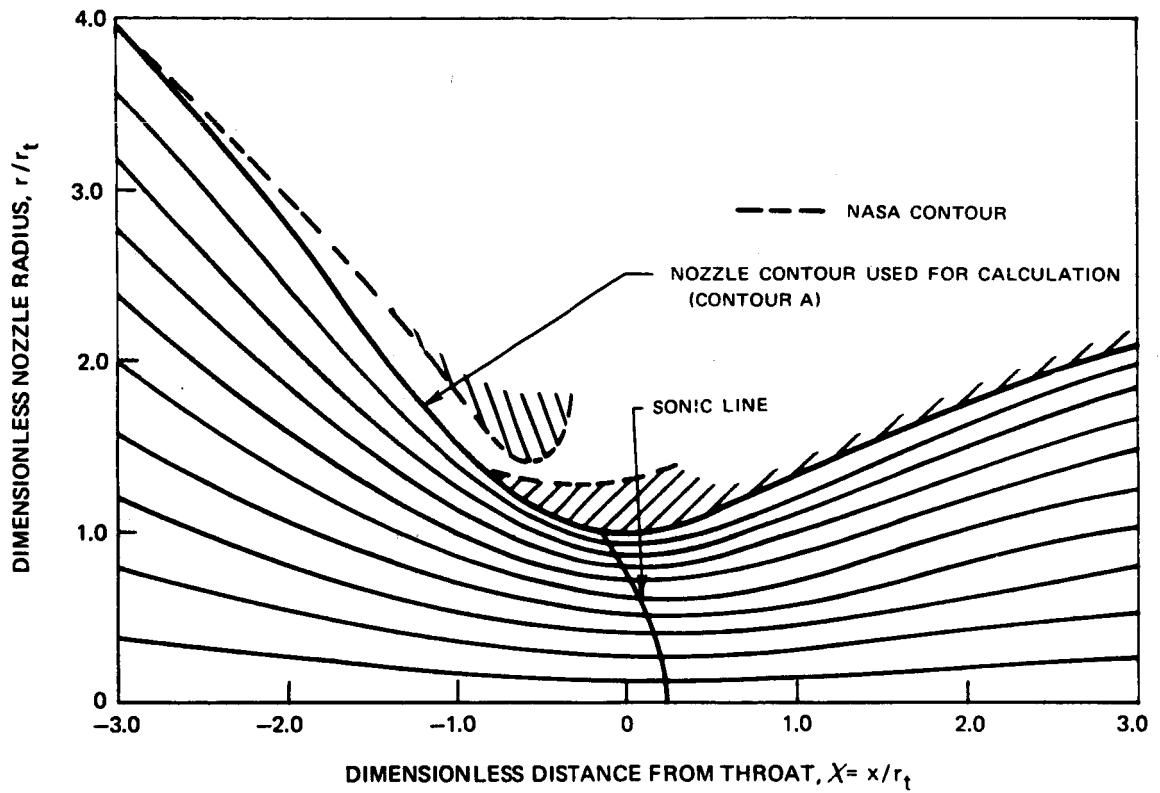


Figure 15. — Calculated streamlines and sonic line for the transonic section of the NASA Mach 5 nozzle with slot fared in—throat and supersonic section follow NASA contour.

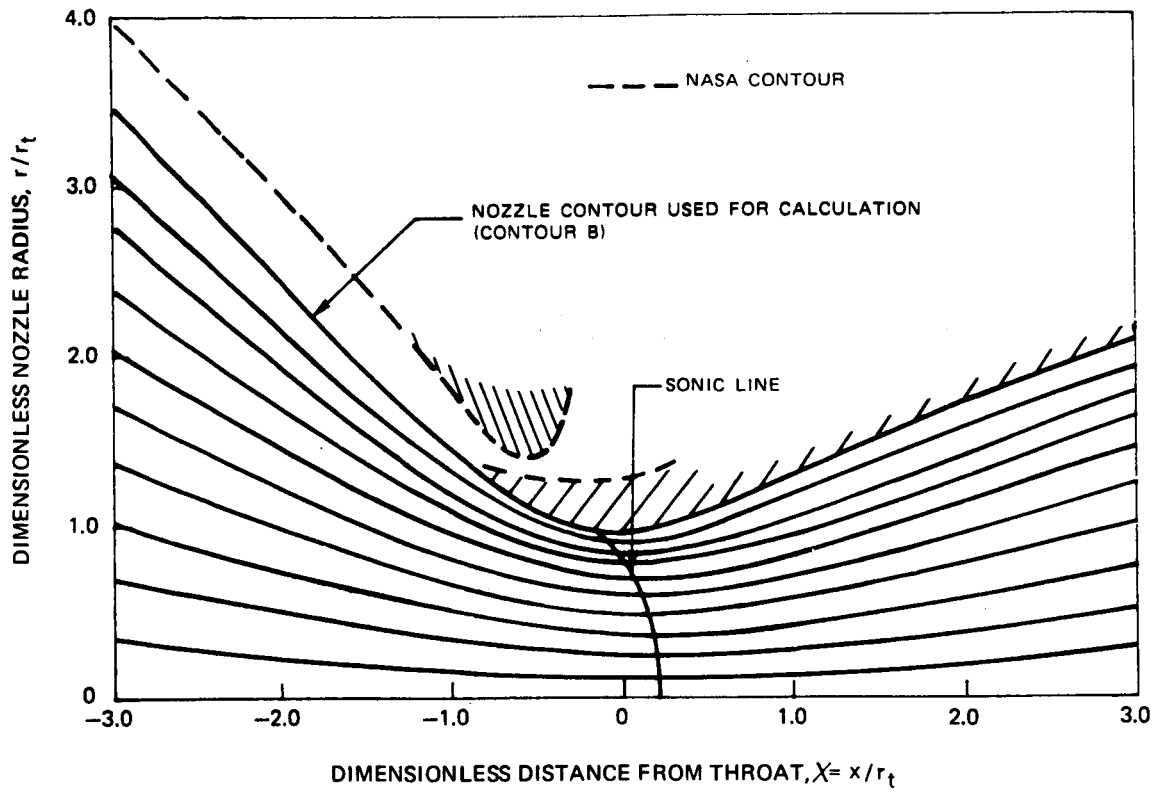


Figure 16. — Calculated streamlines and sonic line for the transonic section of the NASA Mach 5 nozzle using estimated slot stagnation streamline contour— throat and supersonic section follow NASA contour.

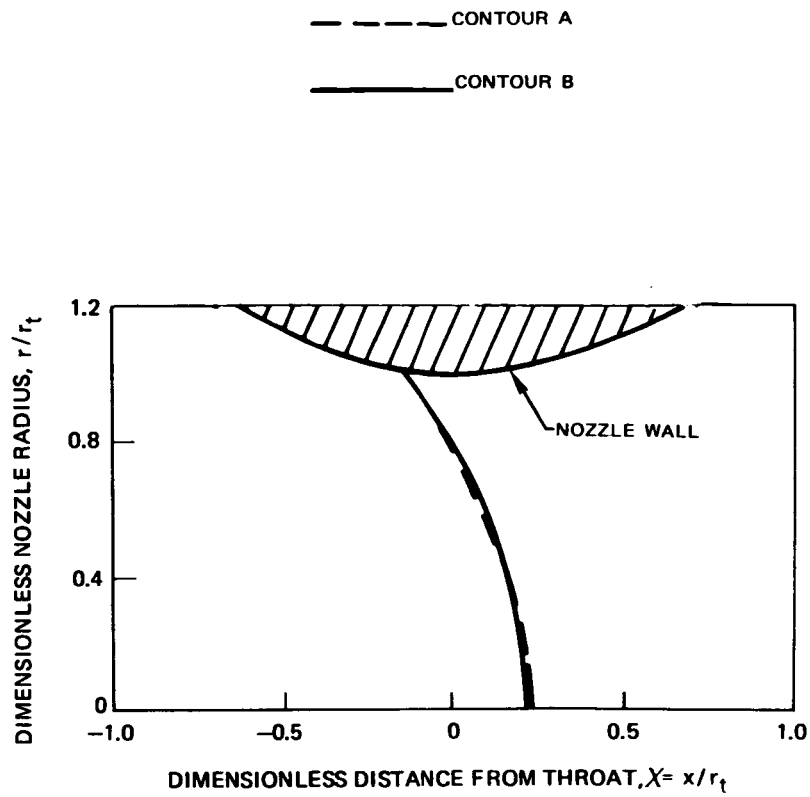


Figure 17. — Comparison of calculated sonic lines in the NASA Mach 5 nozzle using different approach section contours.

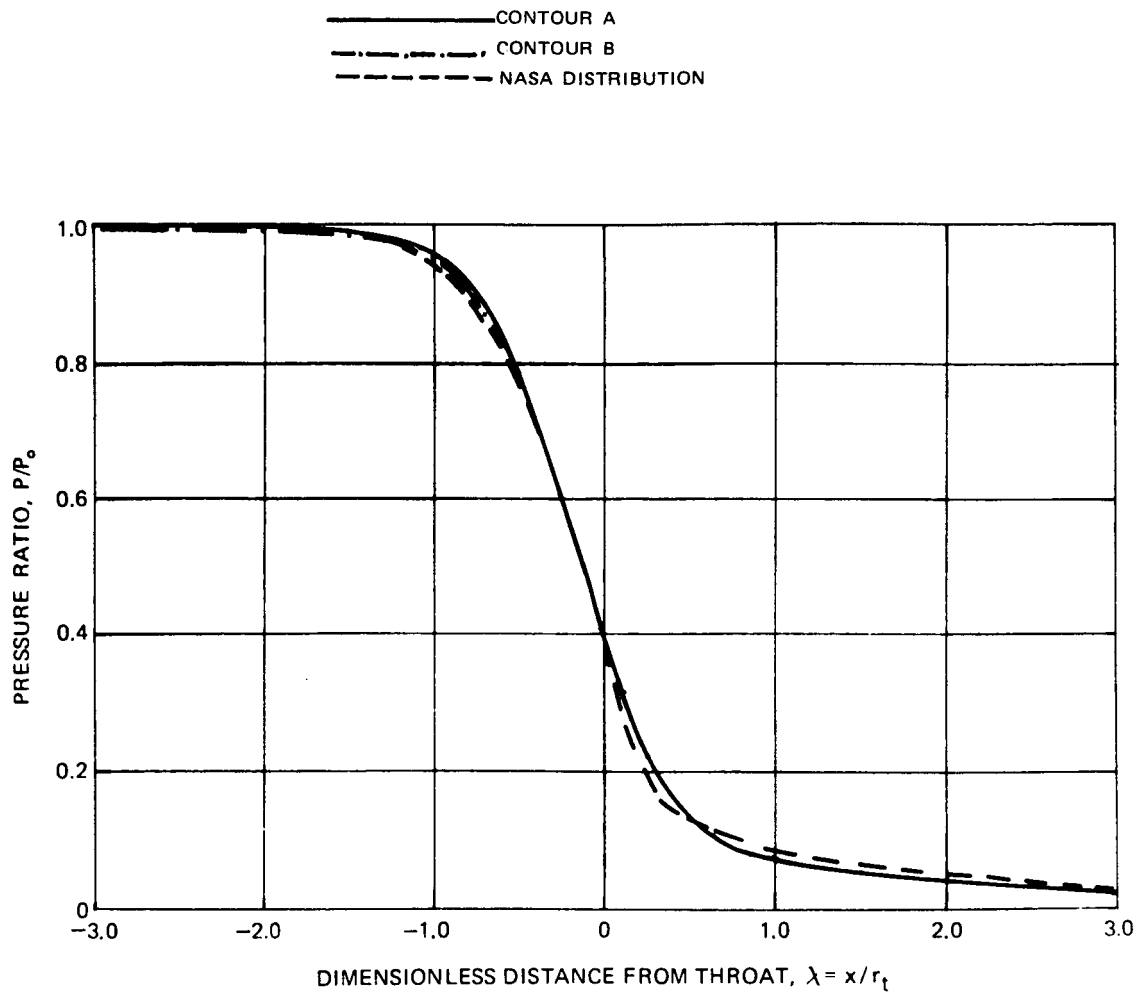


Figure 18. – Comparison between calculated and NASA wall pressure distribution in the transonic section of the NASA Mach 5 nozzle – calculations based on two different approach section contours.

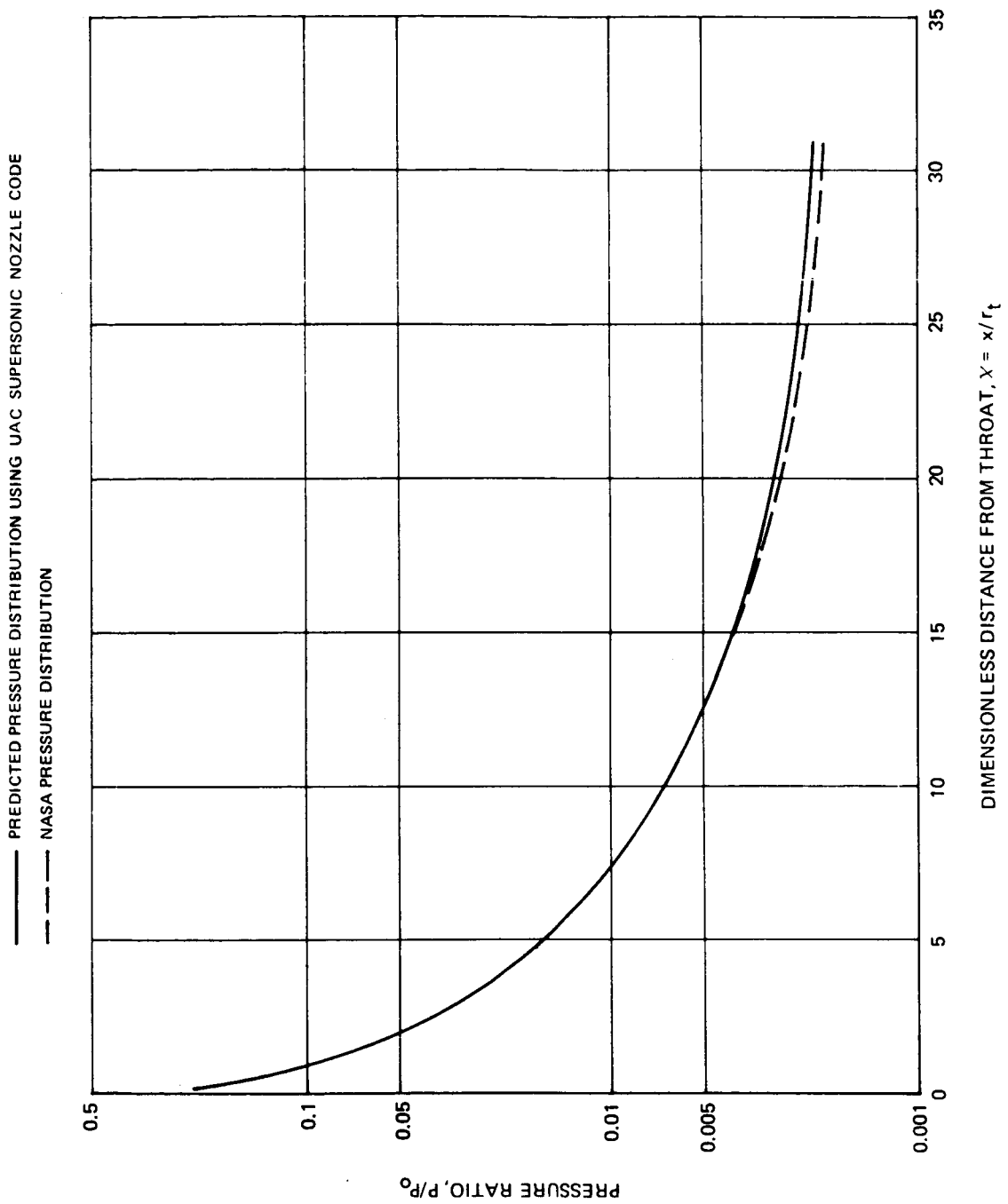


Figure 19. — Comparison between calculated and NASA wall pressure distribution in the supersonic section of the NASA Mach 5 nozzle.

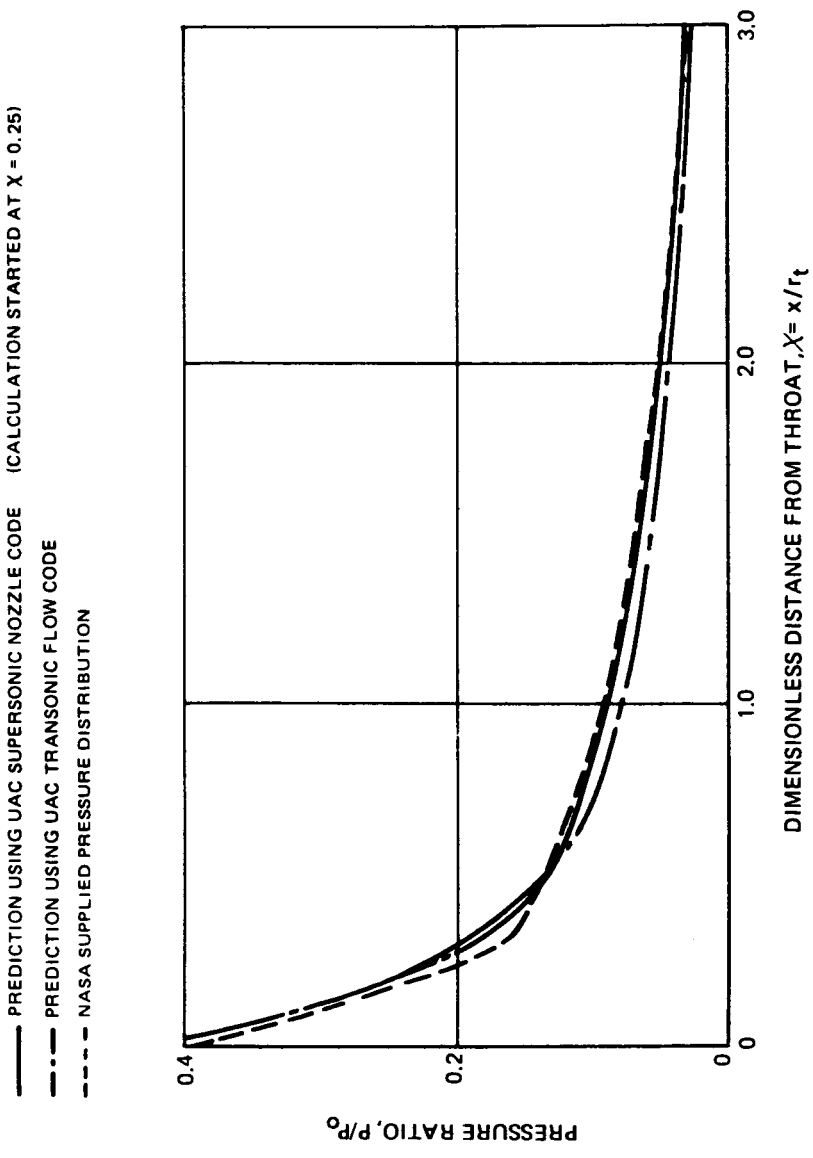


Figure 20. — Comparison between calculated and NASA wall pressure distributions downstream of the throat of the NASA Mach 5 nozzle.

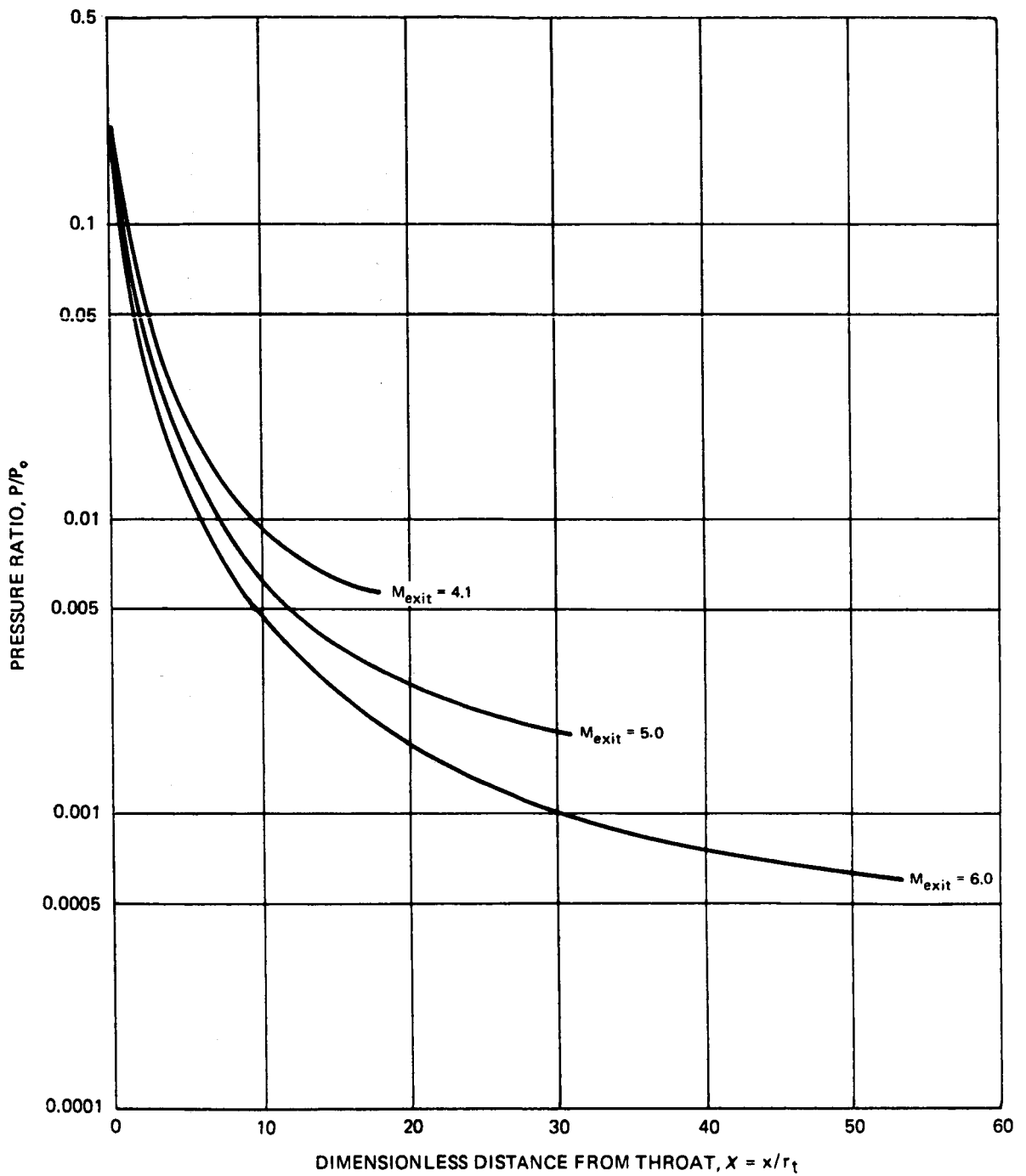


Figure 21. — Predicted pressure distributions in supersonic nozzles with exit Mach numbers of 4.1, 5.0 and 6.0.

————— $\frac{c_1}{c_2} = 0.01$
 - - - - - $\frac{c_1}{c_2} = 0.06$

$T_o = 104.4^\circ\text{C} (220^\circ\text{F})$
 $T_w = 65.5^\circ\text{C} (150^\circ\text{F})$
 $P_o = 10.2 \text{ atm} (150 \text{ psia})$
 $U_1 \approx 213 \text{ cm/sec} (7 \text{ fps})$

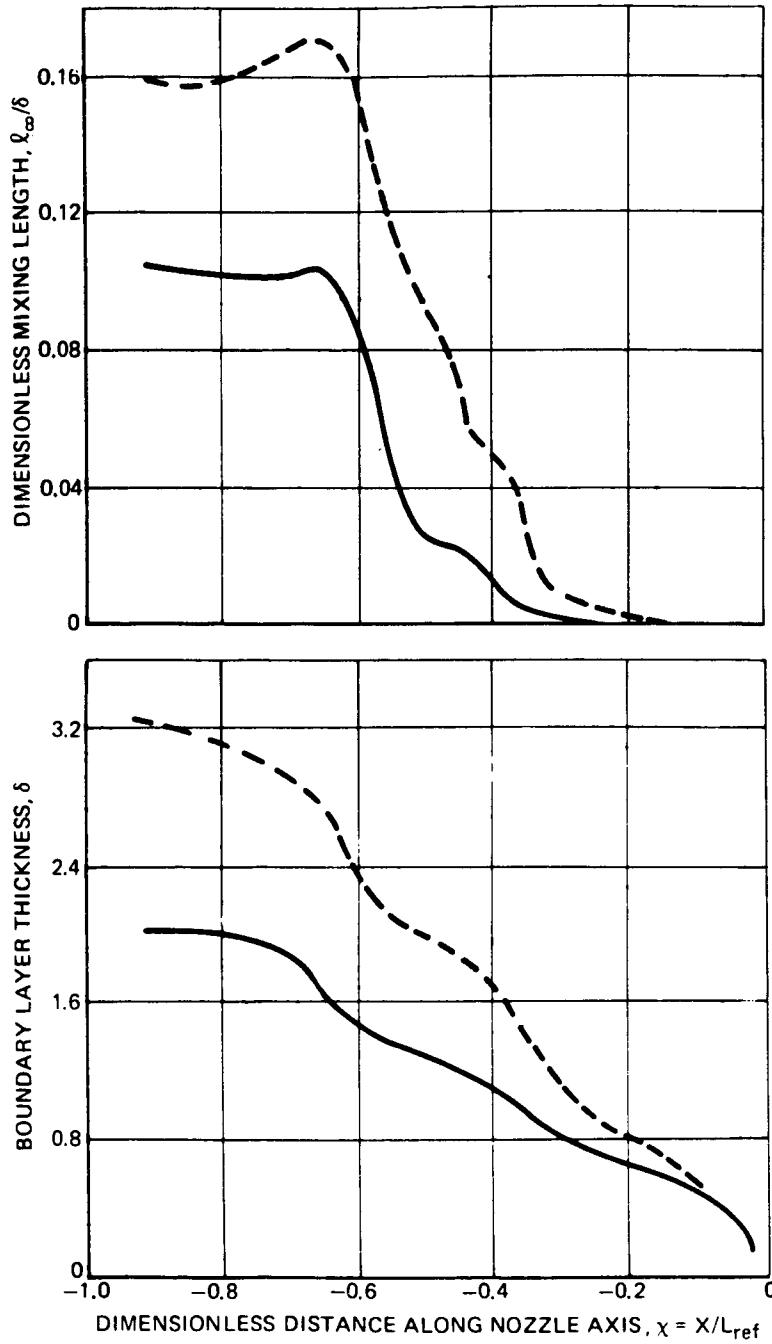


Figure 22.— Prediction of mixing length and boundary layer thickness in the approach section of the NASA Mach 5 laminar flow slotted nozzle.

——— $\frac{u}{U_i} = 0.01$
 - - - $\frac{u}{U_i} = 0.06$
 $T_o = 104.4^\circ\text{C} (220^\circ)$
 $T_w = 65.5^\circ\text{C} (150^\circ\text{F})$
 $P_o = 10.2 \text{ atm} (150 \text{ psia})$
 $U_i \approx 213 \text{ cm/sec} (7 \text{ fps})$

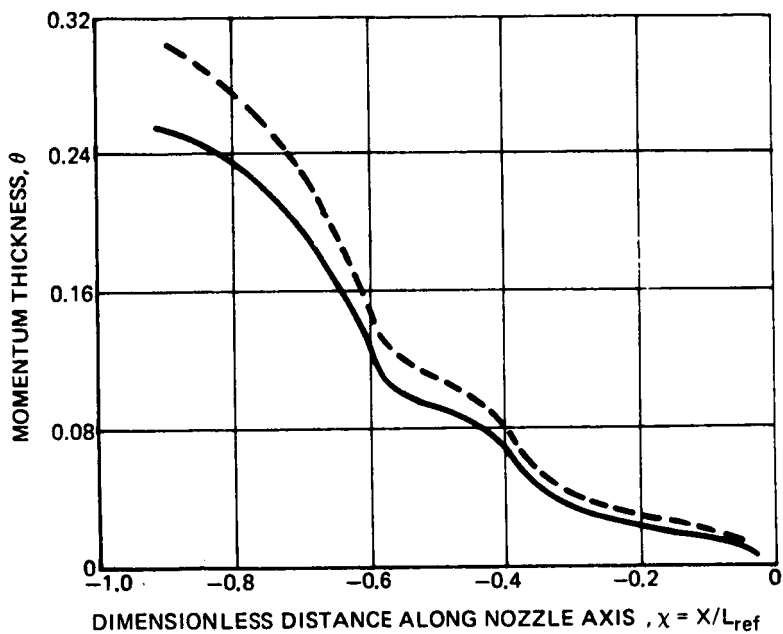


Figure 23. — Prediction of momentum thickness in the approach section of the NASA Mach 5 laminar flow slotted nozzle.

$\frac{u}{U_m} = 0.01$ $T_o = 104.4^\circ\text{C} (220^\circ\text{F})$
 $\frac{u}{U_m} = 0.06$ $T_w = 65.5^\circ\text{C} (150^\circ\text{F})$
 $P_o = 10.2 \text{ atm} (150 \text{ psia})$
 $U_i \approx 213 \text{ cm/sec} (7 \text{ fps})$

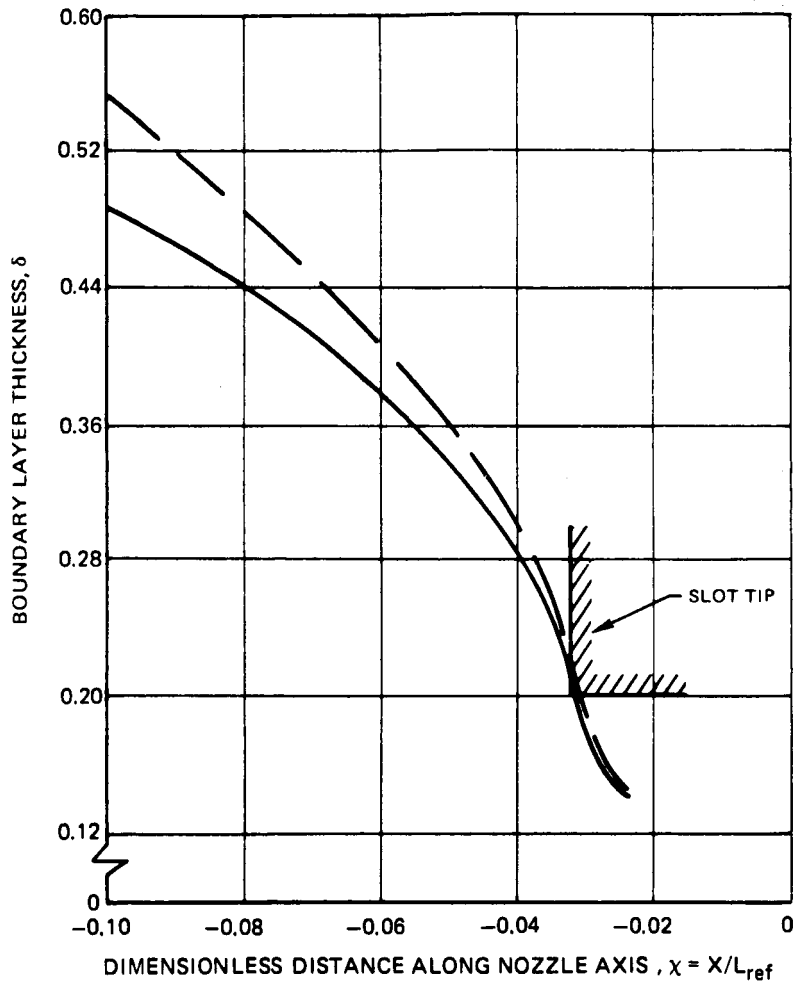


Figure 24. -- Boundary layer thickness in the region near the throat of the approach section of the NASA Mach 5 nozzle.

CALCULATION INITIATED AT SLOT - THROAT AT $\chi = 0$

$\frac{u'_m}{U_i} = 0.01$ (solid line)
 $\frac{u'_m}{U_i} = 0.06$ (dashed line)

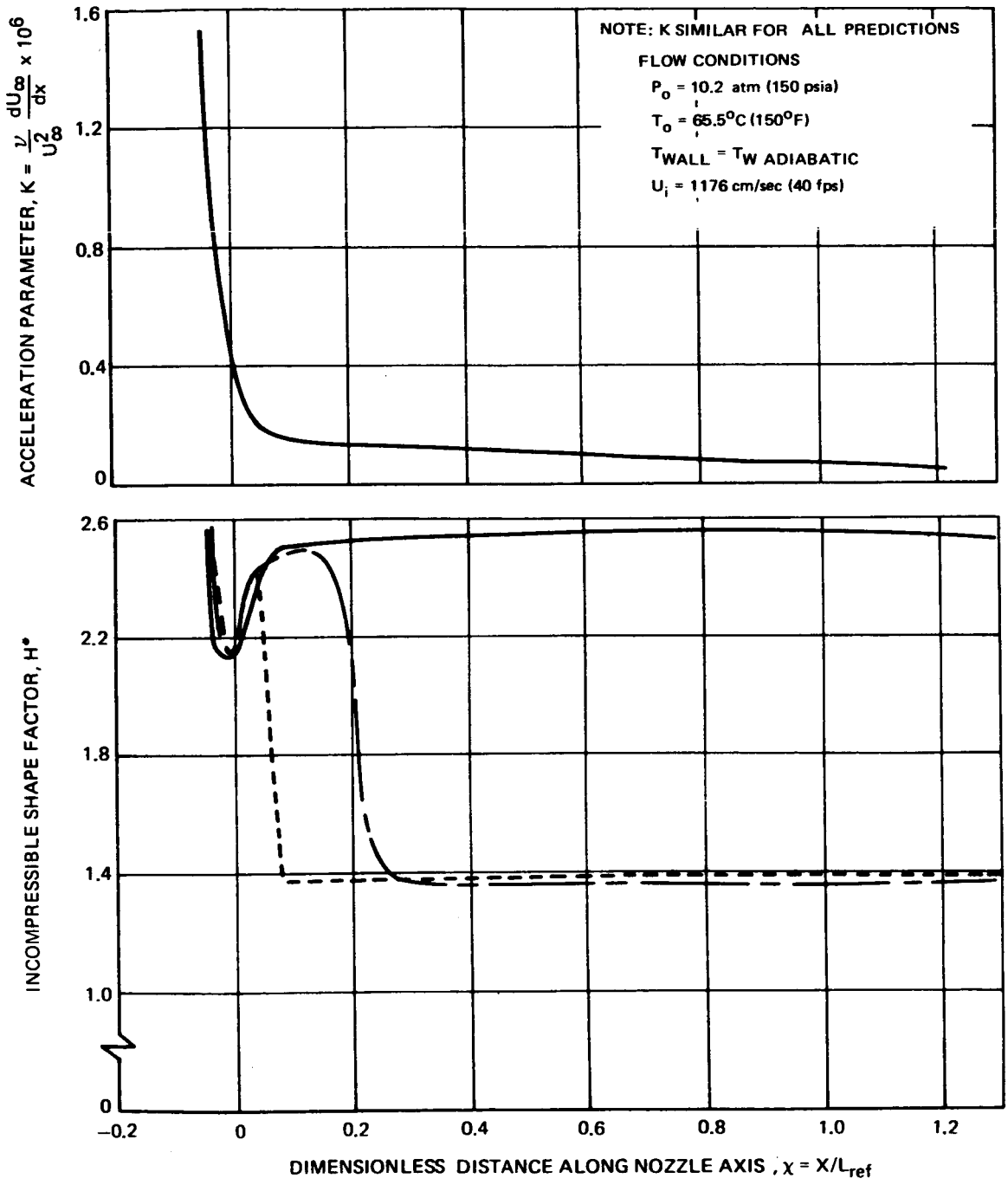


Figure 25. — Acceleration parameter and predicted incompressible shape factor in the transonic and supersonic sections of the NASA Mach 5 laminar flow slotted nozzle.

CALCULATION INITIATED AT SLOT - THROAT AT $\chi = 0$

$\frac{u'_m}{U_i} = 0.01$ $\frac{u'_m}{U_i} = 0.03$
 $\frac{u'_m}{U_i} = 0.06$

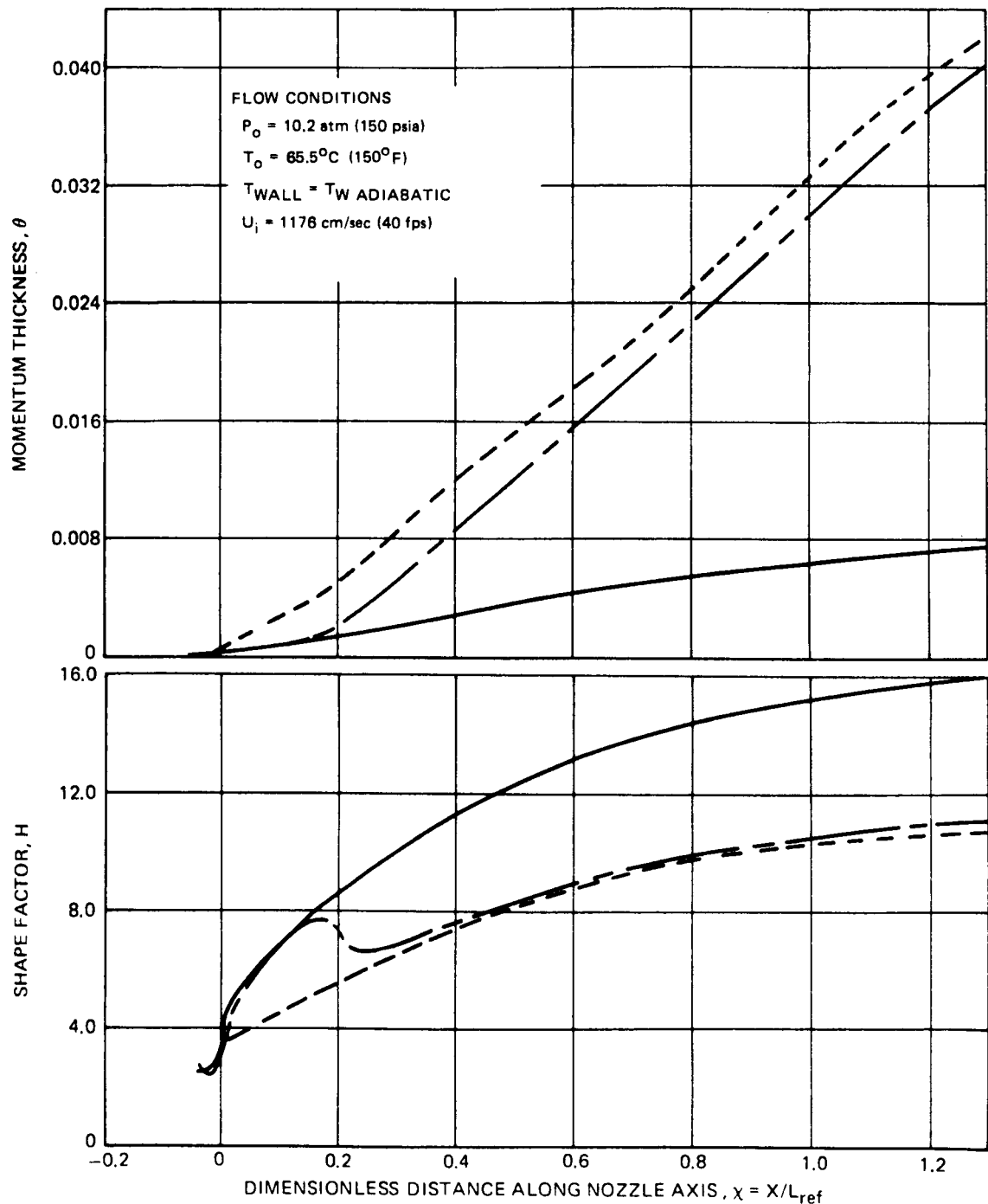


Figure 26. — Predicted momentum thickness and shape factor in the transonic and supersonic sections of the NASA Mach 5 laminar flow slotted nozzle.

CALCULATION INITIATED AT SLOT - THROAT AT $\chi = 0$

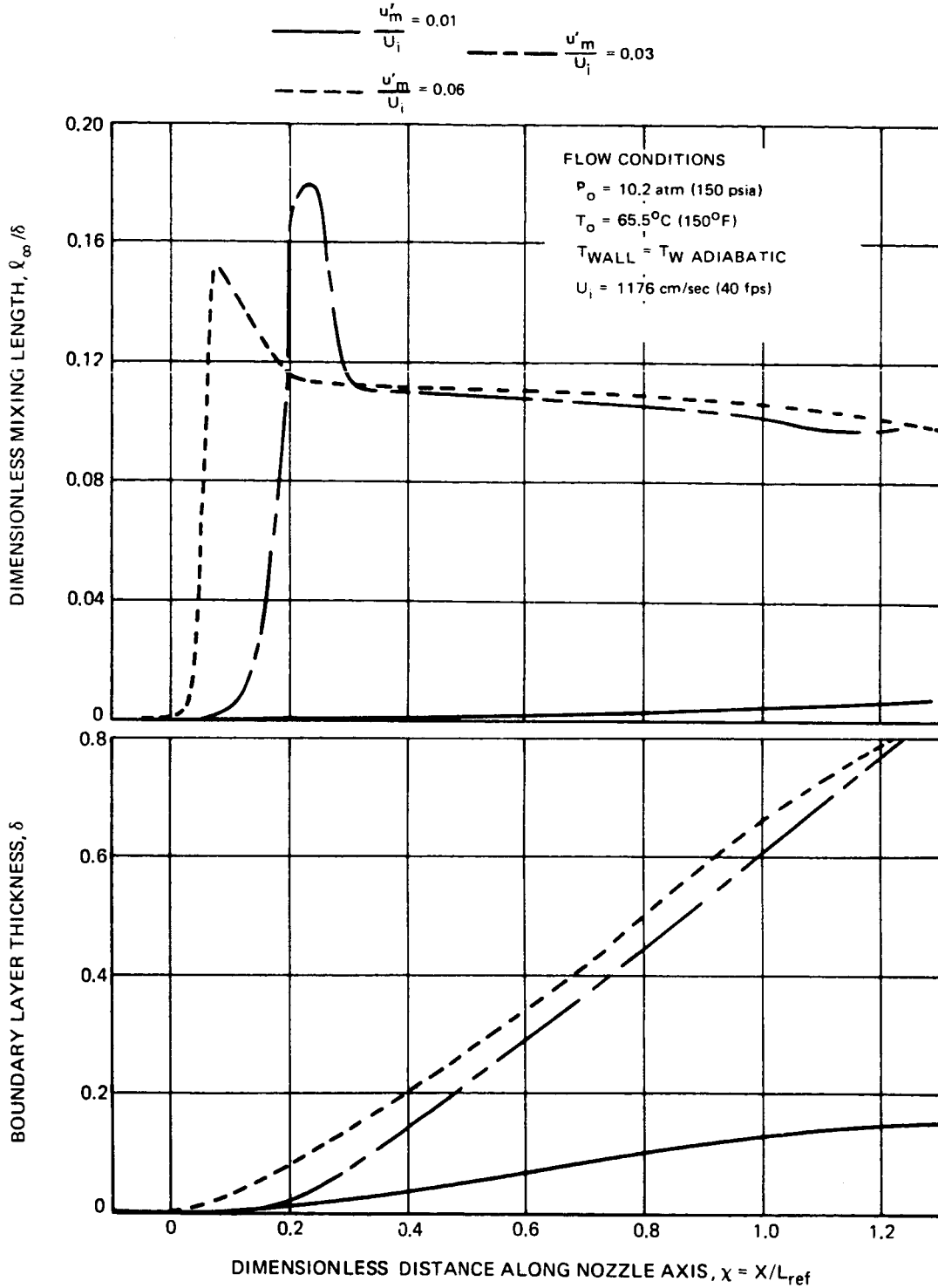


Figure 27. — Predicted dimensionless mixing length and boundary layer thickness in the transonic and supersonic sections of the NASA Mach 5 laminar flow slotted nozzle.

CALCULATION INITIATED AT SLOT-THROAT AT $\chi = 0$

$$\frac{u'_m}{U_i} = 0.01$$

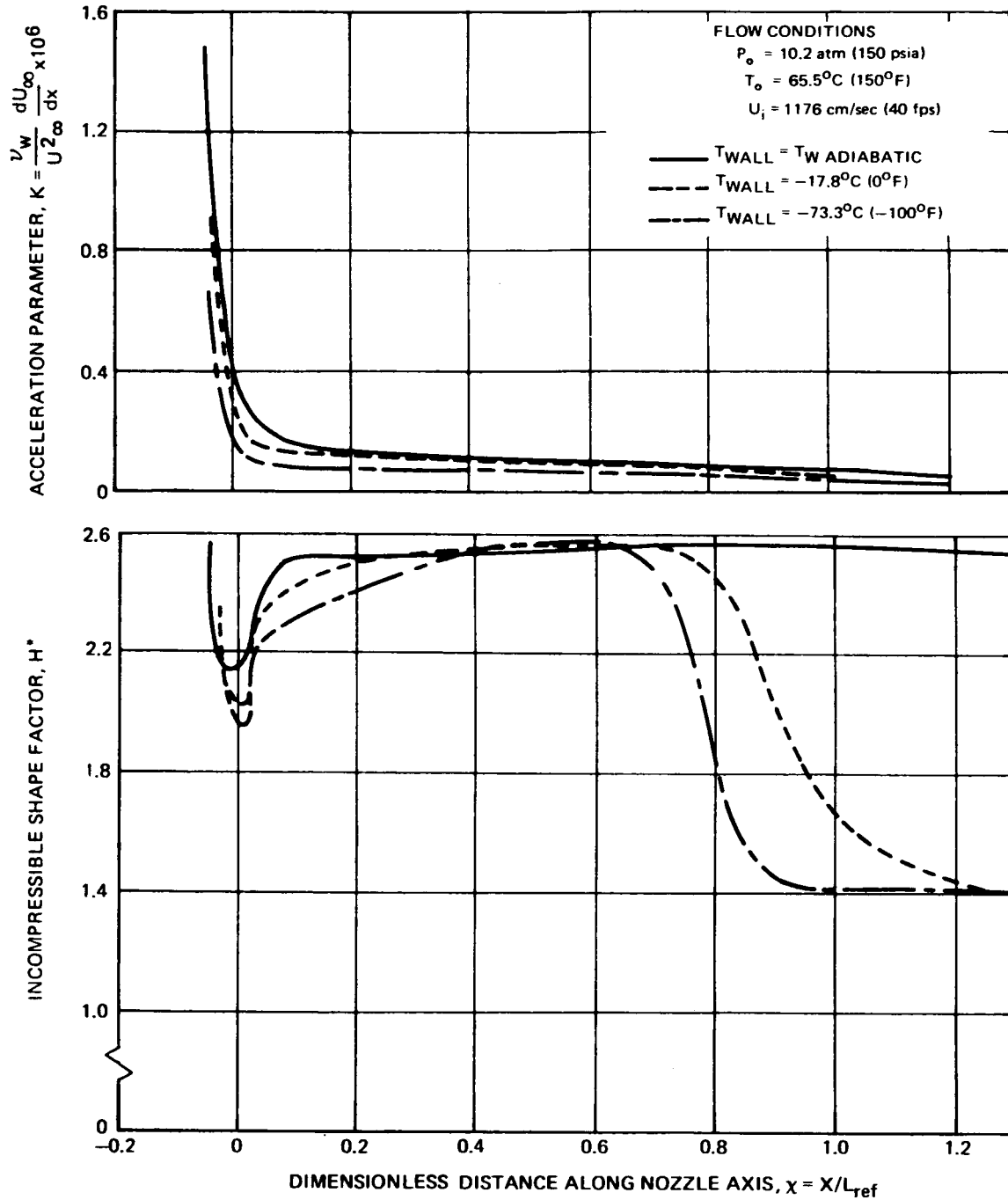


Figure 28. — Effect of heat transfer on acceleration parameter and incompressible shape factor in the transonic and supersonic sections of the NASA Mach 5 laminar flow slotted nozzle.

CALCULATION INITIATED AT SLOT-THROAT AT $\chi = 0$

$$\frac{u'_m}{U_i} = 0.01$$

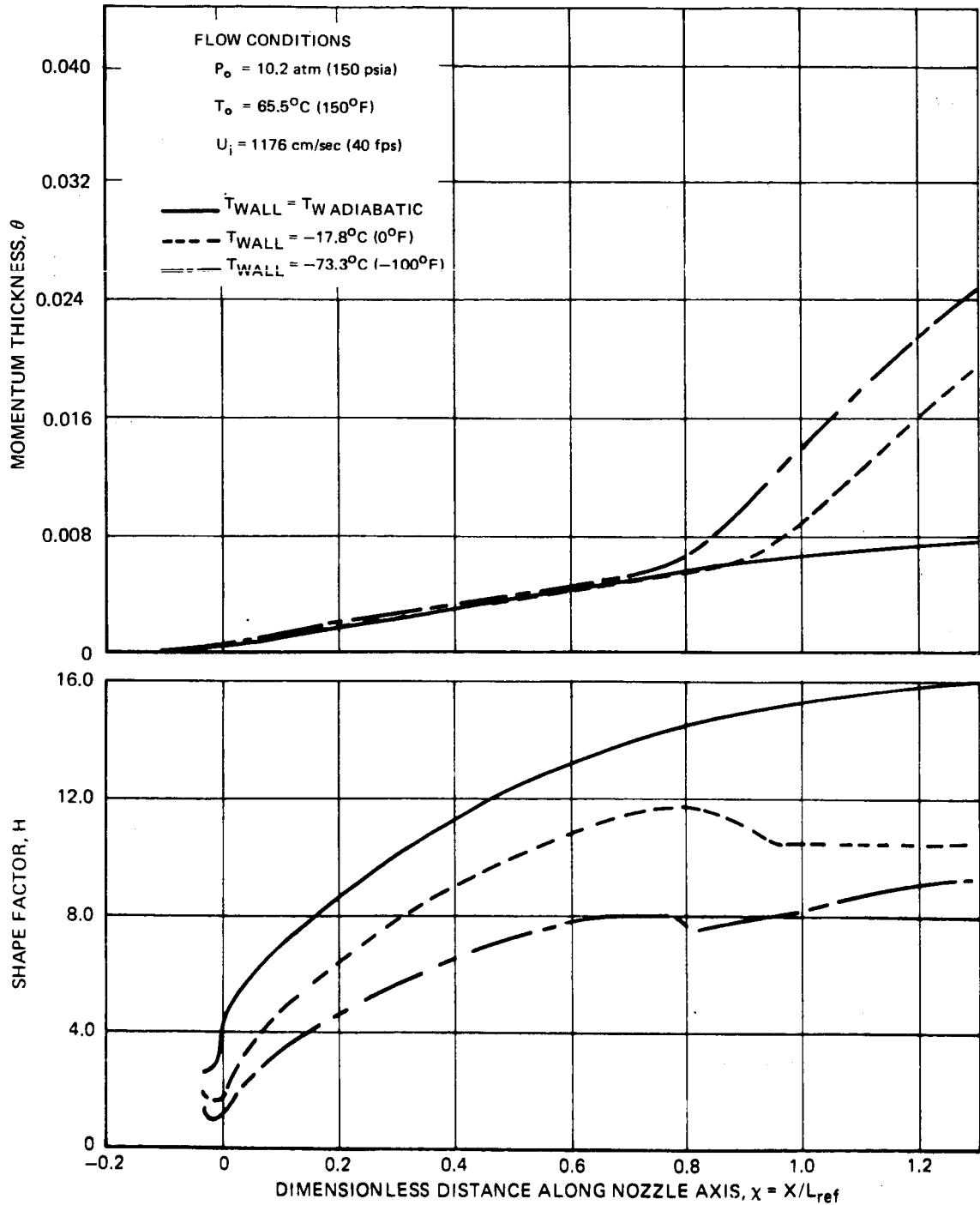


Figure 29. — Effect of heat transfer on momentum thickness and shape factor in the transonic and supersonic sections of the NASA Mach 5 laminar flow slotted nozzle.

CALCULATION INITIATED AT SLOT - THROAT AT $\chi = 0$

$$\frac{u'_m}{U_i} = 0.01$$

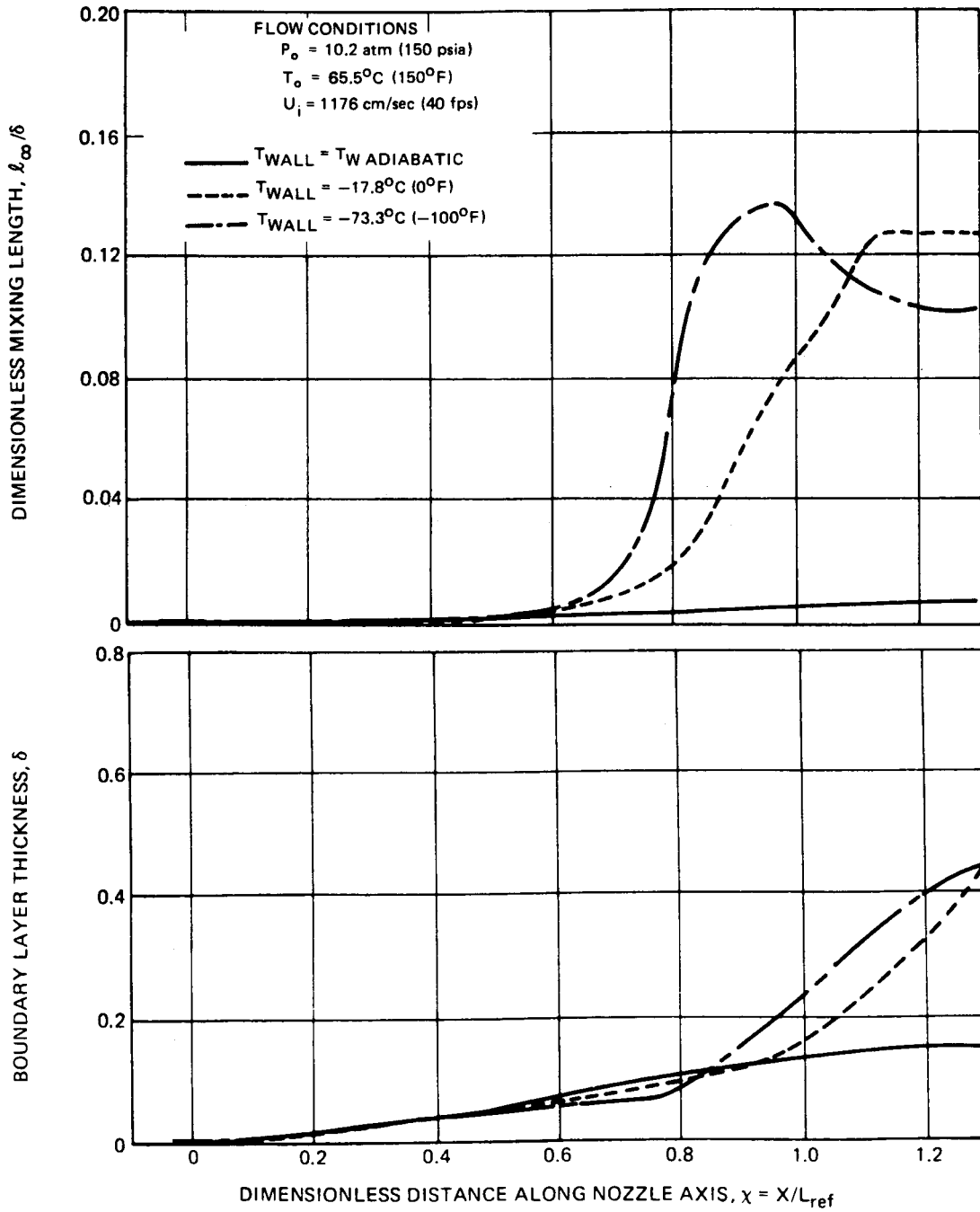


Figure 30. — Effect of heat transfer on mixing length and boundary layer thickness in the transonic and supersonic sections of the NASA Mach 5 laminar flow slotted nozzle.

CALCULATION INITIATED AT SLOT-THROAT AT $\chi = 0$

$$\frac{u'}{U_i} = 0.03$$

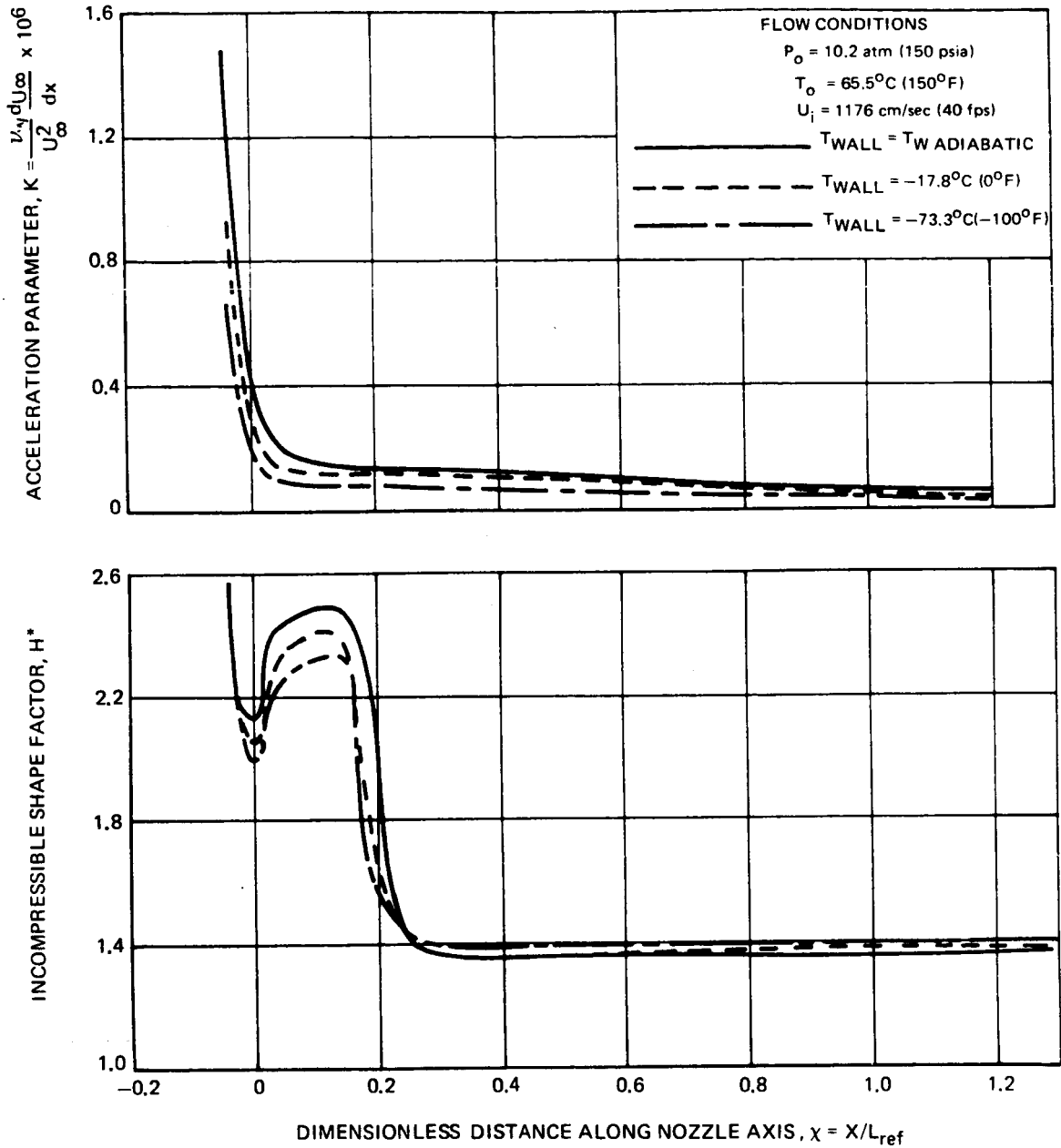


Figure 31. — Effect of heat transfer on acceleration parameter and incompressible shape factor in the transonic and supersonic sections of the NASA Mach 5 laminar flow slotted nozzle.

CALCULATION INITIATED AT SLOT-THROAT AT $\chi = 0$

$$\frac{u'}{U_i} = 0.03$$

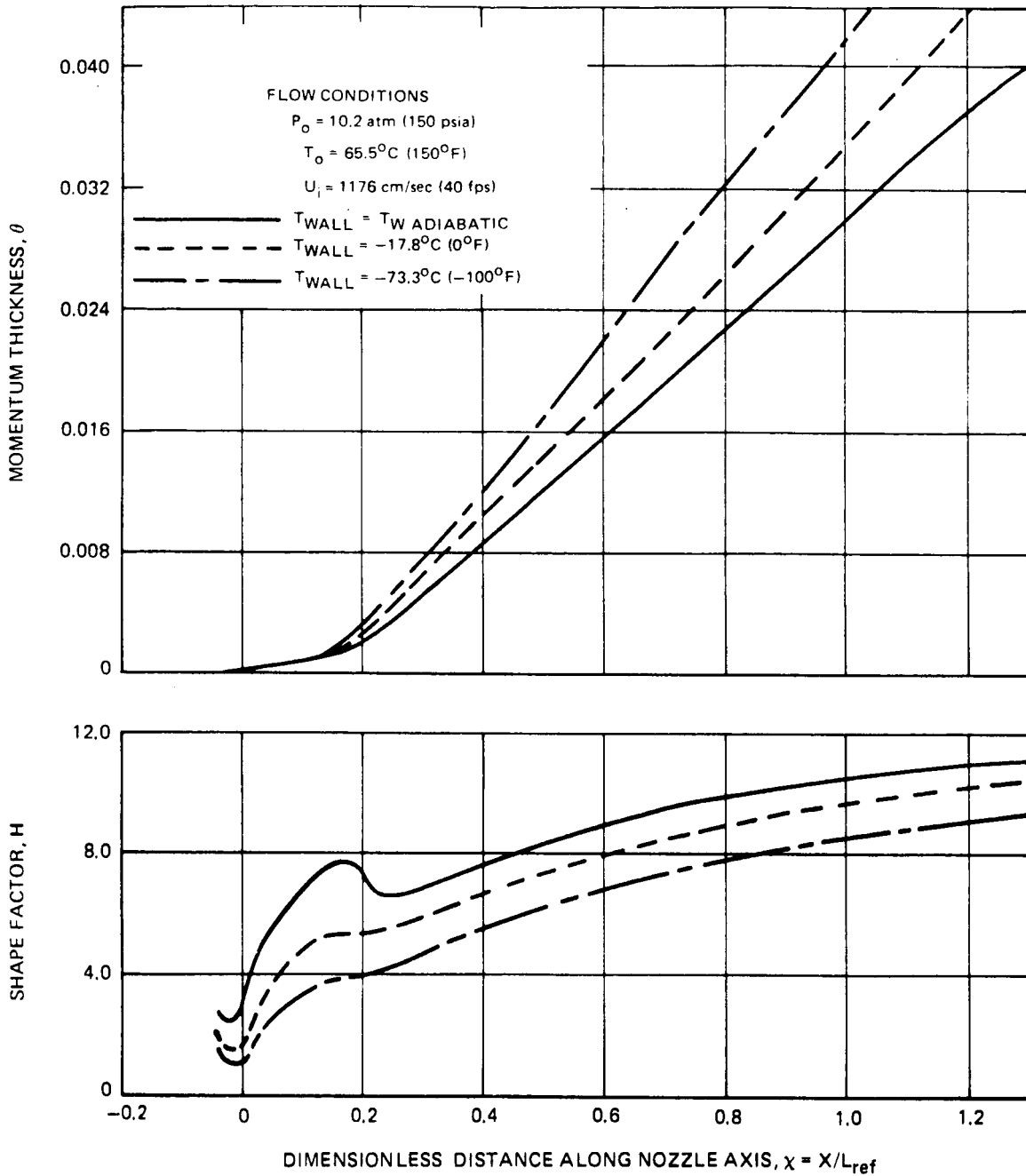


Figure 32. — Effect of heat transfer on momentum thickness and shape factor in the transonic and supersonic sections of the NASA Mach 5 laminar flow slotted nozzle.

CALCULATION INITIATED AT SLOT-THROAT AT $\chi = 0$

$$\frac{u'_m}{U_i} = 0.03$$

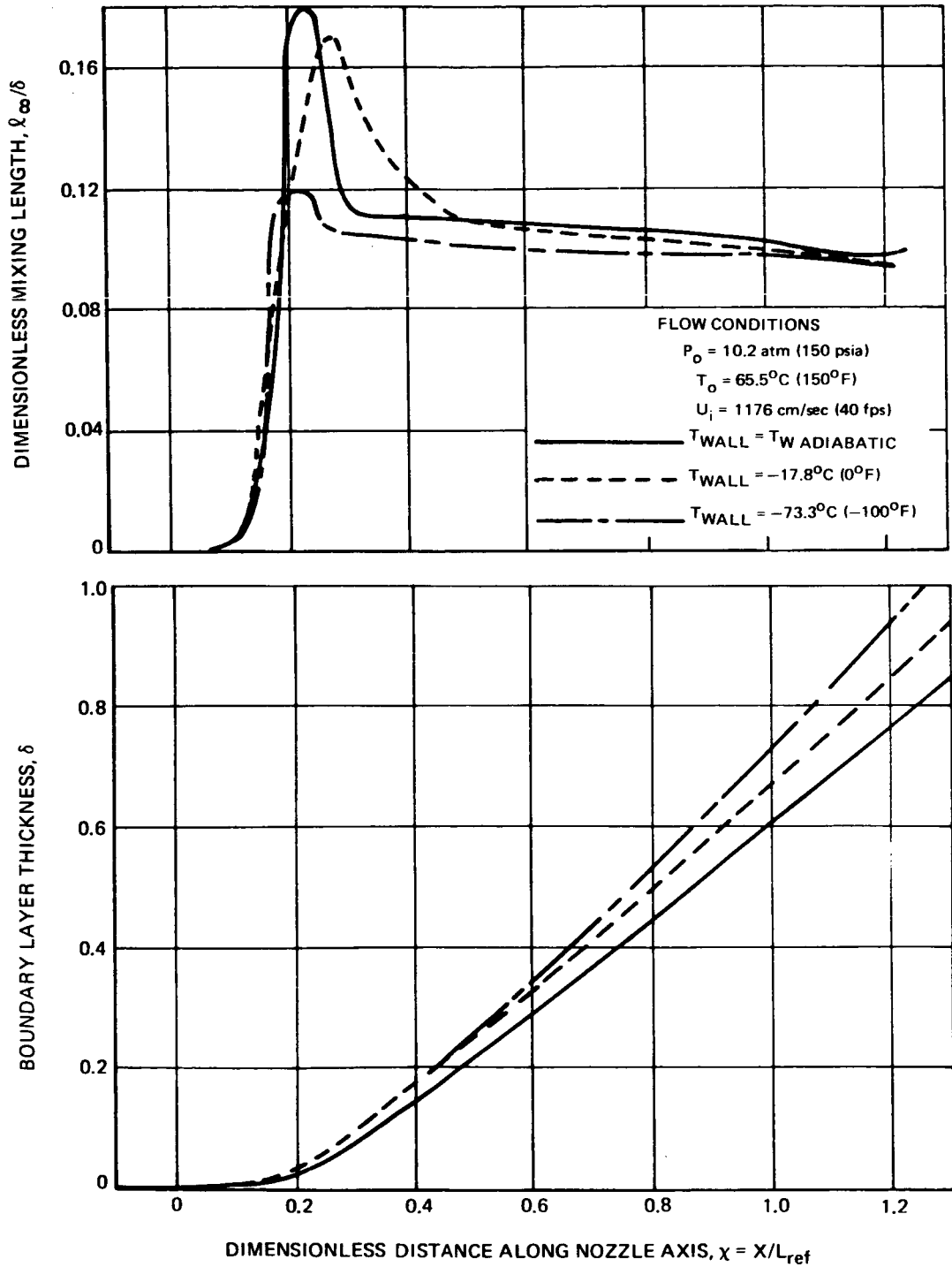


Figure 33. — Effect of heat transfer on mixing length and boundary layer thickness in the transonic and supersonic sections of the NASA Mach 5 laminar flow slotted nozzle.

CALCULATION INITIATED AT SLOT - THROAT AT X = 0

$$\frac{u_m'}{U_i} = 0.01$$

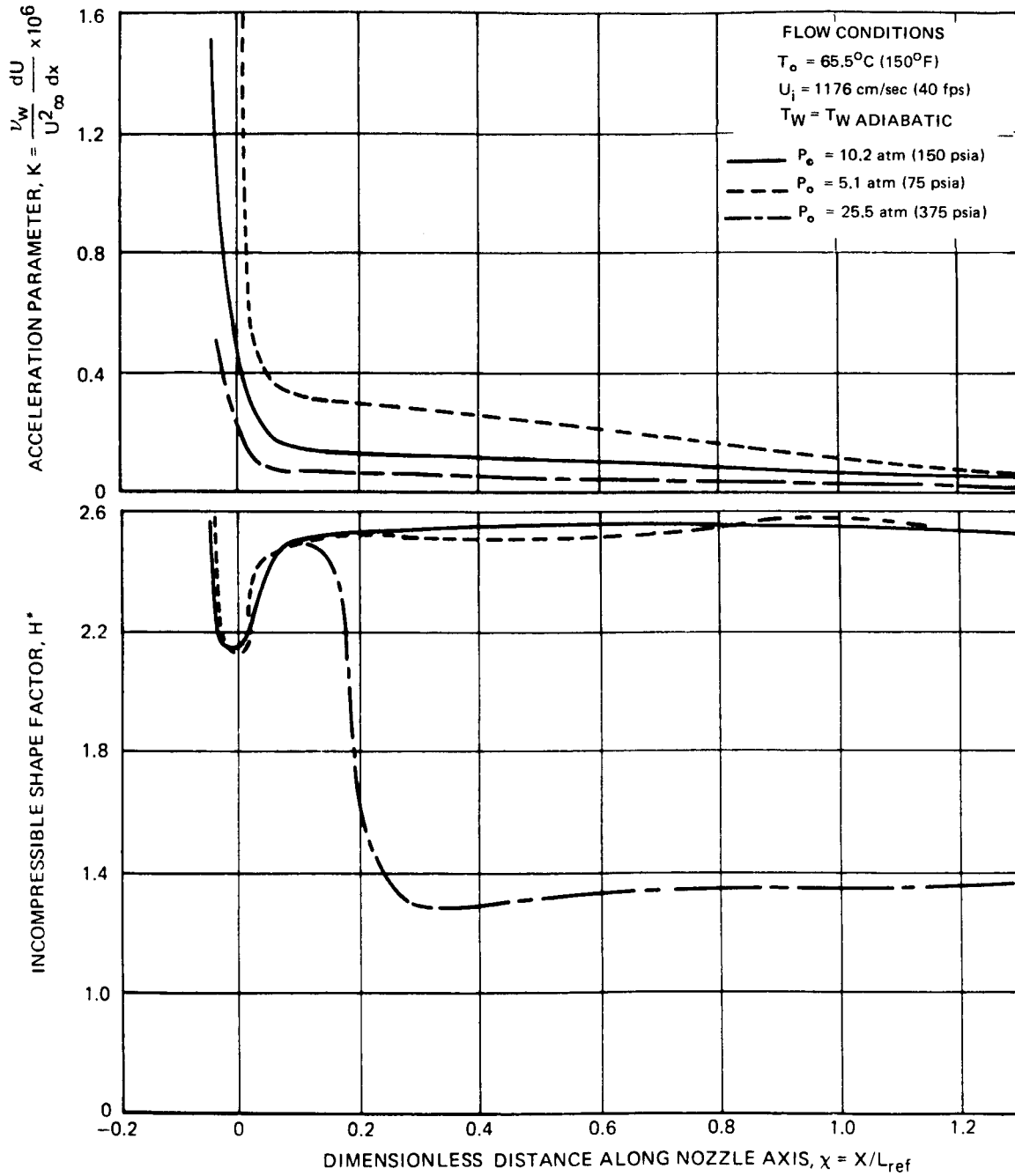


Figure 34. - Effect of stagnation pressure on acceleration parameter and incompressible shape factor in the transonic and supersonic sections of the NASA Mach 5 laminar flow slotted nozzle.

CALCULATION INITIATED AT SLOT - THROAT AT $\chi = 0$

$$\frac{u}{u_i} = 0.01$$

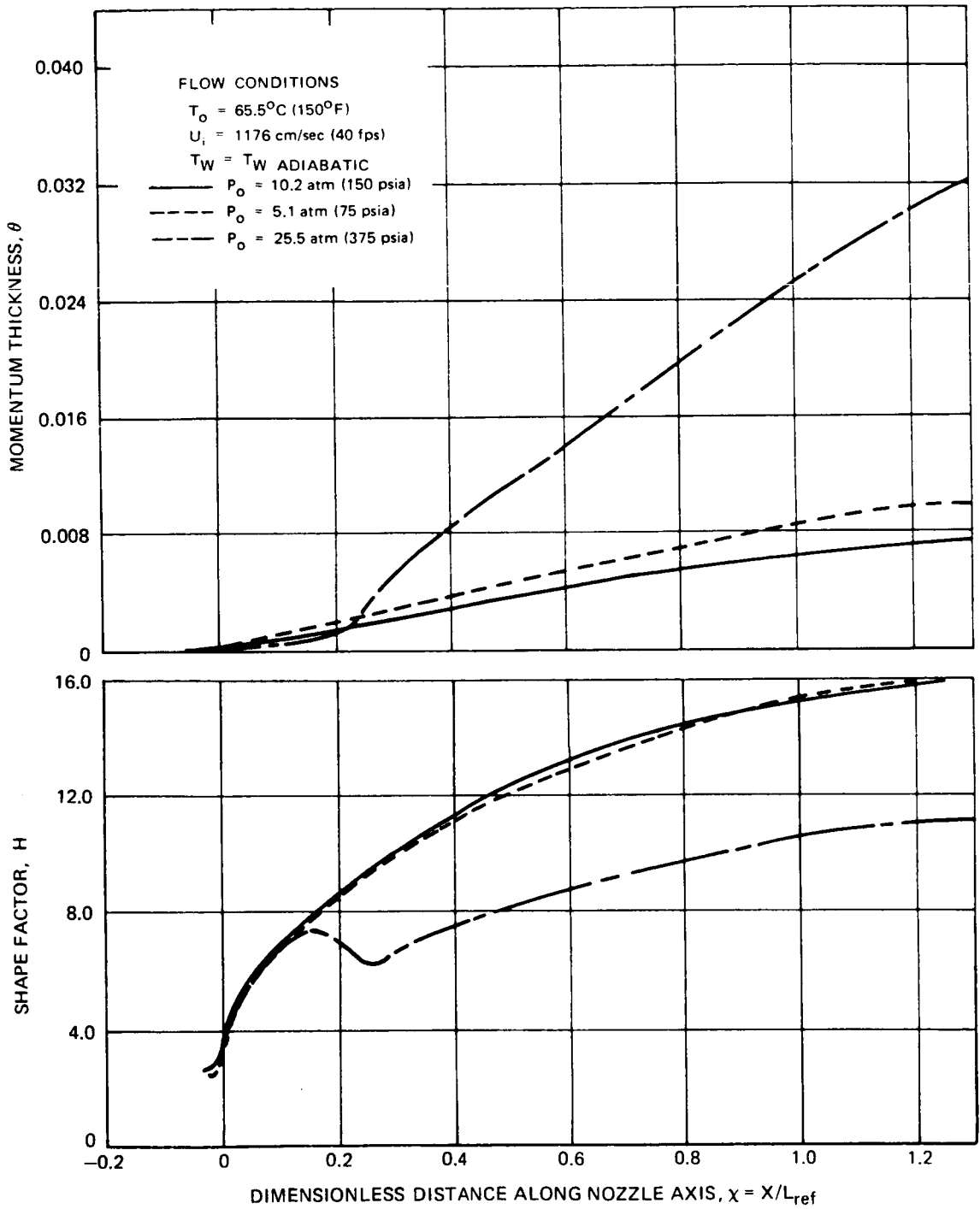


Figure 35. — Effect of stagnation pressure on momentum thickness and shape factor in the transonic and supersonic sections of the NASA Mach 5 laminar flow slotted nozzle.

CALCULATION INITIATED AT SLOT-THROAT AT $\chi = 0$

$$\frac{u'}{u_i} = 0.01$$

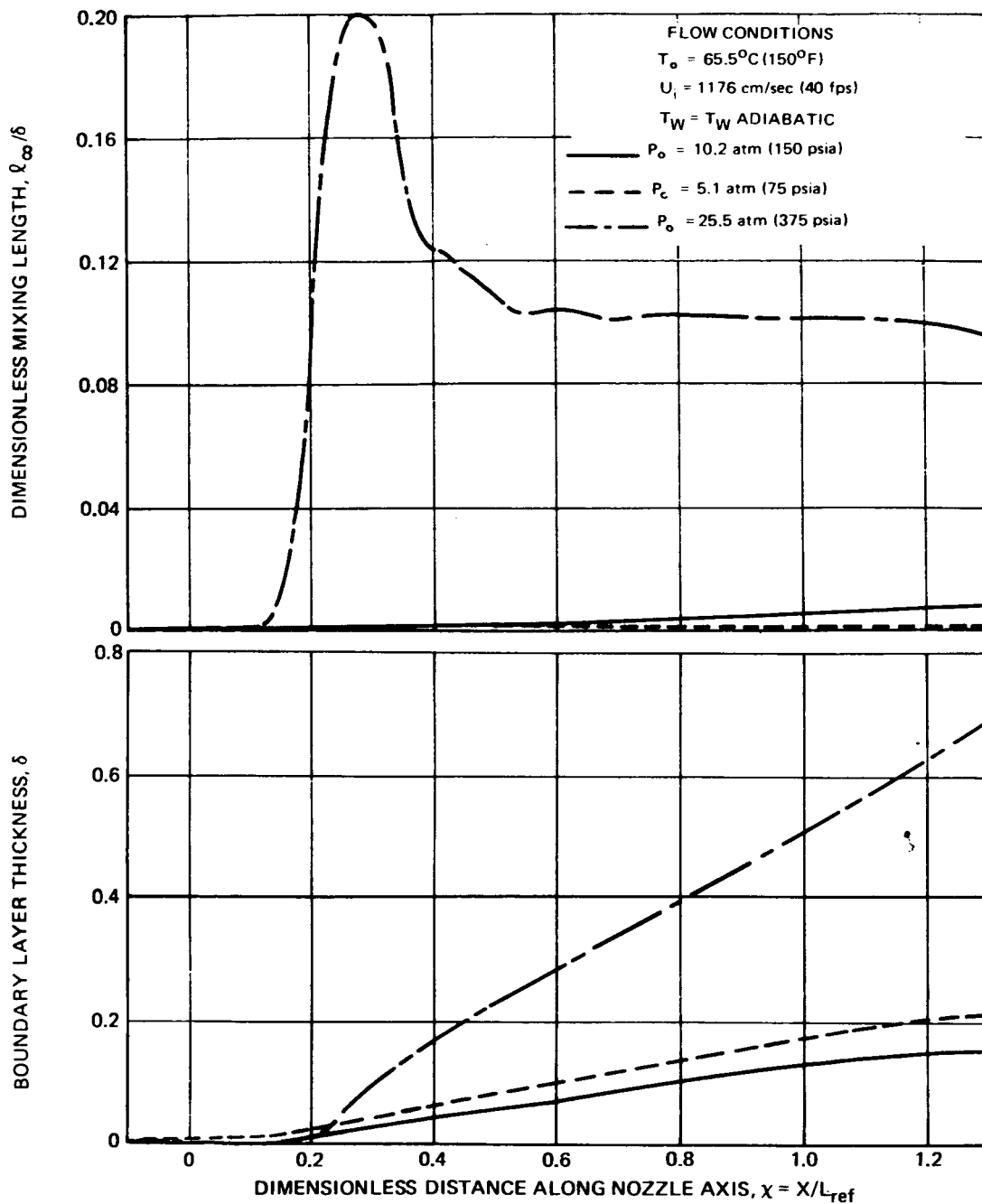


Figure 36. — Effect of stagnation pressure on mixing length and boundary layer thickness in the transonic and supersonic sections of the NASA Mach 5 laminar flow slotted nozzle.

$$\frac{C_{f,w}}{Re} = 0.01$$

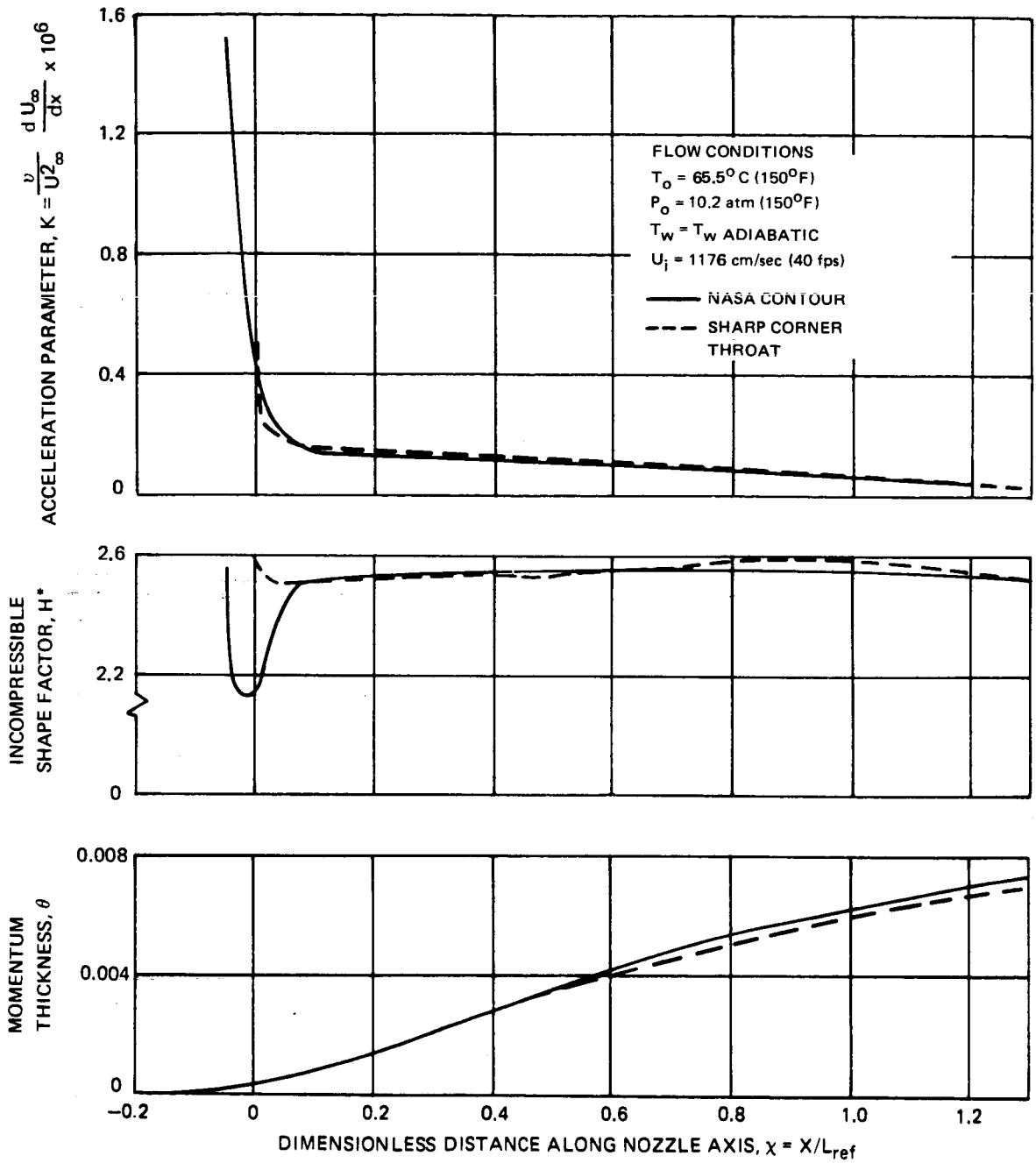


Figure 37. — Effect of nozzle geometry on acceleration parameter, incompressible shape factor and momentum thickness in the transonic and supersonic sections of the NASA Mach 5 laminar flow slotted nozzle.

$$\frac{u}{u_i} = 0.01$$

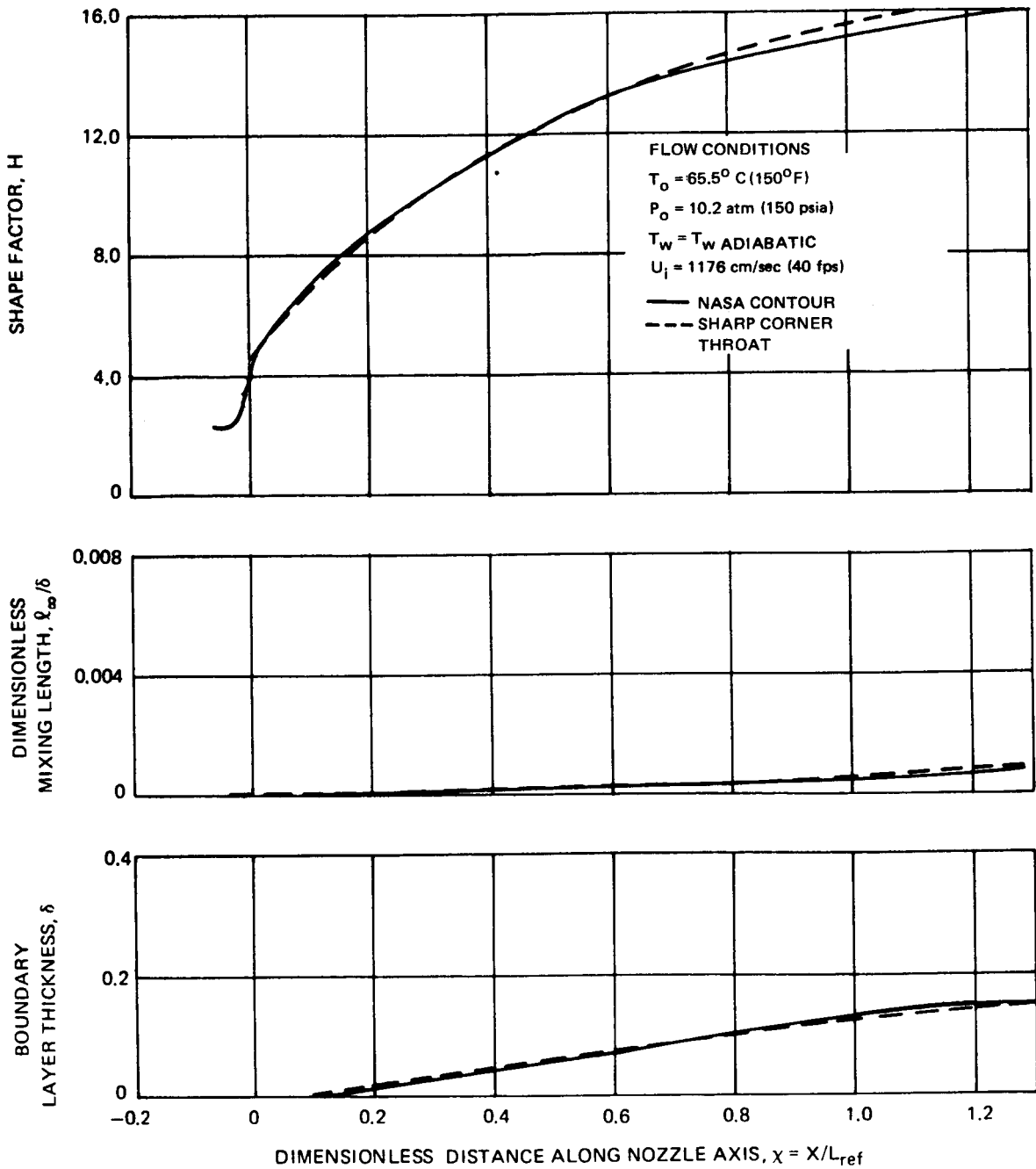


Figure 38. — Effect of nozzle geometry on shape factor, mixing length and boundary layer thickness in the transonic and supersonic sections of the NASA Mach 5 laminar flow slotted nozzle.

CALCULATION INITIATED AT THROAT

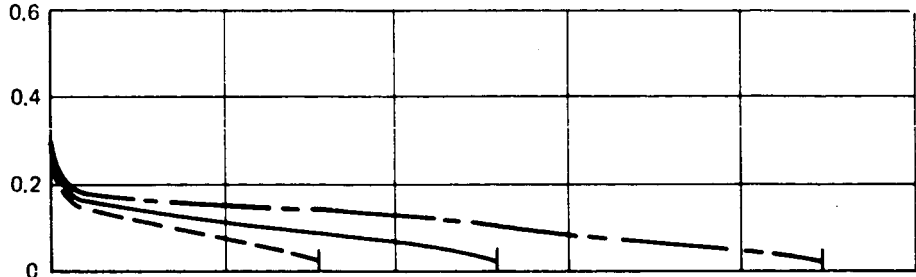
$$\frac{u'_m}{U_i} = 0.01$$

—| INDICATES NOZZLE END

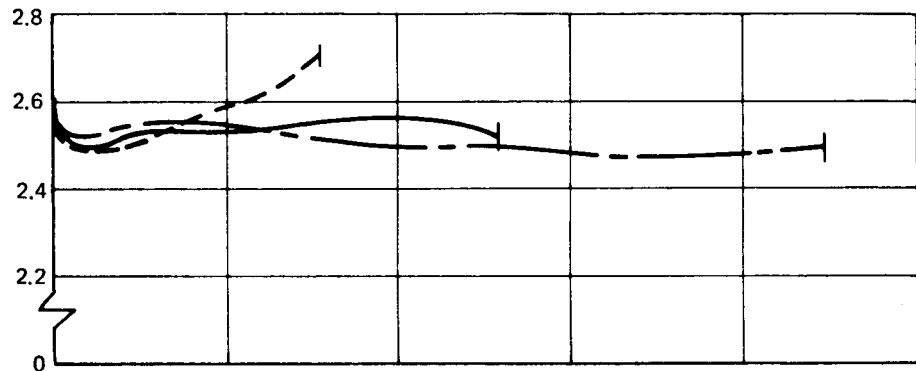
FLOW CONDITIONS

- $P_o = 10.2 \text{ atm (150 psia)}$ --- $M_{\text{exit}} = 4$
 $T_o = 65.5^\circ\text{C (150}^\circ\text{F)}$ — $M_{\text{exit}} = 5$
 $U_i = 1176 \text{ cm/sec (40 fps)}$ - - - $M_{\text{exit}} = 6$
 $T_w = T_w \text{ ADIABATIC}$

ACCELERATION PARAMETER,
 $K = \frac{1/W}{U_\infty^2} \frac{dU_\infty}{dx} \times 10^6$



INCOMPRESSIBLE SHAPE FACTOR,
 H^*



MOMENTUM THICKNESS, θ

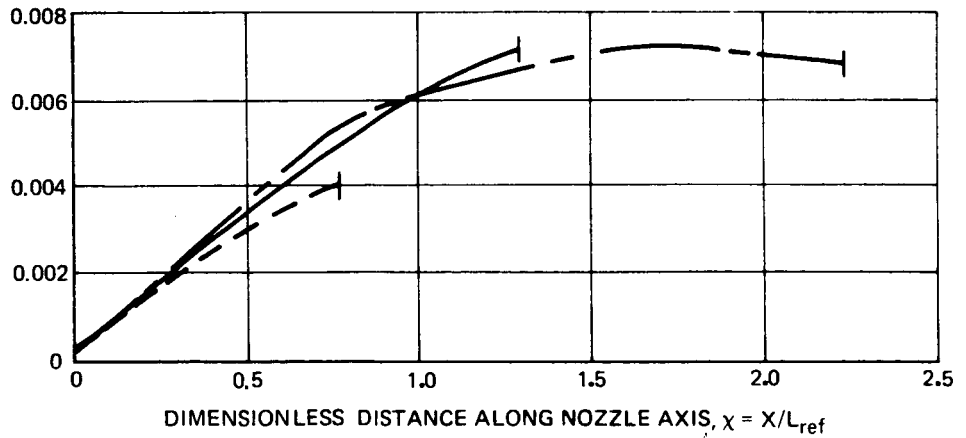


Figure 39. — Effect of Mach number on boundary layer development in supersonic nozzles.

CALCULATION INITIATED AT THROAT

$$\frac{u'_m}{U_i} = 0.01$$

—| INDICATES NOZZLE END

FLOW CONDITIONS

$P_0 = 10.2 \text{ atm (150 psia)}$

$T_0 = 65.5^\circ\text{C (150}^\circ\text{F)}$

$U_i = 1176 \text{ cm/sec (40 fps)}$

$T_w = T_w \text{ ADIABATIC}$

--- $M_{\text{exit}} = 4$

— $M_{\text{exit}} = 5$

- - - $M_{\text{exit}} = 6$

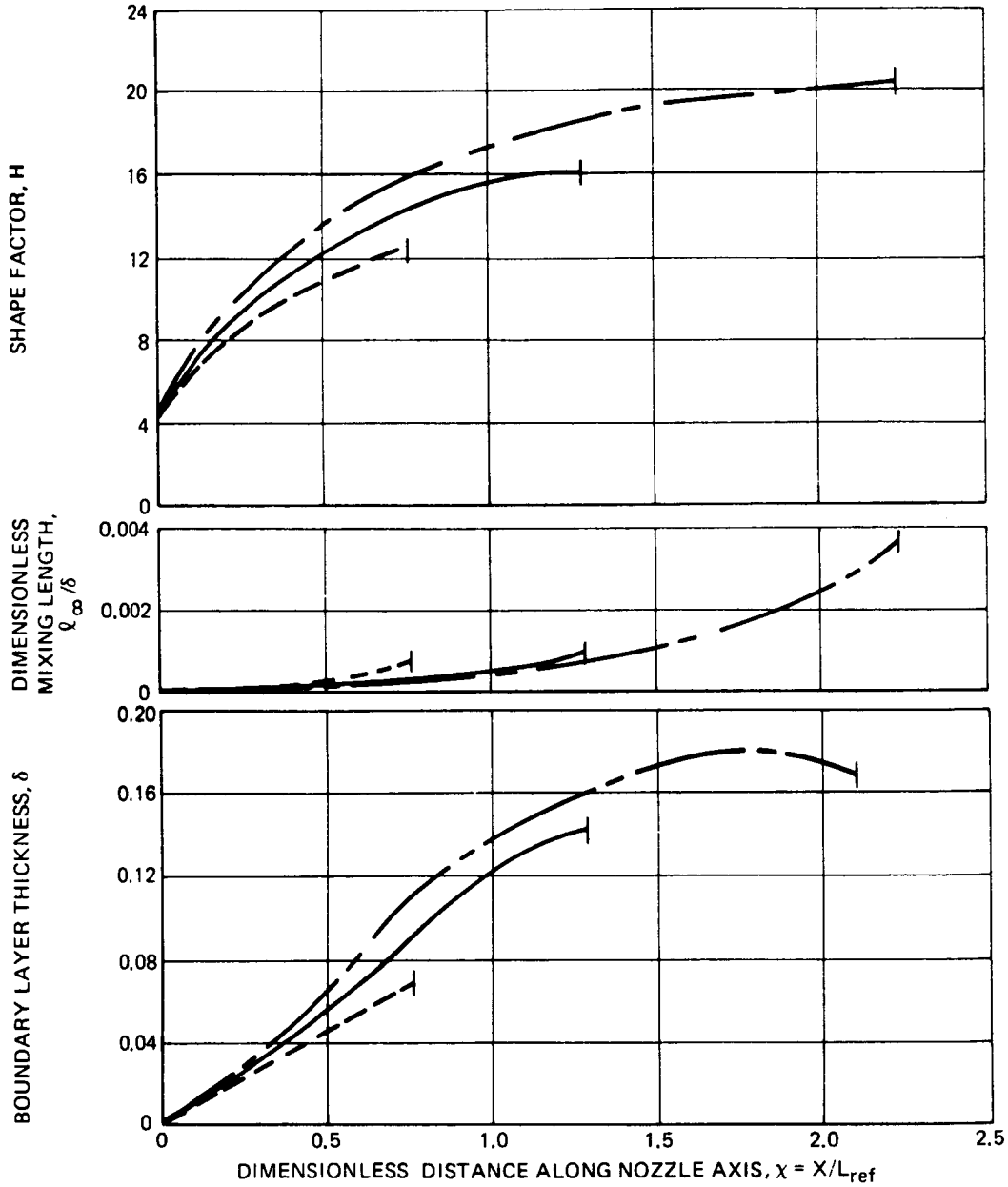


Figure 40. — Effect of Mach number on boundary layer development in supersonic nozzles.

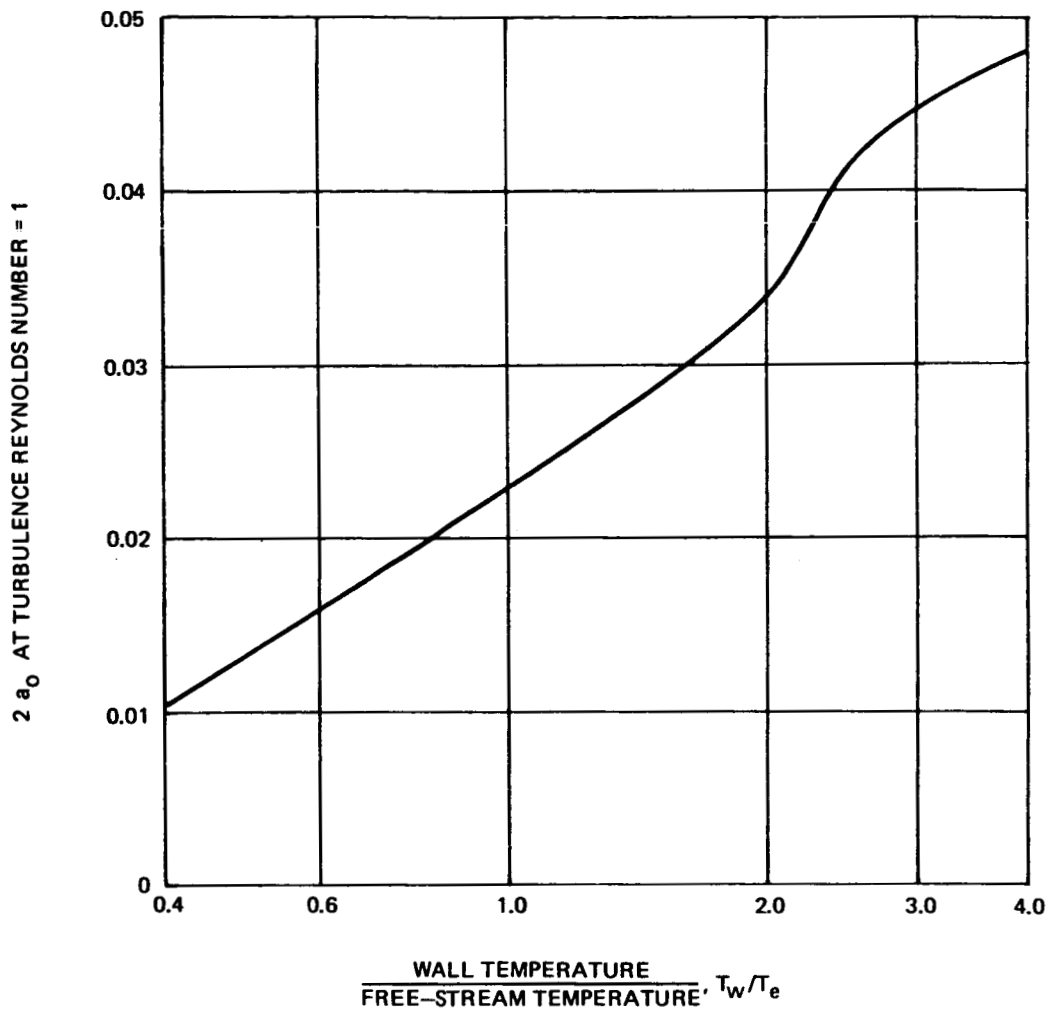


Figure 41. — Variation of structural coefficient with temperature ratio.

☆ U.S. GOVERNMENT PRINTING OFFICE: 1974-739-161/140